D I P L O M A R B E I T

A novel system for continuous temperature swing adsorption: parameter study at bench scale

unter der Leitung von

Univ.Prof. Dipl.-Ing. Dr.techn. Hermann Hofbauer

Dipl.-Ing. Johannes Fuchs

Dipl.-Ing. Gerhard Schöny

Dipl.-Ing. Egon Zehetner

E 166

Institut für Verfahrenstechnik, Umwelttechnik und Technische Biowissenschaften

eingereicht an der Technischen Universität Wien

Fakultät für Maschinenwesen und Betriebswissenschaften

von

Florian Dietrich

0825612

Dr. F.-J. Schichtgasse 16/1; 2340 Mödling

Wien, im Juli 2014

Danksagung

Bedanken möchte ich mich bei den Herrn Dipl.-Ing. Johannes Fuchs, Dipl.-Ing. Gerhard Schöny und Dipl.-Ing. Egon Zehetner für die hervorragende Betreuung sowie die kurzweilige Gestaltung der vielen Versuchsstunden. Bei allen Mitarbeitern der Arbeitsgruppe "Zero Emissions Technolgy" sowie bei allen Professoren, die mein Interesse an den verschiedensten Bereichen der Verfahrenstechnik geweckt haben, bedanke ich mich ebenfalls. Des Weiteren bedanke ich mich bei allen Studienkollegen und Freunden, die mich durch das Studium begleitet haben und mich des Öfteren zum Lernen motiviert haben. Auch meiner Familie möchte ich danken. Ihr habt es mir ermöglicht ein Fachgebiet zu studieren, welches mich nicht mehr hätte faszinieren können. Danke auch an Julia, die mich während des Studiums stets unterstützt hat.

Kurzfassung

Sequestrierung und nachträgliche Speicherung von CO_2 welches aus großen Punktquellen emittiert wird, wie z.B. Kraftwerken oder Industrieanlagen, wird als einer der Schlüsselmaßnahmen gegen den Klimawandel in den kommenden Jahrzehnten angesehen. Während der kitische Teilaspekt von CO_2-Sequestrieung in der öffentlichen Akzeptanz liegt, beeinflusst der Eigenenergiebedarf des CO_2 Abscheidungsprozesses auch die Betriebskosten des eigentlichen CO_2 emittierenden Prozesses.

Deswegen wurden weltweit große Bemühungen zur Entwicklung von kosteneffizienten CO_2 Abscheidungstechnologien unternommen; die Forschungsgruppe "Zero Emission Technologies" (ZET) an der Technischen Universität Wien ist führend in diesem Bereich. Kürzlich wurde ein neuartiges Reaktordesign zur nachgeschaltenen CO_2 Abscheidung, basierend auf Temperatur-Wechseladsorption (auch Temperature Swing Adsorption oder TSA), von der ZET Gruppe, gemeinsam mit einem interationalen Gas- und Ölunternehmen, entwickelt. Eine Anlage im Labormaßstab (auch Bench Scale Unit oder BSU), welche dem entwickelten Reaktordesign zugrunde liegt, wurde errichtet um experimentelle Untersuchungen, im Bezug auf die Abscheideleistung des TSA Prozesses, durchzuführen.

Dieses Werk stellt Ergebnisse vor, die im Zuge einer ausführlichen Versuchskampagne an der BSU, erzielt wurden. Als Adsorbens wurde ein, mit PEI imprägnierter, poröser Silikasand verwendet. Eine Vielzahl verschiedener Betriebsbedingungen wurden untersucht, um ein tiefes Verständnis für die Zusammenhänge zwischen Betriebsbedingungen und CO_2-Abscheideleistung der Anlage zu gewinnen.

Wenn ein Abgas mit einer CO_2 Konzentration von $7,7 vol\% CO_2$ und einem Volumenstrom von $16,8 Nm^3/h$ dem gekühlten Adsorber zugeführt wurde, und $8 Nm^3/h$ Dampf verwendet wurde um das Adsorbens, bei einem Umlauf von circa $30 kg/h$, zu regenerieren, konnte des Öfteren ein Abscheidegrad von über 80% erzielt werden. Des weiteren wurde gezeigt, dass eine Wechselwirkung zwischen Dampf, der zur Regeneration verwendet wird, und dem Adsorbens, eine verbesserte Abscheideleistung zurfolge hat, hervorgerufen durch einen internen Wärmeverschub-Effekt. Eine Verringerung des Volumenstroms an Regenerationsdampf, hatte einen vergleichbar gering Einfluss auf die Abscheideleistung der Anlage; sodass eine Verringerung des Dampfvolumenstroms für die Regeneration bei zukünftigen Versuchen in Betracht gezogen werden kann. Eine erhöhte Fördermenge an CO_2 in den Adsorber, zeigte eine verbesserte Abscheiderate (in $kg_{CO_2 abgesch.}/Tag$), jedoch eine

erheblich geringerer CO_2-Abscheidegrade. Sowohl die Fluidisierungsgeschwindigkeit, als auch die Betthöhe der Wirbelschichtstufen, hatten einen großen Einfluss auf den CO_2-Abscheidegrad; höchst wahrscheinlich aufgrund der Auswirkungen auf die Wärmeübertragungsrate der Bettwärmetauscher. Schließlich, wurde beobachtet dass die Zufuhr einer geringen Menge an Sperrgas, in den Fließbettbereich nach dem Desorber Feststoffauslass, den Dampfschlupf von Desorber zu Adsorber erheblich verringert, was beweist, dass es mit dieser Maßnahme möglich ist, die Kolonnen abzudichten.

Die Versuchskampagne wurde erfolgreich durchgeführt und ein Bereich identifiziert, in dem stabiler Betrieb der BSU bei ausreichend hoher CO_2 Abscheideleistung möglich ist. Aus der Versuchskampagne wurde geschlossen, dass ausreichend hoher Wärmeaustausch mit den beiden Gas-Feststoff Kolonnen, die wichtichste Rolle, im erlangen hoher Abscheidegrade, sogar bei hohen Abscheideraten, spielen könnte. Ausserdem wurde gezeigt, dass Wasserdampfkondensierung innerhalb des Systems stets vermieden werden muss, um die Schädigung des Adsorbens und das Bedecken von Wärmetauscherflächen mit Adsorbens zu verhindern.

Abstract

Capture and subsequent sequestration of CO_2 emitted from large point sources such as power plants or industrial facilities is considered as one of the key mitigation measures against climate change for the next decades to come. While the most critical part of CO_2 sequestration lies in public acceptance, the capture of CO_2 also induces a parasitic energy demand and thus affects the operating costs of the actual CO_2 emitting process. For this reason, a great effort has been put world-wide into the development of cost effective CO_2 capture technologies and the research group Zero Emission Technology (ZET) at the Vienna University of Technology is among the leaders in this field. Recently, a novel reactor design for post-combustion CO_2 capture based on temperature swing adsorption (TSA) has been developed by the ZET group together with an international oil and gas company. A bench scale unit (BSU) has been built basing on the developed reactor design in order to conduct experimental investigations, concerning the performance of the TSA process. This work presents results obtained from an extensive experimental campaign that has been conducted within the BSU using a PEI impregnated porous silica as adsorbent material. A variety of different operating conditions were tested to get an in-depth understanding of the correlations between operating conditions and performance of the unit. When a flue-gas with a CO_2 concentration of $7,7vol\%CO_2$ and a flow rate of $16,8Sm^3/h$ was fed to the cooled adsorber and $8Sm^3/h$ steam was used to regenerate sorbents at a circulating rate of around $30kg/h$, a capture efficiency of over 80% was achieved at various occasions. Furthermore, it was shown that interaction between steam, used for regeneration, and the sorbent material, entailed improved process performance through an internal heat displacement effect. Reduction of the stripping steam feeding rate had a comparatively small influence on the unit's performance; such, that a reduction of the steam flow rate for regeneration can be considered in future experiments. Increased feed rates of CO_2 to the adsorber, showed an improved capture rate (in $kg_{CO_2capt./day}$), however, at significantly lower CO_2 capture efficiencies. The fluidization velocity as well as the bed height of the fluidized bed stages had a strong impact on the CO_2 capture efficiency, most likely through affecting the actual heat transfer rate with the immersed stage heat exchangers. Finally, it was observed that introduction of small amounts of purge gas into the moving bed section after the desorber solids outlet, reduces the steam slip from the desorber to the adsorber significantly, which proved the feasibility of this

measure for proper gas sealing between the columns. The experimental campaign has been conducted successfully and the range of stable operation with sufficient CO_2 capture performance of the BSU has been identified. It was concluded that sufficient heat exchange with both gas-solids contactors may play the most important role in attaining high capture efficiencies, even at higher capture rates. Furthermore, it was shown that condensation of steam within the system needs to be avoided at any time in order to prevent adsorbent damage and coverage of heat exchanger surfaces with adsorbent material.

Contents

List of Symbols

Symbol	Unit	Meaning
a	m^2/s	Thermal diffusivity
Ar	-	Archimedes number
b	-	Langmuir parameter
b_0	-	Constant fit to experimental data
c	$Mole/m^3$	Concentration
c_p	$J/(kg \cdot K)$	Heat capacity
d	m	Diameter
D	m^2/s	Diffusion coefficient
dSl	kg/kg	Dynamic sorbent loading
f	Hz	Frequency
g	9,81 m/s^2	Gravitational acceleration
Δh	$J/Mole$	Heat of Reaction
k_n	$m^3/(Mole \cdot s)$	Reaction rate constant of reaction "n"
k_{SC}	$kg/(h \cdot Hz)$	Screw conveyor constant
L	m	Characteristic length
M_{CO_2}	44,01 $kg/kMole$	Molar mass of CO_2
$\dot{n}$	$Mole/s$	Mass transfer rate
Nu	-	Nusselt number
$\dot{q}$	W/m^2	Heat flux
p	Pa	Pressure
Pr	-	Prandtl number
q	-	Number of occupied sites
q_s	-	Fixed number of sites
R	8,31 $J/Mole \cdot K$	Universal gas constant
Re	-	Reynolds number
Sc	-	Schmidt number
Sh	-	Sherwood number
SCR	kg/h	Solid circulation rate
T	K	Temperature

Symbol	Unit	Meaning
U	m/s	Velocity
u^*	-	Dimensionless fluidization velocity
$\dot{V}$	Sm^3/h	Flow rate at standard temperature and pressure
V_M	22,41 $m^3/kMole$	Molar volume of an ideal gas at $0°C$
α	$W/(m^2 \cdot K)$	Heat transfer coefficient
β	m/s	Mass transfer coefficient
β_{CO_2}	$Mole/kg$	Sorbent loading with CO_2
δ	-	Ratio of desorption and evaporation
η	%	Efficiency
λ	$W/(m \cdot K)$	Thermal conductivity
μ	$Pa \cdot s$	Dynamic viscosity
θ	-	Fractional sorbent loading
ρ	kg/m^3	Density

List of Indices

Symbol	Meaning
Ads	refers to the adsorber step/column
$Adsorptive$	refers to adsorptive
$captured$	refers to captured CO_2
CO_2	refers to Carbon Dioxide
Des	refers to the desorber step/column
$Feed$	refers to the adsorber feed
g	refers to gas
in	refers to an in-flux
max	maximum possible
mf	at minimum fluidization conditions
out	refers to an out-flux
p	refers to particle
$sorbent$	refers to sorbent
$St\#$	refers to Stage number (top = 5; bottom = 1)

Chapter 1

Introduction

1.1 The Greenhouse effect

In the past years the greenhouse effect and its influence on the earth's climate have become
an omnipresent issue. Ever since the industrial revolution carbon dioxide (CO_2) emissions
have constantly been increasing, making them a major contributor to the greenhouse
effect. Treaties such as the Kyoto-protocol, where seven of the EU-15 member states
which committed to greenhouse gas (GHG) emission reductions, "were far from meeting
their targets" [Haita, 2012], exemplify the need for research dedicated to reducing GHG
emissions. Thus, substantial damage to the earth's climate could be prevented.

The greenhouse effect takes place when the earth effectively absorbs infrared radiation in
its troposphere and re-emits this radiation towards the earth's surface, resulting in heat
being trapped between the troposphere and the earth's surface [IPCC, 2012]. Increas-
ing concentrations of greenhouse gases in the atmosphere promote this effect, leading to
an increase of the earth's temperature and ultimately to a change in the global climate.
Greenhouse gases (GHGs) include water vapor, Carbon Dioxide (CO_2), Methane (CH_4),
Nitrous-oxide (N_2O) and many chlorofluorocarbons (CFCs). In order to quantify the im-
pact GHGs have on our climate, a parameter called Global Warming Potential (GWP)
was introduced in 1990 by Houghton et al. in the first assessment report by the Inter-
governmental Panel on Climate Change (IPCC). The GWP refers to the "time-integrated
Radiative Forcing (RF) due to a pulse emission of a given component, relative to a pulse
emission of an equal mass of CO_2" [IPCC, 2013], whereas RF is the "change in net (down
minus up) radiative flux (shortwave plus longwave; in W/m^2) due to an imposed change"
[IPCC, 2013]. In Table 1.1, several greenhouse gases including their GWP for two time
spans are listed.

	Lifetime (years)	GWP time horizon	
		20 years	100 years
Carbon Dioxide (CO_2)	n.A.	1	1
Methane (CH_4)	12,4	86	34
Hydrofluorocarbon ($HFC-134a$)	13,4	3.790	1.550
Chlorofluorocarbon ($CFC-11$)	45	7.020	5.350
Nitrous-oxide (N_2O)	121	268	298
Carbon-tetrafluoride (CF_4)	50.000	4.950	7.350

Table 1.1: Global Warming Potential including climate-carbon feedback of several gases [IPCC, 2013]

Of the GHGs listed above, nowadays CO_2 is regarded as the most relevant. As shown in Figure 1.1, the CO_2 concentration in the earth's atmosphere has varied greatly in the past 400 thousand years, yet only in the past 50 years (see Figure 1.2) has the CO_2 concentration increased to an unprecedented level and is predicted to rise 1,5 to 2 ppm each year [Canadella, 2007].
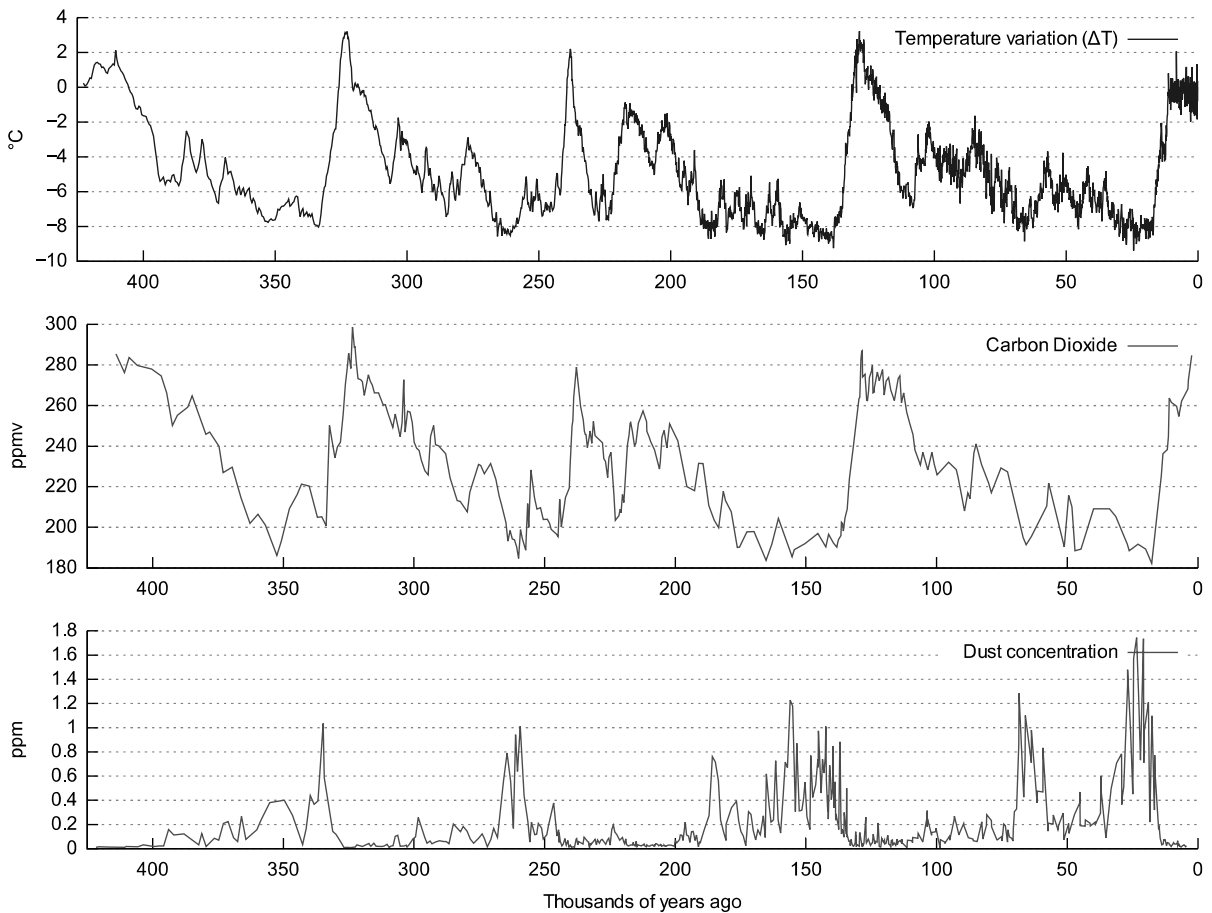

Figure 1.1: Climate and atmospheric history of the past 420,000 years from the Vostok ice core, Antarctica [Petit et al., 1999]
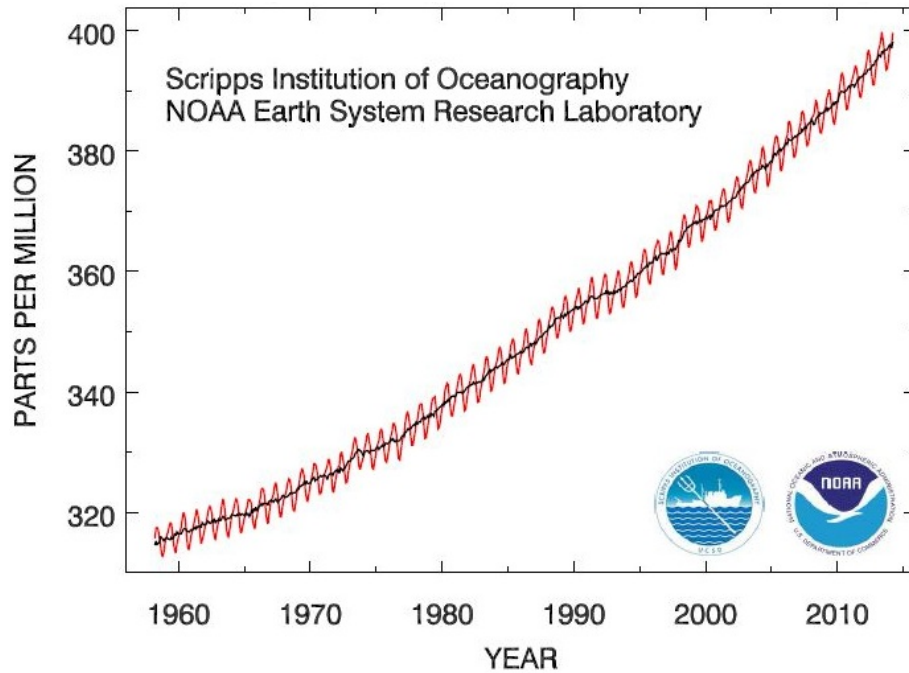
Figure 1.2: Atmospheric CO_2 concentration at Mauna Loa Observatory [ESRL, 2014]

In Figure 1.3, the global annual anthropogenic GHG-emissions in terms of CO_2 equivalent ($CO_2eq.$) of the years 1970 to 2004 (a), as well as global GHG emission data of the year 2004 (b) & (c) are shown.
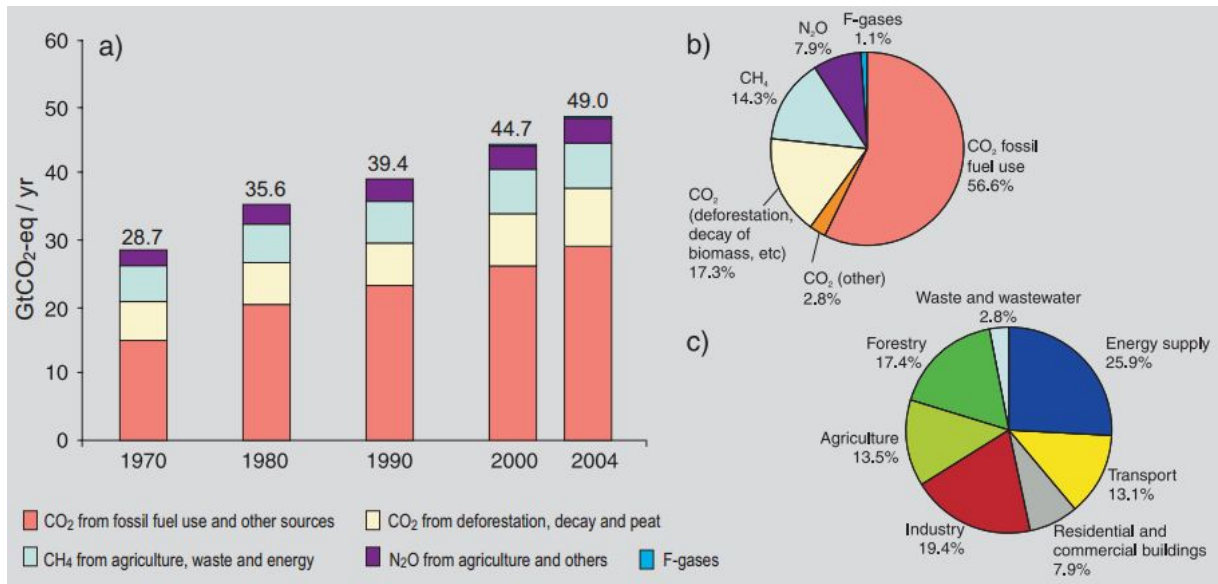
Figure 1.3: (a) Global annual emissions of anthropogenic GHGs from 1970 to 2004 (b) Share of different anthropogenic GHGs in total emissions in 2004 in terms of CO_2-eq. (c) Share of different sectors in total anthropogenic GHG emissions in 2004 in terms of CO_2-eq. (Forestry includes deforestation) [IPCC, 2007].

It can be seen that in the years 1970 - 2004, although all other GHGs have been multiplied by their respective GWP (see Table 1.1), CO_2 emissions from fossil fuels by far outweigh

the GHG emissions from any other source (Figure 1.3 (a)) and have risen to approximately 30 $GtCO_2eq./year$. The annual GHG emission rate, in terms of $GtCO_2eq./year$, has practically doubled from 0,43 $GtCO_2eq./year$, between the years 1970-1994 (24 years), to 0,92 $GtCO_2eq./year$ in only 10 years (1994-2004). Further, by comparing Figure 1.2 and Figure 1.3 (a), one can see an obvious coherence between CO_2 concentration in the atmosphere and anthropogenic CO_2 emissions between 1970 and 2004.

As to avoid climate change, the development of technologies to aid in the reduction of greenhouse emissions has become increasingly important; high potential for future change is seen in the sectors industry, with 19% of total GHG emissions in 2004, as well as energy supply, with 26% of total anthropogenic GHG emissions in 2004 [IPCC, 2007].

1.2 Carbon Capture and Sequestration

There are four measures that can be taken to reduce CO_2 emissions: increases in the efficiency of energy conversion as well as utilization, partial use of carbon neutral fuels such as biomass, utilization of renewable energy sources and carbon capture and sequestration (CCS) [IPCC, 2005]. CCS can contribute in reducing CO_2 emissions, since fossil fuels will be used in industry and power generation, until a system comparable in terms of flexibility with a "sizable contribution from renewables" [IPCC, 2005] is found. The International Energy Agency (IEA) [2013] investigated a scenario, which would limit a long-term increase of the global temperature to $2°C$ and further identified feasible technology options required for reducing GHG emissions.
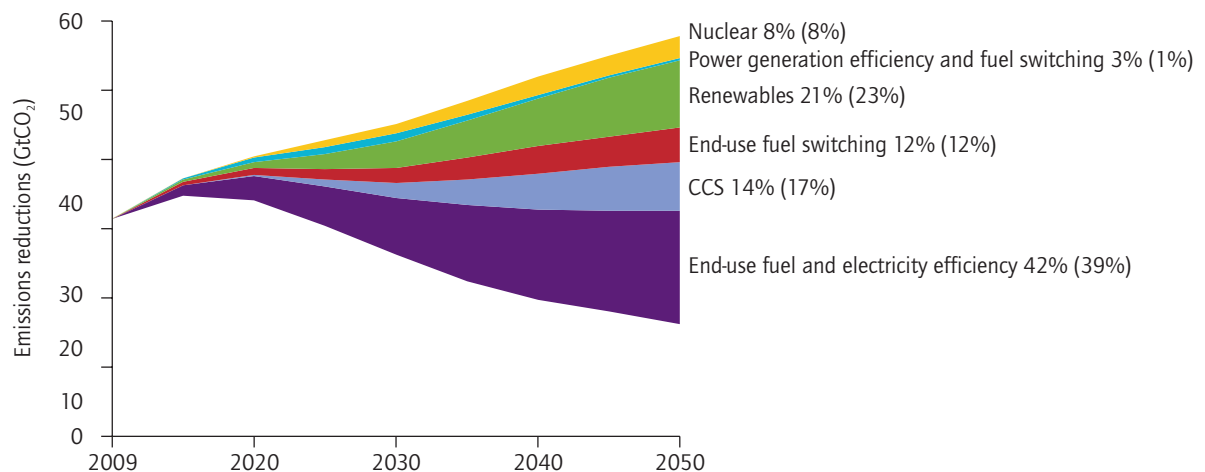
Figure 1.4: Contribution of technologies to reduce GHG emissions until 2050, for a scenario where the global temperature is allowed to increase by $2°C$ (or $6°C$ in brackets) in the long term [IEA, 2013]

As can be seen in Figure 1.4, carbon capture and sequestration will contribute at least 14% to CO_2 emission reductions, should the global temperature be allowed to increase

by $2°C$. In the scenario where the global temperature is allowed to increase by $6°C$, the contribution of CCS must increase to 17%.

In CCS, carbon emissions, in form of CO_2, are captured before, during or after combustion processes; "the CO_2 would then be compressed and transported for storage in geological formations, in the ocean, in mineral carbonates or for use in industrial processes" [IPCC, 2005]. Nevertheless, the greatest cost component of CCS is the cost of capture including compression (15 - 75 $US\$/tCO_2$ net captured from a coal- or gas-fired power plant), relative to 1 - 8 $US\$/tCO_2$ for transport and 0,1 - 30 $US\$/tCO_2$ for storage (excluding mineral carbonation). The anticipated reduction of the capture cost is between 20% and 30% using "new technologies that are still in the research or demonstration phase" [IPCC, 2005]. For this reason, compression, transport and storage will not be discussed herein. As seen in Figure 1.5, there are currently three types of carbon capture processes that can be integrated in the power generation process; namely oxyfuel combustion as well as pre- and post-combustion processes.
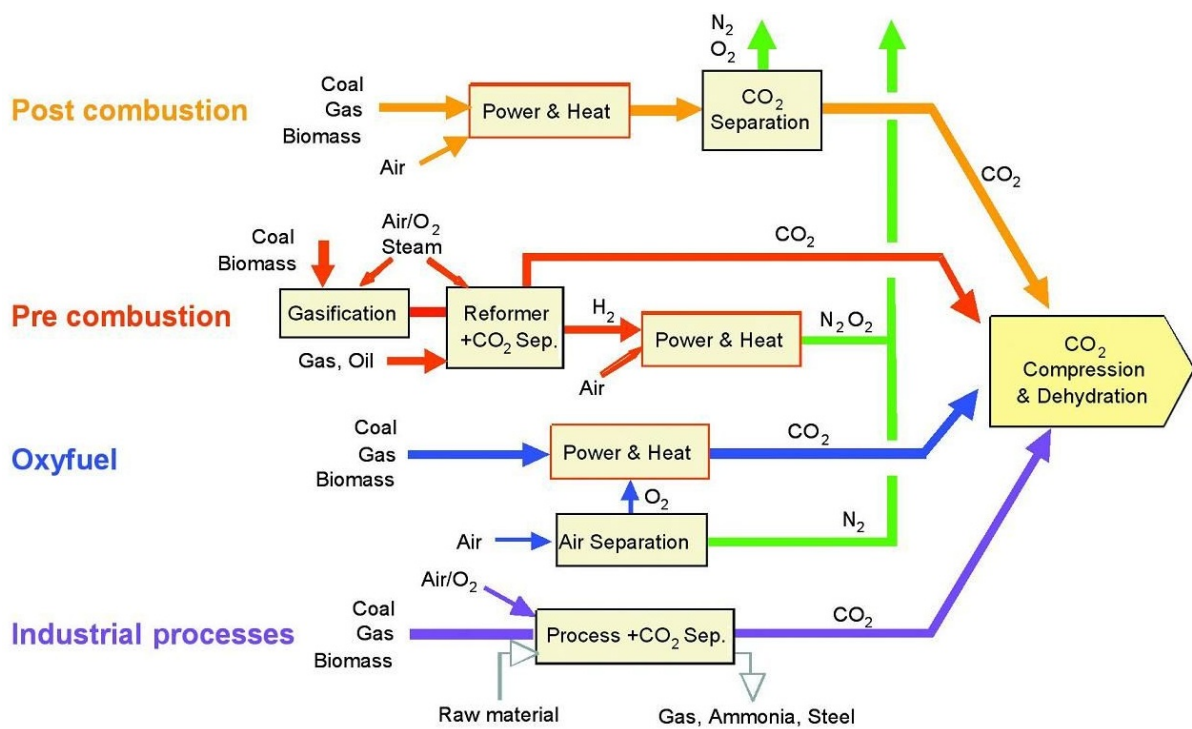

Figure 1.5: CO_2 Capture Systems [IPCC, 2005]
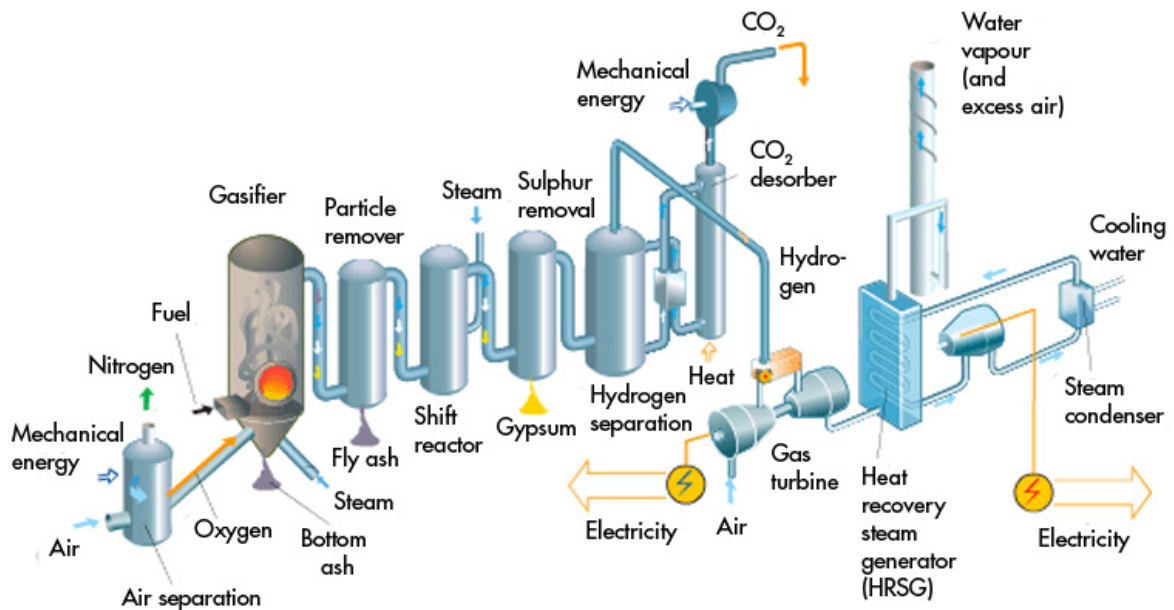
1.2.1 Pre-Combustion Processes

In the pre-cobustion process, a fuel is first gasified by a gasification agent to produce syngas gas, which is also refered to as product gas. As indicated in Figure 1.5 and Figure 1.6, either an air separation process, to separate nitrogen (N_2) from ambient air or a boiler is necessary for the production of the gasification agent (oxygen or steam).

During the gasification process syngas (typically a mixture of carbonmonoxide (CO) and steam) is produced. Before the product gas enters a shift reactor, dust is removed in the particle removal system. Inside the shift reactor a moderately exothermal water-gas shift reaction (see Equation 1.1) takes place, where CO_2 and hydrogen (H_2) are produced [Ratnasamy and Wagner, 2009].

$$CO + H_2O \longleftrightarrow CO_2 + H_2 \tag{1.1}$$

After the sulphur removal unit an absorber unit removes CO_2 from the product gas, by means of absorption. The obtained H_2-rich gas is then combusted in a gas turbine, thus generating electricity in the generator further down the shaft. The efficiency of this cycle is increased by means of a heat recovery steam generator, which generates superheated steam using heat from the gas turbine's off-gas. This steam is then expanded in a steam turbine; a generator connected to the turbine generates electricity.
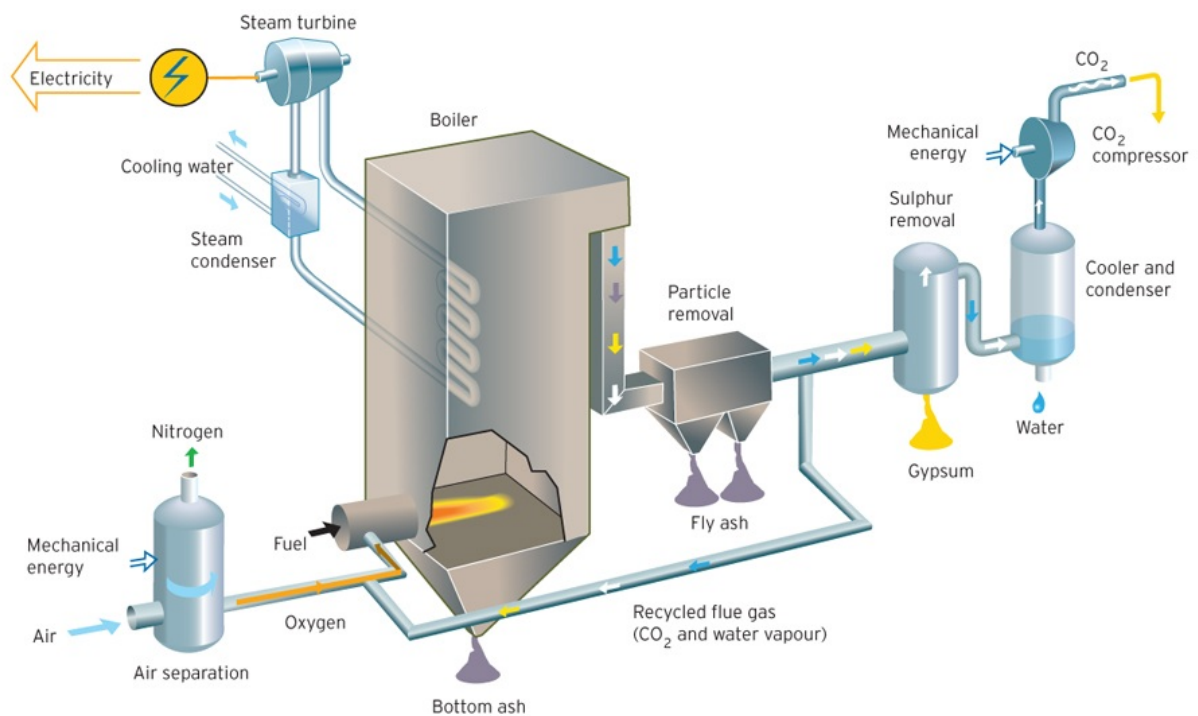

Figure 1.6: Schematic illustration of a pre-Combustion CCS process [Vattenfall, 2014]

In this process the components with particularly high energy demand, thereby substantially influencing the cost for CO_2 capture, are, either the air separation unit, which usually operates under high pressure, or the boiler, if steam is used as a gasification agent. Further, the production of stripping-steam for the desorber unit, is also associated with a high energy demand.
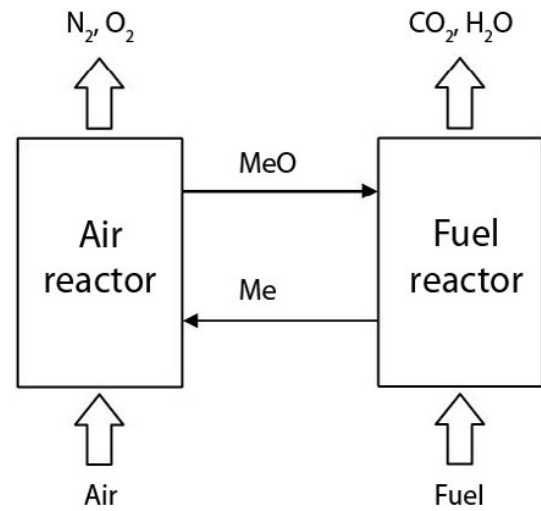
1.2.2 Oxyfuel and Chemical Looping Combustion

During Oxyfuel combustion, combustibles are incinerated using oxygen (O_2) rather than air. This process has the advantage of producing highly concentrated CO_2 during a combustion process. Since higher adiabatic incineration temperatures are reached during Oxyfuel combustion compared to combustion using air, the combustion reaction is often cooled by means of recycled flue gas or steam; in this way increasing the CO_2 concentration or vapor concentration, at the cost of the O_2 concentration in the resulting flue gas. Generally, a stoichiometric reaction of the fuel and O_2 is pursued, resulting in a flue gas with two main components namely, CO_2 and steam, with traces of SO_x or NO_x, depending on the combusted fuel. In a further step, the flue gas is cooled, in order to separate the steam from the flue-gas stream. A schematic illustration of an Oxyfuel process can be seen in Figure 1.7:

Figure 1.7: Schematic illustration of an oxyfuel process [Vattenfall, 2014]

The air separation unit, used for the production of oxygen, represents the highest energy demand in the Oxyfuel process.

Similarly to Oxyfuel combustion, in Chemical Looping Combustion (CLC) a fuel is combusted in an atmosphere ideally devoid of N_2. This process is realized using two interconnected circulating fluidized beds between which a metal (Me) is circulated. The metal is oxidized to form a metal-oxide (MeO) in the Air Reactor (AR), where air is used to fluidize the bed. The bed material is then transported to the Fuel Reactor (FR), which is fluidized with a fuel (e.g. natural gas). Here, the fuel is oxidized using the O_2 bound to the MeO. Thus, the MeO is reduced to a metal, which is then returned to the AR, where it is re-oxidized. The principle of CLC is illustrated in Figure 1.8. The off-gases produced by this

Figure 1.8: Schematic illustration of the principle used in CLC [Kolbitsch et al., 2009]

process are ideally, air low on oxygen at the AR gas-outlet and a mixture of CO_2 and water vapor at the FR outlet [Kolbitsch et al., 2009]. The combustion of solid fuels using CLC is still in development. Further, costly bed material and the complex design of CLC units, make combine-cycle units with integrated post-combustion CO_2 capture more efficient for power generation from gaseous fuels.

1.2.3 Post-combustion Processes

In the post combustion process, CO_2 is separated from the flue-gas after the combustion process. The flue-gas resulting from the combustion of fossil fuels mainly consists of N_2, CO_2, H_2O, O_2, and may include traces of SO_x, NO_x, and ash. Typical flue-gas compositions, resulting from coal combustion and natural gas combustion in power plants, can be seen in Table 1.2:

Gas constituent	Coal (vol%)	Natural gs (vol%)
N_2	70-75	73-76
CO_2	10-15	4-5
H_2O	8-15	8-10
O_2	3-4	12-15
Trace Gases (SO_x, NO_x, etc.)	<1	<1

Table 1.2: Typical compositions of flue-gases from coal- and natural gas-fired power plants (natural gas combustion by means of a gas turbine) [GCCSI, 2012a]

Before CO_2 is captured, the flue-gas is usually cleaned by means of a particle remover, which will remove all fly ash, and a sulfur removal unit, for the removal of sulfurous compounds (see Figure 1.9). An advantage of post-combustion CCS processes is the possibility of implementing CCS in any existing CO_2 emitter. The methods used for CO_2 separation include absorption as well as adsorption and membrane separation processes.

1.2.3.1 Absorption Processes

In absorption processes, a flue-gas is typically brought into contact with a solvent (or absorbent) in a gas-liquid contactor (or absorber). Here, either chemical absorbents, which form chemical bonds or react with acid gases (in this case CO_2) or physical absorbents into which acid gases dissolve, are used [GCCSI, 2012b]. Most-commonly chemicals such as aqueous single amine solutions, blends of amines or aqueous ammonium carbonate are used to chemically bind CO_2. To minimize degradation, thus reducing solvent make-up, a concentration of 10ppmv of sulphur dioxide (SO_2) or sulphur trioxide (SO_3) must not be exceeded, since other acid-gases disrupt the CO_2 capture process [GCCSI, 2012a]. The loaded solvent is then brought to the regenerator (or stripper) unit, where it is regenerated using steam. This process lowers the partial pressure of CO_2 in the gas phase and increases the solvent temperature; both of these changes promote a discharge of CO_2 from the solvent. Yet, exceeding a solvent-specific maximum operating temperature can lead to the evaporation and loss, or degradation of the solvent. The off-gas of the stripper unit (desorbate) is ideally a mixture of CO_2 and water vapor. Subsequently the lean solvent is returned to the absorber unit.
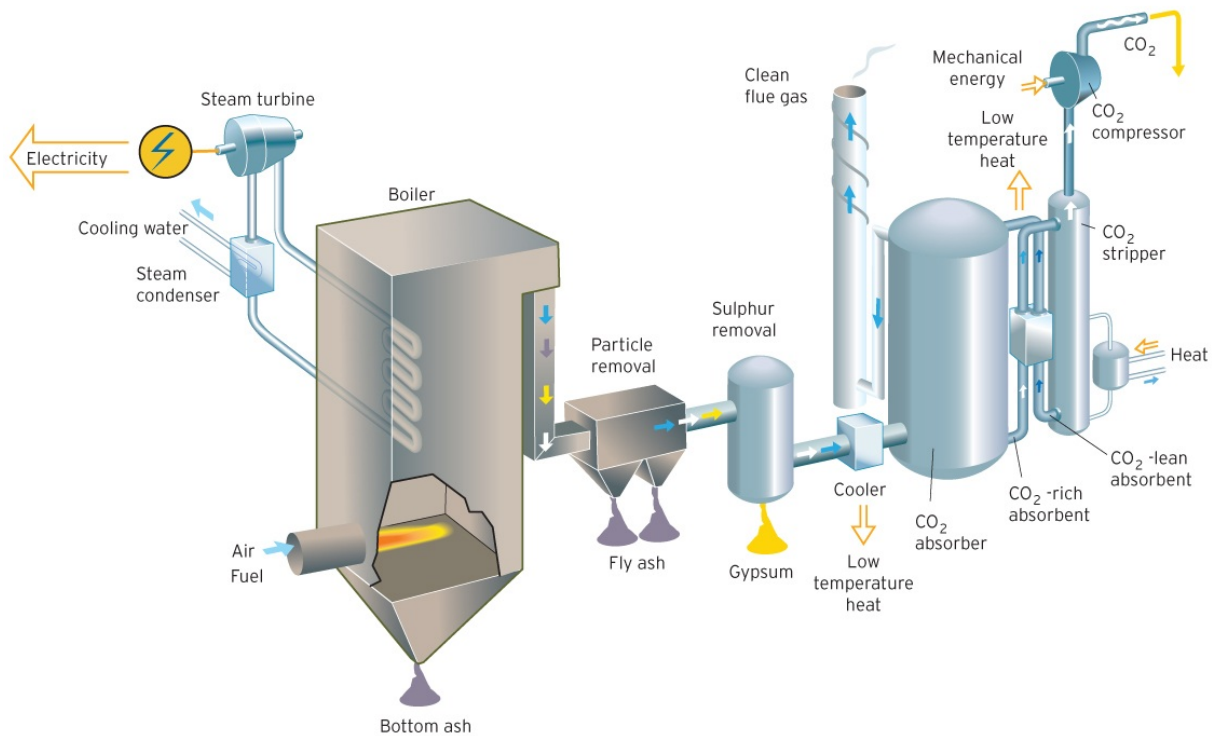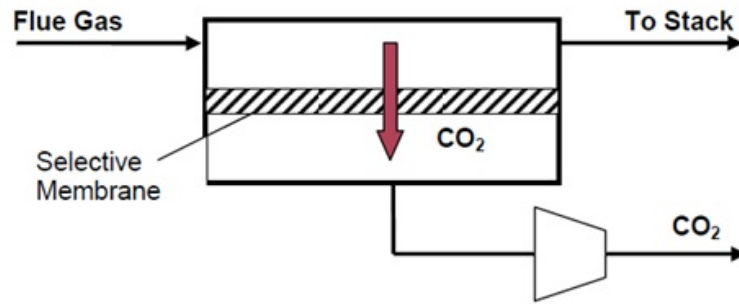
Figure 1.9: Schematic illustration of a post-combustion CCS process [Vattenfall, 2014]

Since heating the regenerator unit is linked to a high energy demand, the regeneration step of the absorption process greatly influences the cost of operation.

1.2.3.2 Membrane Processes

For processes where membranes are used to separate CO_2 from a flue gas, the membrane's selectivity is an important factor. CO_2 must first dissolve into the membrane material before it can permeate through it. A partial pressure gradient is the driving force for the permeation of CO_2; this difference is induced by means of a high pressure on the feed side and/or a vacuum on the permeate side. To increase the selectivity of the membrane material, chemicals which react with CO_2 can be used to further increase the product purity [GCCSI, 2012a]. An example for the configuration of a membrane separation process is given in Figure 1.10.

Figure 1.10: Schematic illustration of a membrane separation process [GCCSI, 2012a]

In membrane processes, the operating costs are governed by the energy demand of the compressor used to induce a pressure difference across the membrane [GCCSI, 2012a].

1.2.3.3 Adsorption Processes

In the adsorptive capture of CO_2, a solid sorbent is brought into contact with a flue-gas. CO_2 is captured either by chemisorption, where the flue-gas chemically reacts with the solid's surface, or by means of weak e.g. van-der-Waals forces; this mechanism is then called Physisorption [GCCSI, 2012a]. For the realization of the gas-solid contact, two different methods are typically used. In the first method a packed bed is operated in batch-mode; the CO_2-rich flue-gas moves through a column filled with sorbent material; CO_2 is then captured on the sorbent's surface. As soon as the capacity of the sorbent is near depletion, the regeneration procedure is initi-

Figure 1.11: Steps of procedure when using a packed bed [GCCSI, 2012a]

ated, so the sorbent can be used again. Similarly to the absorption process, regeneration can be done by means of a temperature or pressure swing. A schematic illustration of the steps of this procedure can be seen in Figure 1.11.

For selectivity reasons chemical sorbents are commonly used in adsorption processes. These adsorbents are however connected to high enthalpies of adsorption which must be supplied or extracted when CO_2 is desorbed or adsorbed respectively. To avoid problems caused by insufficient heat and mass transfer in the reactors, such as local "hot" and "cold" spots during exothermic adsorption or endothermic regeneration, it is recommended to use flu-
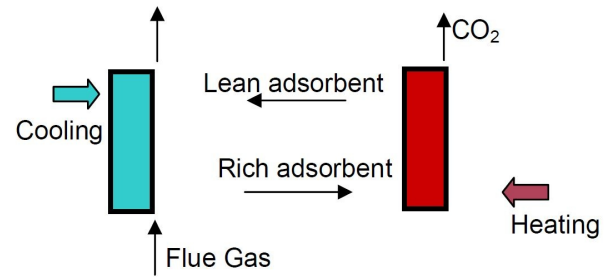
Figure 1.12: Steps of procedure when using a fluidized bed [GCCSI, 2012a]

idized beds for adsorption processes [Yang and Hoffman, 2009]. Here, intense contact between the gaseous and the solid phase is realized by fluidizing the sorbent with either the flue gas (in the adsorber) or a regeneration agent (in the regenerator). As shown in Figure 1.12, the sorbent material circulates between the adsorber column and the regenerator (or desorber) column. To enhance the exothermal adsorption step, the adsorber unit is cooled, thus increasing the sorbents capacity [Yu et al., 2012]. On the contrary, the regenerator is heated, and optionally the CO_2 partial pressure is decreased using a stripping agent to induce the release of CO_2. Analogously to the absorption process, the cost for CO_2 capture is strongly influenced by the energy demand during regeneration.

1.3 Motivation

Currently the absorption process, using aqueous monoethylamine (MEA) is considered the state-of-the-art for post-combustion CO_2 capture [Wang et al., 2011]. Though this process is well-known, a major drawback of this technology is the high energy consumption involved when regenerating the solvent (e.g. 3,1 GJ/tCO_2 [Dinca and Badea, 2012] - 3,7 GJ/tCO_2 [Knudsen et al., 2009]). The National Energy Technology Laboratory [2007] published an evaluation of technical and economic feasibility of a pulverized coal-fired power plant retrofitted with an amine scrubber for post combustion CO_2 capture. It was shown that the integration of CCS by means of chemical absorption would lead to an energy penalty of about 10,5% in terms of net plant efficiency and a CO_2 capture cost of US\$59$ per ton of CO_2 captured, at a capture efficiency of 90% [NETL, 2007].

In recent years chemical adsorption has increasingly been suggested for post-combustion CO_2 capture [Gray et al., 2005, Gray et al., 2008, Yang and Hoffman, 2009]. This technology has the potential of overcoming the shortcomings of the absorption process in respect to energy demand due to "higher CO_2 loading, lower material heat capacity and/or lower heat of reaction" [Sjostrom and Krutka, 2010]. Many amine functional-

ized solid sorbents have been evaluated for their suitability for CO_2 adsorption, such as activated carbon [Houshmand et al., 2012], zeolites [Su et al., 2010], polymers like Polymetylmethacrylate (PMMA) [Gray et al., 2008] and silica material [Gray et al., 2005]. However, for deployment of solid sorbent CO_2 capture technology, the development of suitable reactor systems is also key.

In this work, polyethyleneimine (PEI) impregnated porous silica was used as a sorbent. To realize optimal gas-solid contact during adsorption and regeneration, a double loop multi-stage fluidized bed system was used. Unlike fixed bed reactors, mixing conditions make fluidized beds reactors exhibit excellent heat and mass transfer properties; thus making these systems ideal for adsorption and regeneration [Yang and Hoffman, 2009].

1.4 Aim & Scope

Extensive testing on a multistage fluidized bed bench scale unit (BSU), designed for continuous adsorptive post-combustion capture of CO_2, was carried out. To better understand and further optimize the process, a variety of different operating conditions were tested. In this work, the experimental campaign, which was carried out in the first half of 2014, is analyzed. The experiments include variations of flue-gas composition and fluidization rate variations as well as a variation of regeneration agent composition and weir-height variations in both columns.

1.5 Organization of this Thesis

In Chapter 2, the fundamentals of adsorption and fluidized bed system are discussed; whereas Chapter 2.3 addresses how these principles were considered in the design of a unit capable of continuously separating CO_2 from a flue-gas. The setup used for data acquisition during the experimental campaign, as well as details concerning the BSU's design and operation will be introduced within Chapter 3. Results obtained during the experimental campaign are shown in Chapter 4, and interpreted in Chapter 5, while Chapter 6 will be dedicated to the conclusions thereof.

Chapter 2

Literature Research

2.1 Fundamentals of Adsorption

In the late 18th century, C.W. Scheele and F. Montana, discovered adsorption independently from another; Scheele, for example, found that by applying heating on charcoal, adsorbed gases were desorbed, and re-adsorbed when the charcoal was cooled [Masel, 1996]. Only in 1881, was the term "adsorption" introduced by Kayser [Kayser, 1881]; he distinguished "between adsorption, where a gas binds directly to the surface of a solid, and absorption where gas dissolves directly into the bulk of a fluid" [Masel, 1996]. This statement rests upon the observation, that in absorption, the amount which can be absorbed depends on the volume or mass of solvent, whereas adsorption is independent from the mass of sorbent (or adsorbent), but rather depends on its surface area [Masel, 1996]. In more recent literature [Masel, 1996, LeVan et al., 1997, Rouquerol et al., 1999, Dabrowski, 2001], adsorption is generally described as a phenomenon, where "molecules accumulate in an interfacial layer" [Masel, 1996]; whereas these interfaces include gas-liquid, liquid-liquid and solid-gas interfaces [LeVan et al., 1997]. The opposite effect, where molecules deplete at an interface is called desorption. The following will only treat gas-solid adsorption; more on other adsorption systems can be found elsewhere [Ruthven, 1984, LeVan et al., 1997]. As mentioned in Chapter 1.2.3, the bond which is formed between the species which is adsorbed (adsorptive) and the sorbent's surface, can either be physical in nature, this form of adsorption is also called physical adsorption or physisorption, or is formed by means of chemical bonds, which is then called chemical adsorption or chemisorption [Dabrowski, 2001]. The basic properties of chemisorption and physisorption can be seen in Table 2.1:

Property		Physisorption	Chemisorption
Selectivity of sorptive gases		low	high
Intensity of adsorption increased	Pressure (p)	$p \to \infty$	-
for sorptive gas	Temperature (T)	$T \to 0$	T
Kinetics		rapid	slow
Ratio (δ) of enthalpy of desorption and evaporation		$2 \leq \delta \leq 3$	$\delta > 5$
Structure of sorbate		Monolayer Multilayer Pore fluid	Monolayer

Table 2.1: Basic properties of physisorption and chemisorption systems and phenomena at the example of ammonia or water sorption on hydrophilic zeolites (adapted from [Keller and Saudt, 2005])

As the basis of chemisorption are chemical reactions, the selectivity towards specific species is higher than in physisorption, where van-der-Waals forces or dipole-dipole interaction define which species are adsorbed. The ability to adsorb an adsorptive gas can be increased, by an increase in pressure or decrease of temperature in physisorption, whereas in the example illustrated in Table 2.1, this attribute depends on a reaction-specific temperature for chemisorption. A change of the chemical structure of the adsorbent's surface is responsible for slow kinetics in chemisorption, while this change doesn't occur in physisorption. An indicator for the strength of the bond, between adsorptive and the sorbent's surface, is the "ratio (δ) of desorption and evaporation". For the example given in Table 2.1 the enthalpy of desorption ($\Delta h_{Desorption}$) in chemisorption can be in the range of -70 to -200 kJ/mole, hence considerably larger than values for $\Delta h_{Desorption}$ in physisorption (typically -10 to -50 kJ/mole) [Keller and Saudt, 2005]). The structure of the molecules chemisorbed on an adsorbents surface (adsorbate) is usually a single molecular layer (or monolayer), while in physisorption other structures such as multilayers or pore fluids can be formed [Keller and Saudt, 2005]; this information is essential for modeling of adsorption processes.

The equilibrium conditions of adsorptive systems are described by so-called "adsorption isotherms". These isotherms show the relation between the number of occupied adsorption sites (q) and the concentration (c) or partial pressure (p) of adsorptive in the fluid phase at constant temperature (T) after a sufficiently long time [Suzuki, 1990]. A model commonly used to describe the chemisorption process is the Langmuir equation [Langmuir, 1918]:
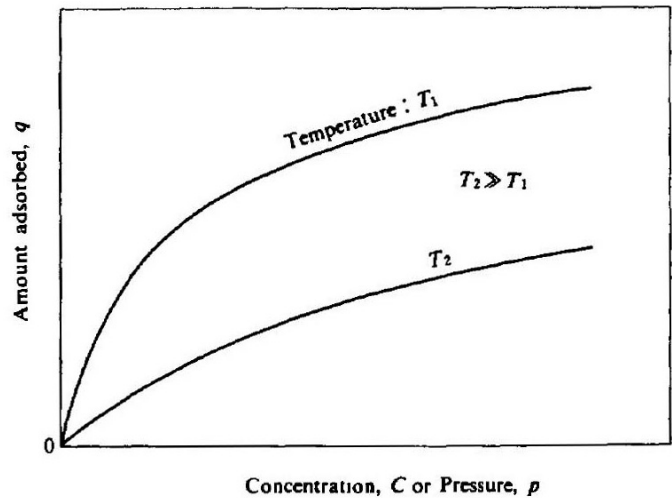
$$\frac{q}{q_s} = \frac{b_{Adsorptive}(T) \cdot p_{Adsorptive}}{1 + b_{Adsorptive}(T) \cdot p_{Adsorptive}} \tag{2.1}$$

with the van't Hoff equation:

$$b_{Adsorptive}(T) = b_0 \cdot e^{\frac{-\Delta h}{R \cdot T}} \tag{2.2}$$

The assumptions this model makes are, that there is a definite number of adsorption sites, which are all energetically equivalent, which means their enthalpy of adsorption are the same, and that each site is able to adsorb one molecule of an ideal gas, as long as the bond is "sufficiently strong to prevent displacement of adsorbed molecules" [Dabrowski, 2001]. Further, this model assumes the formation of a mono-layer of adsorbate on the sorbents surface, which makes this model better applicable for the description of chemisorption, whereas physisorption is comparable to the

Figure 2.1: General appearance of Langmuir adsorption isotherms [Suzuki, 1990]

condensation process of an adsorptive [Dabrowski, 2001]. An example of the general appearance of Langmuir adsorption isotherms can be seen in Figure 2.1; the amount of gas that can be adsorbed (or the number of occupied sites q) on a solids surface increases with decreasing temperature, similar behavior can be seen for increasing partial pressure or concentration of adsorptive in the fluid phase.

2.1.1 Adsorption in gas separation processes

"Industrial adsorption processes normally are cyclic processes in which adsorption and desorption of sorbent material alternate periodically" [Keller and Saudt, 2005]. However, the desorption step is often involved with a higher energy demand relative to adsorption, since energy needed for cooling can be neglected in most cased; thus the thermodynamic efficiency of the cycle is determined by the desorption [Keller and Saudt, 2005]. Ruthven [1984] mentions four methods, listed below, which are commonly used for regenerating sorbent material, whereas two or more of these methods can be combined with each other:

Thermal swing The loaded sorbent is heated, often by steam, to a temperature at which desorption of the adsorbed species is favorable (i.e. regeneration temperature is larger than the adsorption temperature). Due to the changing operating temperature, this process is commonly referred to as temperature swing adsorption.

Pressure swing This form of regeneration is limited to gaseous systems, since the pressure is systematically decreased, at constant temperature; at the decreased pressure the bed is purged.

Purge gas stripping This regeneration method is only efficiently applicable at low bonding energies between adsorptive and adsorbent. Temperature and pressure is held constant, while an inert gas is used as purge gas to reduce the adsorbate concentration in the surrounding atmosphere of the adsorbent.
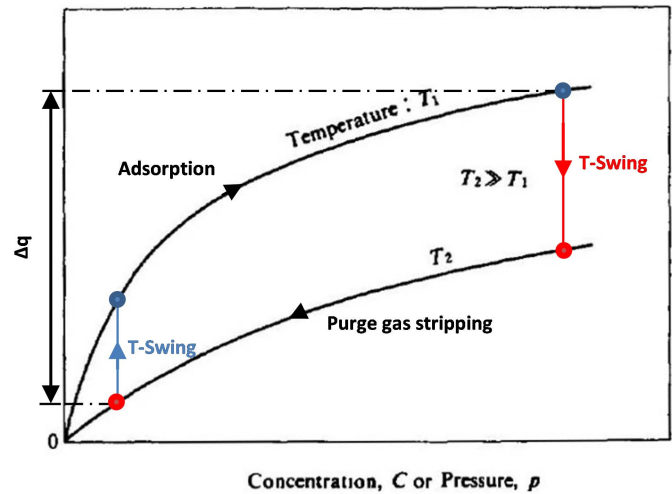
Displacement desorption The only difference between purge gas stripping and displacement desorption is, that instead of using an inert gas for purging, a competitively adsorbed species is used.

Of the regeneration methods mentioned, thermal swing regeneration is probably the method used most commonly in industrial adsorption processes [Ruthven, 1984]. As the adsorption step is exothermic (governed by Equation 2.2), and therefore associated with the release of adsorption enthalpy, a slight increase in temperature at the equilibrium state concentration, can have a large effect on the number of sites which become vacant; indicated by Δq in Figure 2.2. However, observations such as a high energy demand for heating [Ruthven, 1984], a reduction of sorbent life-time after repeated thermal cycling [de Rosset et al., 1981] and slow cycling in batch-mode operation, due to time delays, which arising during heating and cooling the bed and the vessel, can make TSA processes unfavorable. In pressure swing adsorption (PSA), on the other hand, fast cycling in batch-mode operation is possible, at the cost of lower adsorption efficiencies, since part of the product gas is usually used as purge gas. However, electrical energy, which is commonly more expensive than heat, is necessary to realize PSA. A popular combination of methods used to regenerate loaded adsorbent is the combination of TSA and purge gas stripping [Ruthven, 1984]. In such processes the loaded sorbent is heated, while being purged with an inert gas, in this way promoting desorption by two means; decreasing the ambient adsorptive concentration, and by supplying heat (see Figure 2.3).
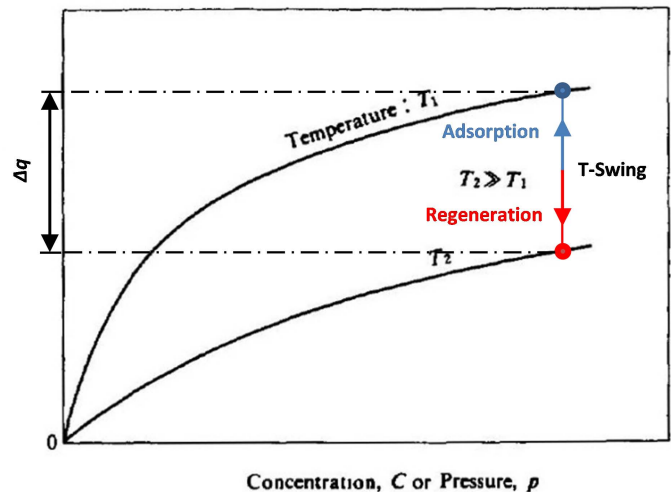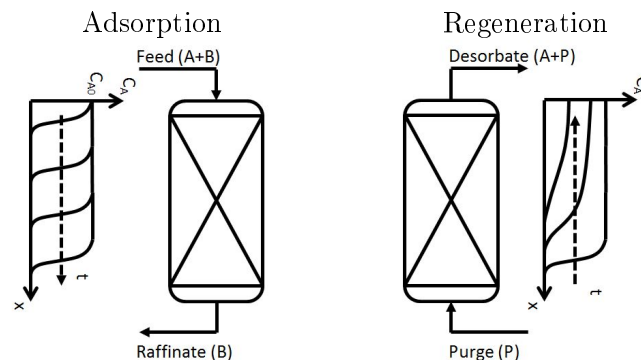

**Figure 2.2:** Example for temperature swing adsorption (adapted from [Suzuki, 1990])

Adsorption processes are either operated in batch-mode or continuously. An example for a cyclic batch-mode adsorption system can be seen in Figure 2.4. A concentration front of adsorptive travels through the reactor, as the sorbent gets more and more saturated with adsorptive; during this procedure the raffinate is more or less pure in the adsorber outlet. As to not reach saturation of the entire sorbent bed and therewith contaminate the raffinate with the adsorptive, "the adsorption cycle is generally terminated prior to breakthrough" [Ruthven, 1984]. Similarly to the ad-

Figure 2.3: Example for a combination of temperature swing adsorption and purge gas stripping (adapted from [Suzuki, 1990])

sorption cycle, the desorption cycle is not carried out to completion, as this would result in an immoderate demand of regeneration agent and/or heat. In forward flow systems, where feed gas and purge gas flow in the same direction, this generally leads to an accumulation of adsorbate in the outlet and to a contamination of the raffinate during the next adsorption cycle. In reverse-flow systems, this draw-back is eliminated and particularly pure raffinates can be obtained, as the residual adsorbate accumulates at the adsorber inlet (or desorber outlet). In continuous systems so called "counter-current flow" is pursued. This operating mode (see Figure 2.5) enables the maximization of the driving force for mass transfer; by doing so, "more efficient utilization of the adsorbent capacity than is possible in a simple batch-contacting system" [Ruthven, 1984] can be achieved. These highly effective systems are capable of reducing the required inventory of adsorbent compared to batch-mode adsorption. More detail on counter-current adsorption systems can be found elsewhere [Ruthven, 1984].

Figure 2.4: Cyclic batch two-bed system (adapted from [Ruthven, 1984])
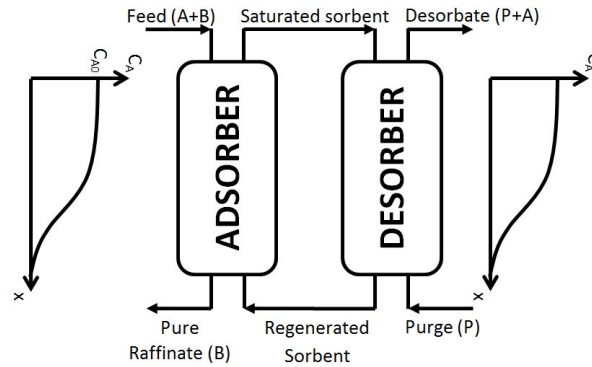
Figure 2.5: A steady-state continuous countercurrent system with adsorbent recirculation (adapted from [Ruthven, 1984])

2.2 Fundamentals of fluidized bed systems

In 1926, the German chemist, Fritz Winkler first implemented a fluidized bed system on an industrial scale for coal gasification purposes [Grace, 2006]. Sixteen years later, in 1942, the first industrial scaled circulating fluidized bed reactor was first put into operation by the Standard Oil Company of New Jersey, in order to crack heavy gas oils [ACS, 2014]. Today, fluidized beds are applied in numerous processes that take advantage of the unique properties of these systems. Physical processes such as mixing, heating and cooling, drying, adsorption, agglomeration or coating processes are being realized with fluidized beds. Furthermore, fluidized beds are used in chemical processes in which the bed material acts as a heat carrier (combustion, gasification etc.), a catalyst (e.g. catalytic cracking, Fischer-Tropsch synthesis) or a reactant (ore processing, calcination etc.) [Hofbauer, 2012]. "Fluidized-bed reactors include gas-solid, liquid-solid and gas-liquid-solid fluidized bed reactors in terms of the fluid-particulate systems." [Grace, 2006]. As seen in Figure 2.6, a reactor is filled with a bed of particles to a certain height. In a fixed bed regime the flow rate of fluid, or rather the fluidization rate (U, see Equation 2.3), is kept below the minimum fluidization velocity (U_{mf}), thus leaving the bed height unchanged.

$$U = \frac{\dot{V}_{Fluidization\ agent}}{A_{Reactor\ cross-section}} \tag{2.3}$$

The minimum fluidization velocity is reached when "the buoyed weight of the particles is completely supported by the drag forces imposed by the fluid" [Grace, 2006]; the bed expands and particles start moving [Hofbauer, 2012]. The term fluidization refers to the fluid-like properties of the fluidized bed. Figure 2.7 shows that the pressure drop across the bed flattens out when the minimum fluidization velocity is exceeded. Bubbles, which are formed by the gas on its way through the bed, are responsible for the mixing conditions

in a fluidized bed system. Mixing significantly contributes to the unique properties of flu-
idized bed systems; not only does it influence gas-solid contact as well as the temperature
distribution within the fluidized bed reactor, it also increases the heat transfer coefficient
between the bed and heat exchangers [Hofbauer, 2012]. When increasing the fluidization
rate beyond aggregative fluidization conditions, particles are entrained from the reactor;
these high fluidization rates are used in circulating fluidized beds, where entrained solids
are separated from the fluidization agent and returned to the reactor. There can also be
other phenomena, which can have a negative impact on mixing conditions in the bed,
such as channeling, where "the gas finds fissures or other fixed passages through station-
ary particles" [Grace, 2006] or slug flow, where the shape and ascent rate of bubbles is
significantly affected by reactor walls
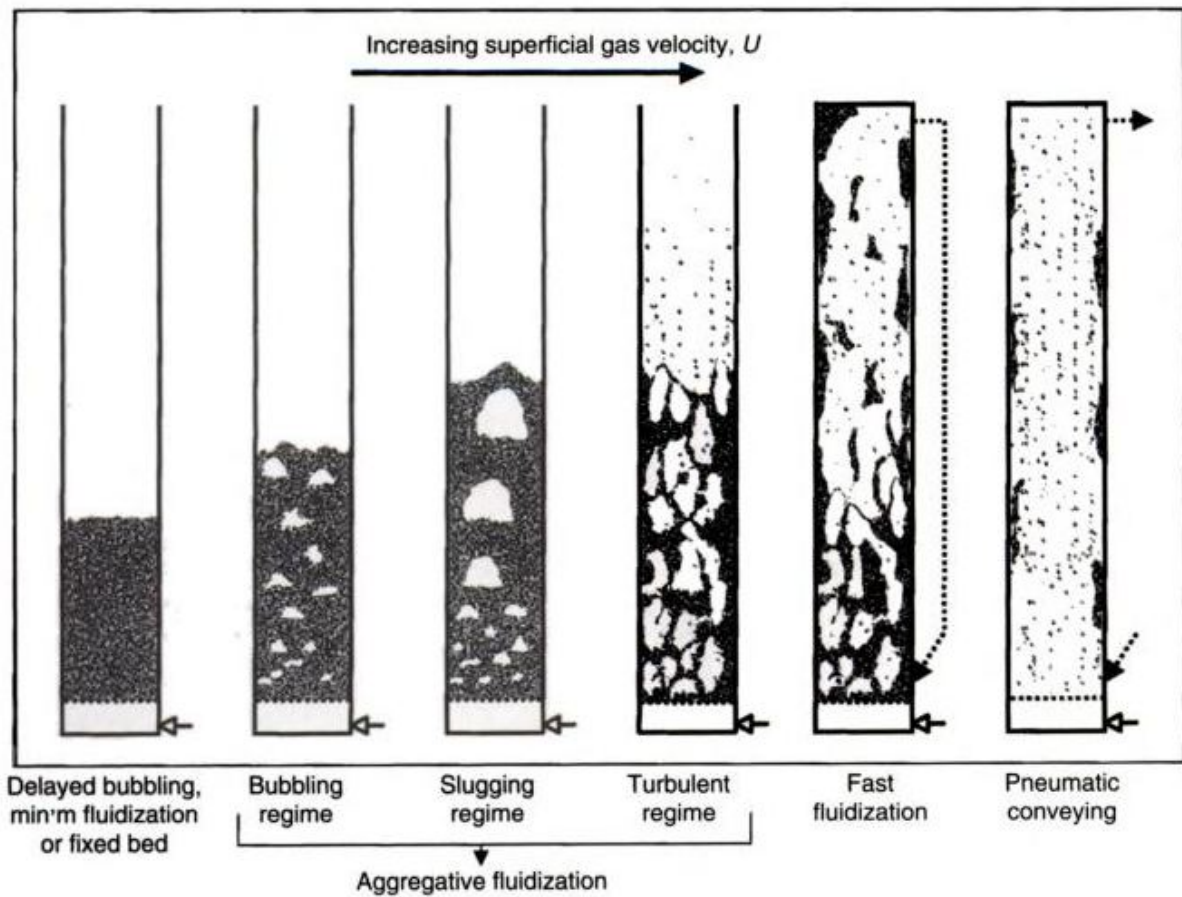
Figure 2.6: Schematic representation showing the appearance of flow regimes relevant to gas-solid flu-
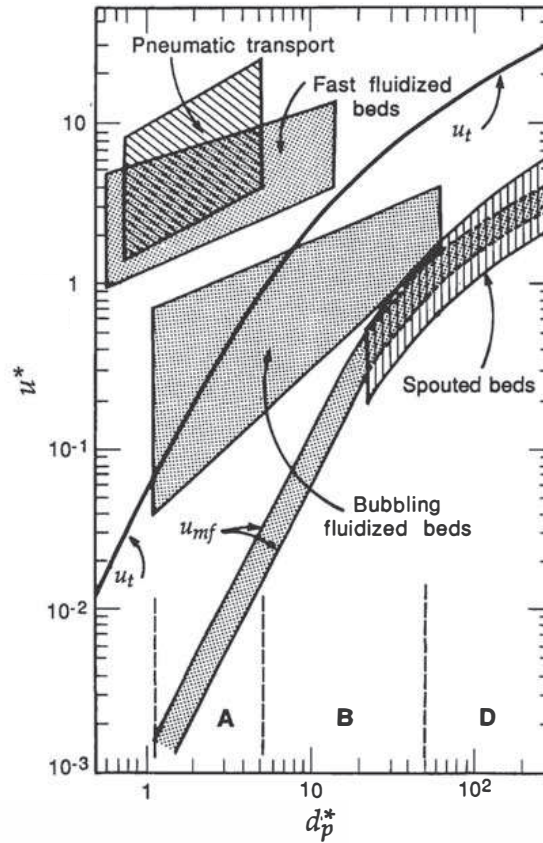idization [Grace, 2006]
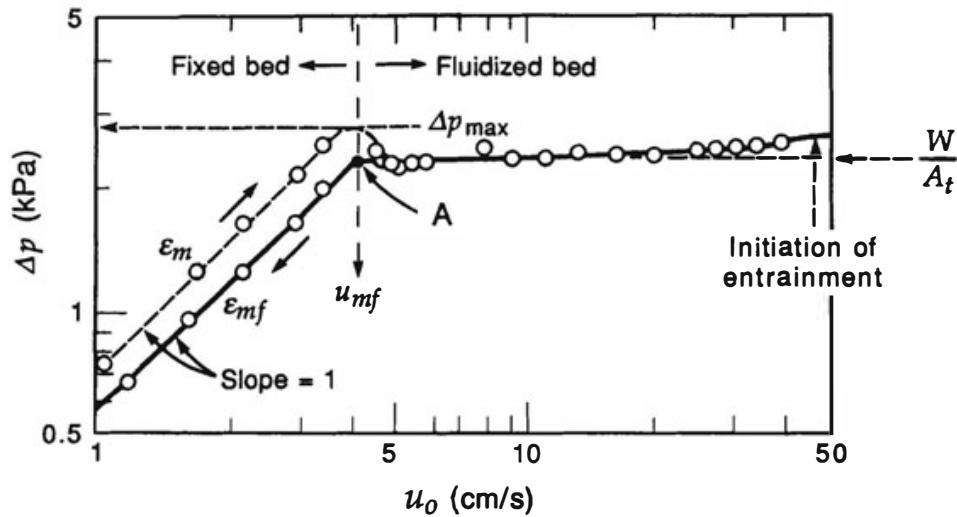
Figure 2.7: Graph showing the pressure drop across a bed of solid particles as a function of gas velocity [Kunii and Levenspiel, 1991]

Geldart [Geldart, 1973] identified particle properties that are decisive for fluidization. The results shown in Figure 2.8, where a bed of particles is fluidized by air at room temperature and atmospheric pressure, show that there are four powder groups that are relevant for fluidization. C group powders are cohesive; their inter-particle forces are dominant relative to weight-buoyancy, making these powders inapplicable in fluidized beds. Group A powders fluidize excellently, deaeration occurs slowly after the gas flow is turned off and solid mixing takes place rapidly; here inter-particle forces are poor, yet not negligible relative to weight-buoyancy. In group B and D

Figure 2.8: Geldart's powder groups for fluidization by air at room temperature and atmospheric pressure (Solid lines indicate AB and BD boundaries, whereas the dashed line indicate AC boundary) [Geldart, 1973])

powders inter-particle forces are negligible relative to weight-buoyancy. Both particle groups show large bubbles and deaerate quickly after the gas flow is turned off. Solid mixing is intermediate in group B powders and poor in group D [Geldart, 1973]. The possible fluidization regimes that can be achieved with Geldart powder groups at different dimensionless fluidization rates (u^*) can be seen Figure 2.9.

Figure 2.9: Dimensionless flow regime map for upward gas flow through solid particles diagram (Adapted from [Grace, 1986])

The dimensionless fluidization velocity is defined as:

$$u^* = \frac{Re}{d_p^*} \tag{2.4}$$

Whereas the definition of the dimensionless particle diameter can be given as:

$$d_p^* = Ar^{\frac{1}{3}} \tag{2.5}$$

The Reynolds number (Re) is the ratio of inertial forces to viscous forces:

$$Re = \frac{\rho_g \cdot U \cdot d_p}{\mu_g} \tag{2.6}$$

Whereas the ratio of buoyancy forces to viscous forces is defined by the Archimedes number:

$$Ar = \frac{\rho_g \cdot d_p^3 \cdot (\rho_p - \rho_g) \cdot g}{\mu_g^2} \tag{2.7}$$

Whereas u_t is the terminal velocity (or free-fall velocity) of a single spheric particle falling through a fluid [Kunii and Levenspiel, 1991].

2.2.1 Heat & mass transfer in fluidized beds

"Gas-solid fluidized bed heat exchangers are well-known for significantly large tube-to-bed heat transfer rates than conventional gas heat exchangers" [Grewal and Cheung, 1985]. As relatively small particles are used, a high surface area of particles is available for heat and mass transfer. Further, mixing due to bubbles moving through the bed of particles contribute to a reduction in thermal gradients, producing virtually isothermal conditions [Hofbauer, 2012]. Kim et al. [2003] carried out heat transfer experiments with a bundle of steel tubes used as heat exchangers immersed in a bed of Geldart group B particles fluidized by air. As shown in Figure 2.10 the gas velocity (U) has a great influence on the heat transfer coefficient (α). At the minimal fluidization velocity, there is a steep increase in the heat transfer coefficient between the fluidized bed and the surface of the heat exchangers. This is due to enhances of particle convection induced by bubble motion, which is the predominant mechanism of heat transfer in low temperature fluidized bed systems [Saxena, 1989]. In Figure 2.10 this increase apparently occurs below U_{mf}. This is owed to a lower cross-sectional area of the bed at the height of the immersed heat exchangers, leading to an acceleration of the gas flow. A maximum in heat transfer coefficient is surpassed when an increasing surface area of the tube is being engulfed by rising bubbles [Grewal and Cheung, 1985]. Similarly to Kim et al. [2003], Grewal and Cheun [1985] have also shown that heat transfer coefficients, between a fluidized bed and heat exchanger surfaces, can reach well over 300 W/m^2K. However, the heat transfer between heat-exchanger tubes and fluidized beds "is often adjusted and controlled not by changing the bed temperature but by raising or lowering the bed level" [Kunii and Levenspiel, 1991]. An increase of the bed height induces an increase of the heat-exchanger surface area immersed in the fluidized bed, at the cost of a decreasing heat-exchanger surface in the splash zone above the bed's surface; hence improving heat transfer [Kunii and Levenspiel, 1991].
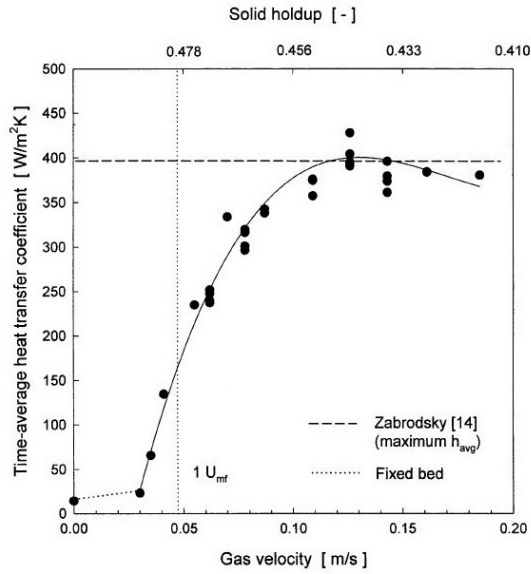
Figure 2.10: Effect of gas velocity on the average heat transfer coefficient [Kim et al., 2003]
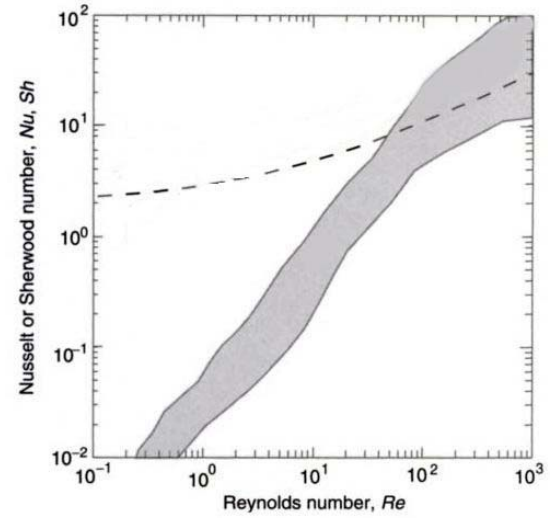
Figure 2.11: Dimensionless heat and mass transfer coefficients as a function of the Reynolds number (adapted from [Palchonok et al., 1998]).

Whereas the Nusselt number is given as:

$$Nu = \frac{\alpha \cdot L}{\lambda} = \frac{\dot{q} \cdot L}{\lambda \cdot \Delta T} \tag{2.8}$$

The Sherwood number defined as follows:

$$Sh = \frac{\beta \cdot L}{D} = \frac{\dot{n} \cdot L}{D \cdot \Delta c} \tag{2.9}$$

The dashed line in Figure 2.11 is calculated with the Frössling-Ranz-Marschall equations [Grace, 2006]. The Frössling-Ranz-Marschall equation for heat transfer is given as:

$$Nu = 2 + 0.6 \cdot Re^{0.5} \cdot Pr^{0.33} \tag{2.10}$$

Whereas for mass-transfer, the Frössling-Ranz-Marschall equation is defined as:

$$Sh = 2 + 0.6 \cdot Re^{0.5} \cdot Sc^{0.33} \tag{2.11}$$

Further, the Prandtl number is:

$$Pr = \frac{\mu}{\rho \cdot a} = \frac{\mu \cdot c_p}{\lambda} \tag{2.12}$$

And the Schmidt number is written as:

$$Sc = \frac{\mu}{\rho \cdot D} \tag{2.13}$$

In Figure 2.11, the grey area represents results from literature, concerning dimensionless gas-solid mass or heat transfer coefficients (Nu & Sh) of fluidized bed systems, whereas the dashed line represents values calculated from the Frössling-Marschall-Ranz equation (see Equation 2.10 & 2.11) for a single spheric particle in one phase flow. It can be seen that values for a single particle are only surpassed by values acquired from fluidized bed systems, if the velocities are high enough. "For small particles and low velocities, the overall coefficients of an active bed appear to be much lower than those of single particles" [Grace, 2006]. This is owed to the fact that with small particles, the fluidization gas preferably passes through the bed in the bubble phase, rather than though the emulsion phase; "thus, the overall resistance at the surface of the particles includes the additional resistance caused by the transfer from the bubble phase to the particulate phase" [Grace, 2006]. Adding to this, the driving force for heat and mass transfer, between the fluidization gas and the particles in the top-most section of the bed almost diminishes, as most of the gas-solid interaction occurs near the gas inlet, where the gas encounters a large particle surface area. With large particles, a higher portion of the fluidization gas moves through the particulate phase and the gas flow reaches farther into the bed before saturation. At low velocities or small particles, the influence of these two effects lead to smaller heat and mass transfer coefficients between solids and gas in a fluidized bed, despite higher heat and mass transfer coefficients for the individual particles in the bed. [Grace, 2006]

2.2.2 Multistage fluidized bed systems

In fluidized bed processes where the bed material undergoes a transformation (e.g. drying, adsorption or oxidation), obtaining uniform products is important for achieving a high product yield. In most cases, the uniformity of the bed material is linked to the residence time of solids in the fluidized bed. "The fraction of solids staying in the bed for a time between t and $t + dt$" [Kunii and Levenspiel, 1991], is described by the residence time distribution (RTD or $E(t)dt$). The function $E(t)$ for a single fluidized bed, which is seen as a perfectly stirred tank reactor, is:

$$E(t) = \frac{1}{\tau} \cdot e^{-\frac{t}{\tau}} \tag{2.14}$$

The mean residence time (τ) is given as:

$$\tau = \frac{W}{\dot{m}_{Solids}} \tag{2.15}$$

For the calculation of the RTD of multistage fluidized bed systems, a cascade of ideally stirred tank reactors, with N reactors and a mean residence time (τ_i) in each tank, is used as a model:

$$E(t) = \frac{1}{(N-1)! \cdot \tau_i} \cdot \left(\frac{t}{\tau_i}\right)^{N-1} \cdot e^{-\frac{t}{\tau_i}} \qquad (2.16)$$

The mean residence time of solids in each stage (τ_i) is defined as:

$$\tau_i = \frac{W_i}{\dot{m}_{Solids}} \qquad (2.17)$$

As can be seen in Figure 2.12 the RTD of solids in a multistage fluidized bed ($N > 1$ in Equation 2.14) is narrower, than in the case of a single fluidized bed (Equation 2.16), and can be further improved by increasing the number of stages.
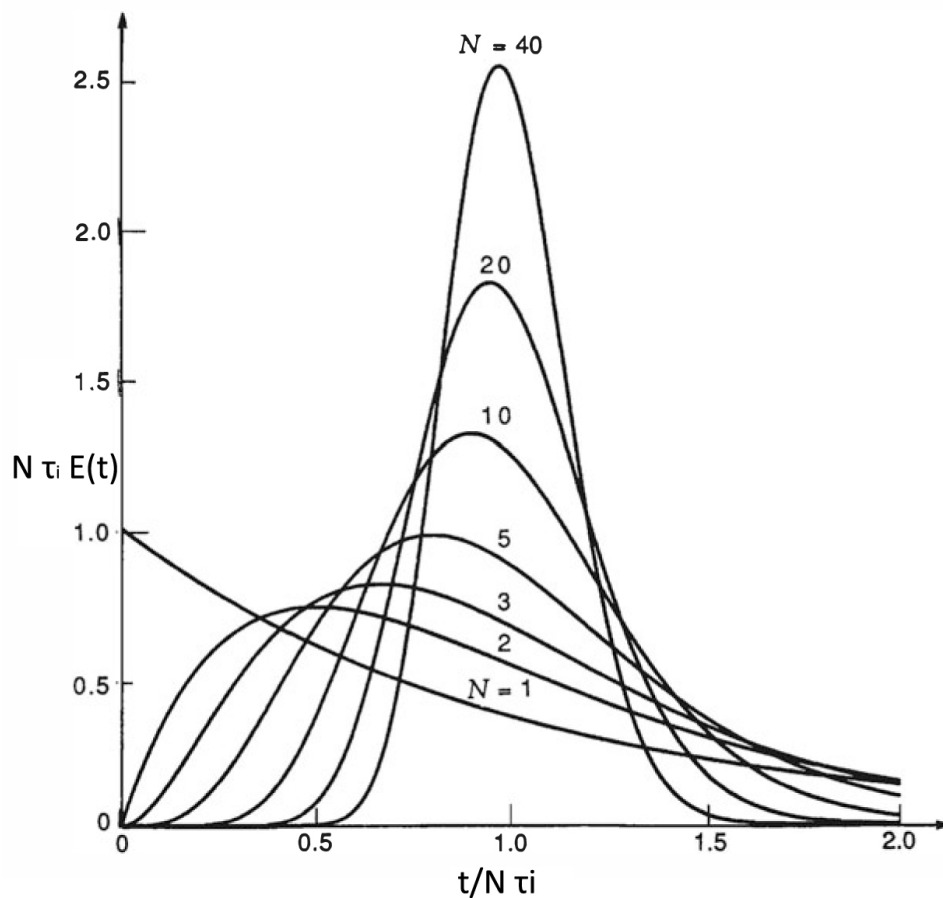
Figure 2.12: Exit age distribution (RTD) for solids in ideal multistaged fluidized beds, from Equation 2.16 [Kunii and Levenspiel, 1991]

There are various possibilities of designing multistage fluidized beds. As shown in Figure 2.13 A, the fluidized bed stages can be placed side-by-side and be separated by weirs, over which solids are transported from one stage to the next. The notable disadvantage of this design is the high amount of fluidization agent needed to achieve the required solid transportation. In the remaining examples (see Figure 2.13 B & C) the reactor stages are placed on top of each other, making the design of such units similar to that of a

distillation column; further, the footprint as well as the volumetric flow of fluidization agent are identical to a single stage reactor. Solid transport from stage to stage can be carried out using perforated distributor plates (Figure 2.13 B) or overflow standpipes, or rather downcomers (Figure 2.13 C). When using perforated distributor plates for solids transport, solids as well as the fluidization agent, are transported through the same perforations in the distributor plates. With the design suggested in Figure 2.13 C, the stages are also separated by perforated distributor plates, yet at normal operating conditions, only the gas flows through the perforations, whereas a downcomer immersed in the bed below, is responsible for solids transport. In the downcomer, a moving bed or an aerated bed regime is maintained, by keeping the fluidization rate and/or the solids throughput in the downcomer within a specific range. This acts as a pressure seal between the high pressure zone in the stage below, and the low pressure zone in the stage above. Should the fluidization velocity in the downcomer or the solids throughput become unfavorable, the pressure gradient across the downcomer cannot be maintained and measures, such as the installation of constrictions or longer downcomers, must be taken to reattain the pressure seal [Kunii and Levenspiel, 1991].
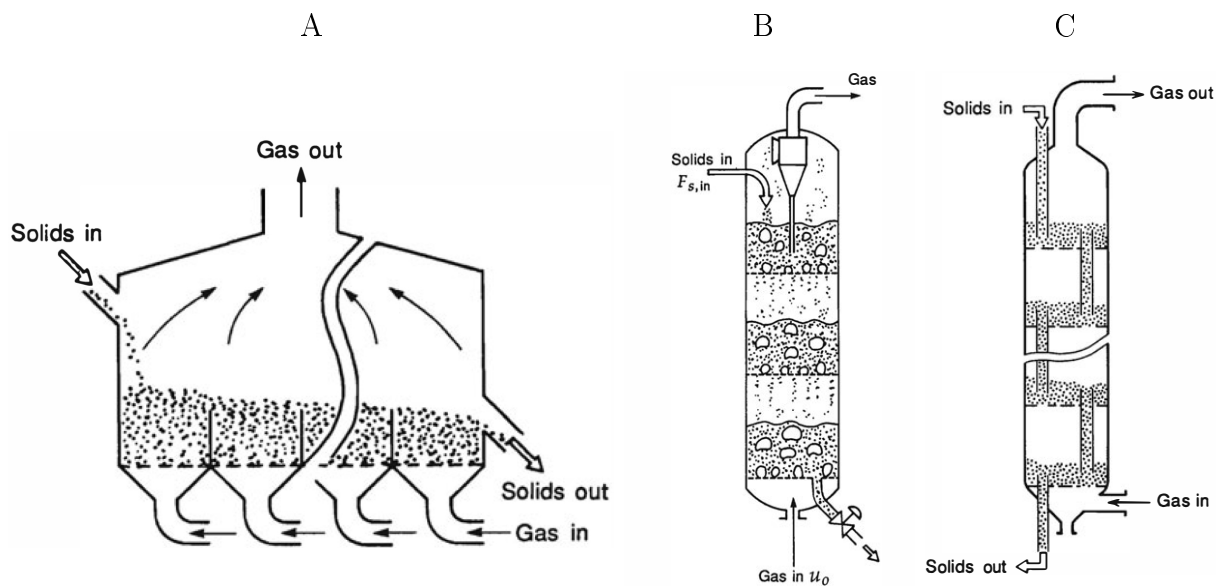
Figure 2.13: Example for multistage fluidized bed designs [Kunii and Levenspiel, 1991]

In multistage fluidized bed systems, operating conditions, such as the temperature, in each stage can be altered with e.g. heat exchangers immersed in each bed. Depending on the task of each stage, specific parameters can be individually controlled, making reactions, such as pyrolysis and gasification of fuels in a high temperature stage and gas upgrading in a low temperature stage above possible [Xu et al., 2009].

2.3 Design considerations

2.3.1 Sorbent material

The task of separating CO_2 from flue-gases is generally characterized by a low concentration or partial pressure of CO_2; hence a high selectivity towards CO_2 is necessary to sufficiently exploit the adsorbent's capacity and generate a high purity desorbate, which is essential for later storage. The sorbent material used to put the chemical adsorption of CO_2 into practice, is porous amine impregnated silica. The high porosity of the adsorbent material is an important property, as the pores provide high specific surface areas; depending on the pore size, the specific surface area of silica can range from 200 m^2/g to 660 m^2/g [Veneman et al., 2012, Hammache et al., 2013]. In order to give the sorbent the property of selectively binding CO_2, the silica support is impregnated with polyethyleneimine (PEI). This is done by forming a slurry consisting of PEI, methanol and the sorbent, subsequently the methanol is removed at elevated temperature and low pressure. Since PEI consist of a mixture of approximately 30% primary amines, 40% secondary amines and with the remainder being tertiary amines [Heyardi-Gorji and Sayari, 2012], the reaction mechanisms of each of the amine groups with CO_2 must be taken into account.
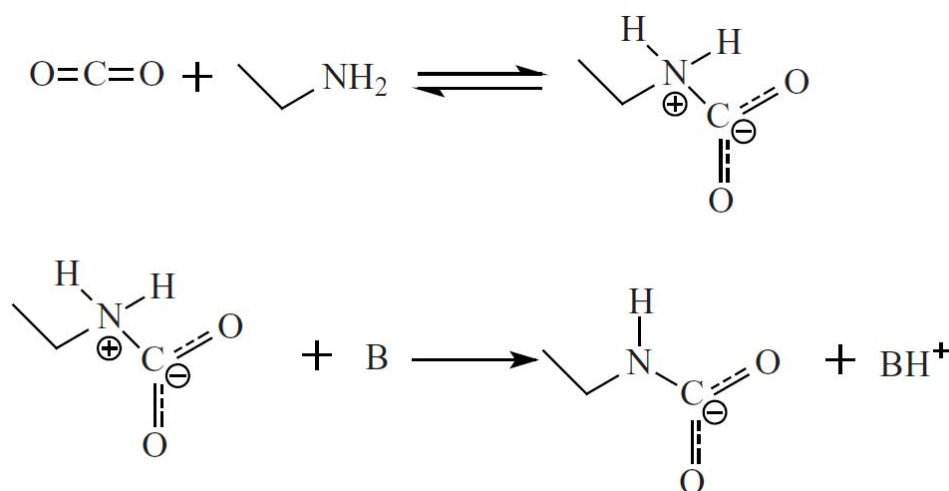
Figure 2.14: Mechanism for carbamate formation between CO_2 and primary, secondary and hindered amines, on the example of a primary amine [Zhao et al., 2013].

As can be seen in Figure 2.14, CO_2 can directly react with primary, secondary and hindered amine groups, to form an intermediate, which is deprotonated to form a carbamate. The deprotonation step is carried out with a nearby base, such as water or another amine group.
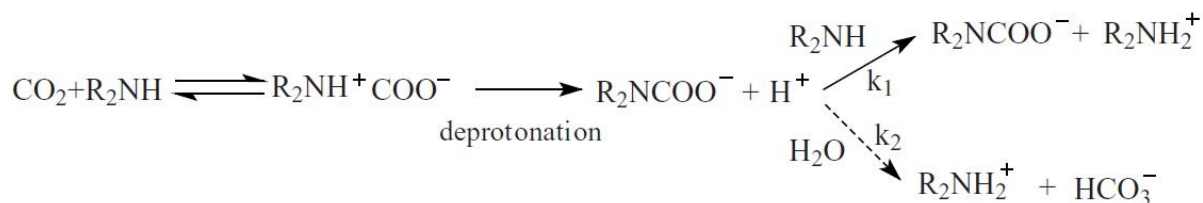
Figure 2.15: Deprotonation of the intermediate species with an amine yields a carbamate whereas deprotonation using water forms carbonate [Zhao et al., 2013].

When water is used as a base in the deprotonation step, a carbonate is formed (see Figure 2.15), whereas when another amine group carries out the deprotonation, a carbamate is produced. As indicated in Figure 2.15, the reaction rates (k_1 & k_2) of each of these deprotonation steps are different. Despite the favorable stoichiometry of the carbonate formation ($N : CO_2 = 1 : 1$ relative to $N : CO_2 = 2 : 1$), the kinetics of the reaction are slower ($k_2 < k_1$) than the reaction kinetics involved in the formation of carbamate; thus carbonate is barely formed, even in humid environments. Therefore the effect of moisture only has a slight effect on the adsorption of CO_2 on primary, secondary or hindered amine groups.
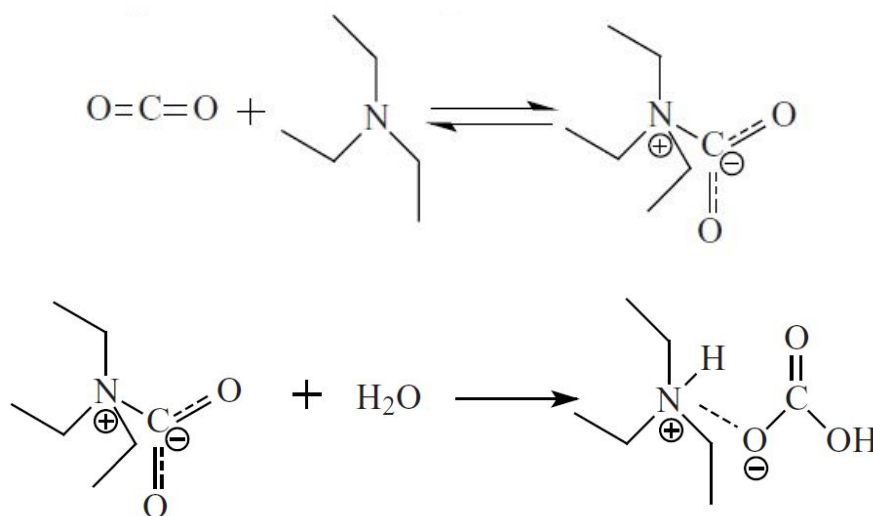
Figure 2.16: Mechanism for carbamate formation between CO_2 and tertiary amines [Zhao et al., 2013].

In contrast to primary, secondary or hindered amines, water is necessary for the tertiary amine to react with CO_2 to form a bicarbonate (see Figure 2.16). As a large share of PEI consists of tertiary amines, moisture will increase the adsorption capacity of sorbent material impregnated with amine groups using PEI [Zhao et al., 2013].
The thermogravimetric analyser (TGA) profiles of an inorganic support impregnated with PEI, in various atmospheres between $25°C$ and $200°C$ were investigated by Drage et al. [2008]. In these experiments the sorbent material was first dried at $100°C$ in an N_2 atmosphere for half an hour, were then exposed to air, CO_2 or an unchanged N_2

atmosphere, while being heated from 25°C to 200°C at a rate of $0,25°C/minute$.
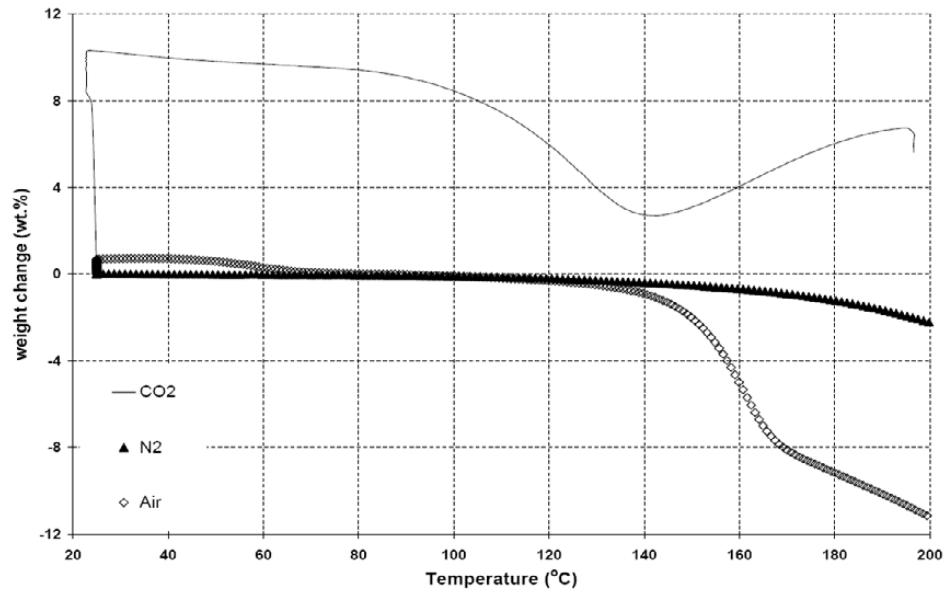
Figure 2.17: TGA profile of the behaviour of a PEI based adsorbent in N_2, CO_2 and air, whilst slowly heated from 25 °C to 200 °C at 0.25 °$C/minute$ [Drage et al., 2008]

As can be seen in Figure 2.17, in a CO_2 atmosphere the adsorbent's weight increases dramatically at the beginning of the experimental procedure, and stays fairly constant up to approximately 85°C; "above this temperature CO_2 adsorption becomes less favorable and the adsorption capacity decreases to a minima at 135°C" [Drage et al., 2009]. At approximately 140°C a weight increase was observed, which indicates the formation of a thermostable complex with CO_2. In air or a N_2 atmosphere the sorbent's weight starts decreasing above 135°C, which suggests thermal degradation or volatilization of amine groups [Drage et al., 2009].

With this knowledge, the regeneration temperature is limited to approximately 120°C (393,15K). The adsorption temperature is limited by findings of Xu et al. [2002], who performed TGA experiments on PEI-modified MCM-41 (a mesoporous molecular sieve). Contrarily to the Langmuir model, Xu and colleagues found, that the adsorption capacity of the tested sorbent reached it's maximum when the temperature was increased to 75°C.

Low temperature   High temperature
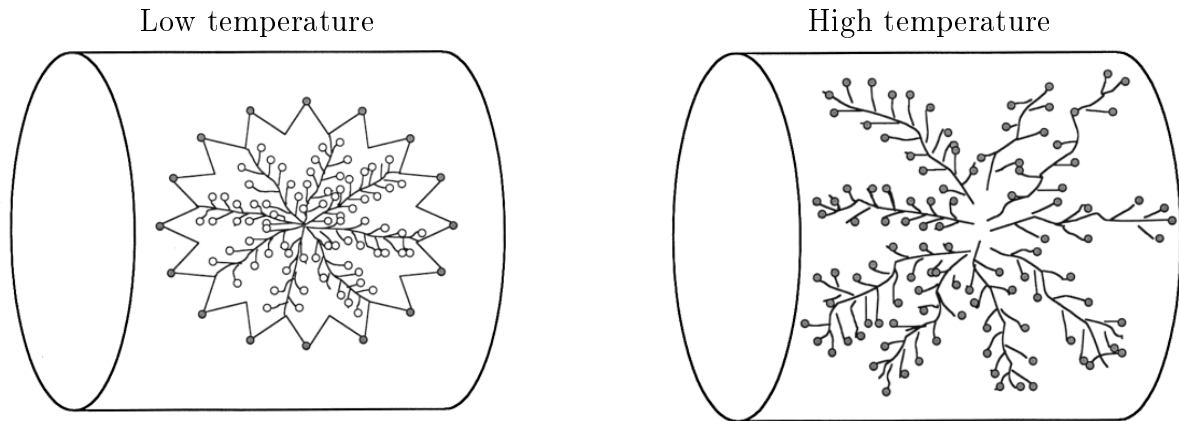
Figure 2.18: Schematic illustration of PEI on MCM-14, whereas at low temperature there are many hidden, vacant adsorption sites $\bigcirc$, only at higher temperatures are these sites accessible to CO_2 [Xu et al., 2002]

This behavior was explained by nano-sized PEI particles (see Figure 2.18) which exist in the pores of the sorbent at low temperatures, and into which CO_2 must diffuse. If the adsorption time is too short, CO_2 isn't able to react with the amine groups inside the particles, hence the "true" capacity of the sorbent can't be taken advantage of. This hypothesis was verified, after an increase of adsorption capacity was observed, when decreasing the temperature to $25°C$ after a sufficiently long adsorption time at $75°C$; this shows that "low adsorption capacity at low temperature was caused by the kinetic limitation" [Xu et al., 2002]. For this reason an adsorption temperature of approximately $75°C$ ($348,15K$) was chosen for the adsorber.

Recently, Fauth et al. [2012] investigated the effect of different amine-methanol mixtures used to impregnate silica material; for silica impregnated with a mixture of $25wt\%$ PEI and $25wt\%$ 3-(aminopropyl)triethoxysilane (APTES), Langmuir CO_2 sorption isotherms were fit to experimental data at different temperatures and CO_2 partial pressures (see Figure 2.19). It's assumed that the sorbent material used throughout this experimental campaign behaves similarly.
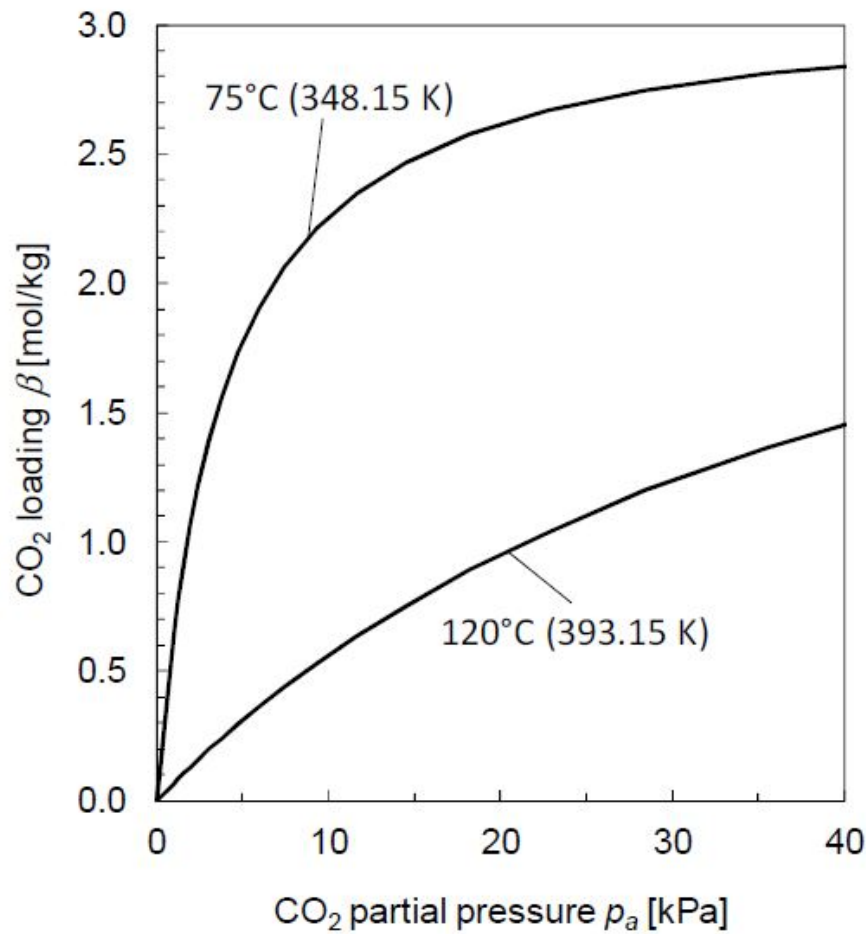
Figure 2.19: CO_2 sorption isotherms for a sorbent at different temperatures and CO_2 partial pressures [Fauth et al., 2012].

As can be seen in Figure 2.19 the term q, for the number of occupied adsorption sites, was replaced by β, the number of *Moles* of CO_2 adsorbed on a *kg* of sorbent. This can be done by altering Equation 2.1 to:

$$\frac{\beta}{\beta_{max}} = \frac{b_{CO_2}(T) \cdot p_{CO_2}}{1 + b_{CO_2}(T) \cdot p_{CO_2}} \tag{2.18}$$

2.3.2 Counter-current TSA in a multistage fluidized bed systems

One of the most important indicators for an adsorption process is the working capacity; which is defined as the difference in adsorbent loading "between the low temperature, low purity adsorption from the flue gas stream and the high purity, high temperature desorption from the regeneration step" [Berger and Bhown, 2011]. In Figure 2.20, the adsorptions isotherms of two sorbents, identical in every respect, except in adsorption enthalpy, are shown; it can be seen, as postulated by the van't Hoff equation (Equation 2.2), that the temperature dependency of the isotherms of the sorbent with a higher enthalpy

of adsorption is stronger. This means, that sorbents with a high enthalpy of adsorption, such as the chemical sorbent used in this experimental campaign, exhibit a higher working capacity in a TSA process running with the same operating temperatures, than a sorbent with a low enthalpy of adsorption.
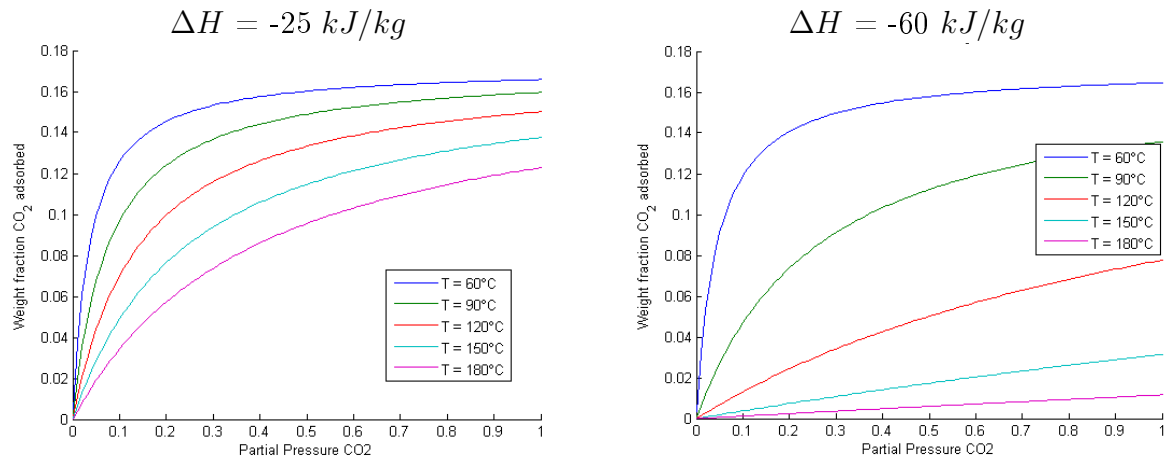
Figure 2.20: Isotherms for sorbents with a heat of adsorption (ΔH) of -25 kJ/kg and -60 kJ/kg [Berger and Bhown, 2011]

To further increase the working capacity, as well as accelerate regeneration by maintaining the driving force of mass transfer (Δc), the desorbate is diluted or rather purged by steam. Ideally a mixture of CO_2 and steam is produced at the desorber gas-outlet, which can easily be conditioned, by means of condensation of steam, to obtain highly pure CO_2 for further utilization or sequestration. Pirngruber et al. [2013], even claim, that depending on the adsorbent material and the reactor system used, it could be indispensable to use a purge gas for a TSA process in fluidized bed systems.

To realize a TSA process continuously, moving beds can be implemented, where the sorbent is circulated between adsorber and desorber. However, unlike in a fluidized bed system, the fluidization velocity (U) is kept below U_{mf}. This implies, that relative to a fluidized bed system, a moving bed system with the same footprint will not be able to treat the same volumetric flow of flue-gas. Furthermore, fluidized beds are at a considerable advantage over moving beds concerning heat and mass transfer properties.

Concerning TSA in fluidized bed systems, Pirngruber et al. [2013] found that a single fluidized bed adsorber, modeled as a perfectly stirred tank reactor, is at a disadvantage to a fixed bed reactor design. Differently to a fixed bed system, where the sorbent loading is at equilibrium with the adsorber inlet CO_2 concentration, in a single fluidized bed adsorber, loading of adsorbents leaving the adsorber is at equilibrium with the adsorber outlet CO_2 concentration. This is because solids within a fluidized bed can be considered as well (to ideally) mixed. Thus, the sorbent loading can be assumed to be in equilibrium with the adsorber off-gas. If, for example, a capture rate ($\eta_{captured}$) of 90 % should

be achieved, it would entail that sorbents with low loading enter the regenerator. The fractional sorbent loading (θ) obtained in a single fluidized bed reactor is calculated by rewriting the Langmuir equation (Equation 2.1) using Dalton's law (Equation 2.19) and the capture rate ($\eta_{captured}$) to Equation 2.20 [Pirngruber et al., 2013]:

$$p_{CO_2} = \frac{p_{Ads}}{y_{CO_2}} \tag{2.19}$$

$$\theta_{Ads} = \frac{q}{q_s} = \frac{b(T_{Ads}) \cdot p_{Ads} \cdot y_{CO_2,Feed} \cdot (1 - \eta_{captured})}{1 + b_T(Ads) \cdot p_{Ads} \cdot y_{CO_2,Feed} \cdot (1 - \eta_{captured})} \tag{2.20}$$

In a single fluidized bed regenerator, the same phenomenon occurs. Pirngruber et al. [2013] calculated the global minimum required energy input for the regeneration of sorbent material with a fractional loading of 0,85, at $403K$ and a CO_2 partial pressure of 0,5bar in the purge gas. The global minimum required heat for regeneration was 9 $kJ/MoleCO_2$ higher in the single fluidized bed regenerator, than in the fixed bed regenerator.

To eliminate this disadvantage and yet continuously operate a TSA process, with the advantages of fluidized beds, a counter-current multistage fluidized bed design was chosen; in Figure 2.21 an illustrative representation of such a process can be seen.
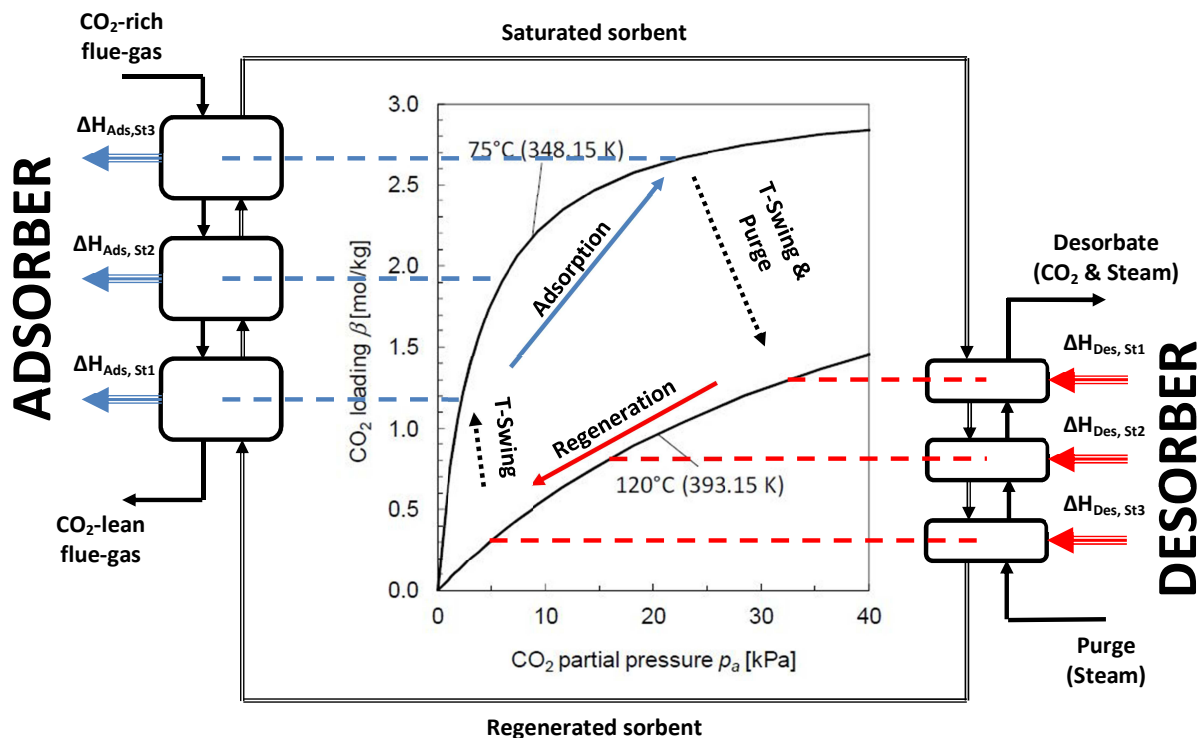
Figure 2.21: Illustrative representation of equilibrium conditions in a counter-current multistage fluidized bed system.

The sorbents in each of the fluidized bed stages are at equilibrium with the respective off-gas CO_2 concentration; counter-current flow enables high working capacities, as the

driving force for mass transfer is maintained. Heat-exchangers immersed in each fluidized bed stage supply and extract heat, thereby making virtually isothermal conditions across each of the columns possible. In the adsorber column, the lean sorbent is gradually loaded, while given the time to reach equilibrium conditions in each stage; hence lean sorbents are in equilibrium with a low CO_2 concentration, whereas saturated sorbents are in equilibrium with a high CO_2 concentration. In a similar way, the regenerations is also enhanced by counter-current flow, as the saturated sorbent is gradually regenerated, stage for stage, until it is at equilibrium with a low CO_2 concentration in the bottom-most stage. Generally, this design reduces the required circulation rate of sorbent material for achieving a specified capture performance, which in turn is linked to a reduction of energy requirement and a decreased stripping steam demand relative to a single stage fluidized bed design.

Chapter 3

Methodology

3.1 Experimental Setup

In Figure 3.1, a basic scheme of the BSU, used to realize continuous adsorptive separation of CO_2 from simulated flue-gas (FG), is shown. As can be seen, a design where the stages are on top of each other was chosen. Further, the walls of the adsorber are made of glass, whereas the desorber is entirely made of steel. In each stage (adsorber & desorber) distributor plates are used to ensure optimal aeration of each of the ten fluidized beds; for the fluidization rates tested herein, a bubbling fluidized bed was formed in each stage. In order to supply and discharge sufficient amounts of heat to and from the fluidized beds, in the desorber and adsorber respectively, every stage is equipped with a copper heat exchanger (position 11 & 12 in Figure 3.1) immersed in the bed of sorbents. The flow of coolant is controlled by valves which must be adjusted manually; hence the temperature of each adsorber stage can be altered individually. The thermal oil pump permanently runs at maximum power, while heating rods in the thermal oil reservoir heat the thermal oil to a specified temperature ($\approx 140°C$). Further, electrical heating, controlled by a temperature controller, is installed on all gas lines, to achieve the desired process temperatures.

Each stage is also equipped with a weir, over which solids are propelled by means of bursting bubbles; in this way solids are entrained into the downcomer, which is capable of transporting solids from an above stage to one below. All weirs can be replaced, to make testing of different bed heights or solids residence times possible.

In steady state conditions, the lean sorbent (position 14 in Figure 3.1) enters the adsorber (position A in Figure 3.1) at the top of the column, via a downcomer which is immersed in the fluidized bed of the top-most stage. Once in the fifth stage, the sorbent is fluidized by simulated FG which is poor in CO_2 relative to the adsorber gas-inlet. Nevertheless, adsorption takes place, resulting in a heat which is discharged from the fluidized bed by the heat-exchanger to maintain isothermal conditions. As the sorbent is transported from one stage to the next, the sorbents get more and more loaded with CO_2, while the CO_2 concentration in the fluidization gas increases from top to bottom.

At the bottom-most stage of the adsorber, the sorbent is again carried over a weir and into a stand-pipe leading to the bottom screw conveyor (BSC, position F in Figure 3.1). Subsequently, the solids are transported into a adiabatic riser (position C in Figure 3.1) which is operated at a fast fluidization regime (see Chapter 2.2), causing the solids to be entrained into a gas-solid separator (position D in Figure 3.1). Finally, the solids fall into a downcomer, which leads to the top-most stage of the desorber column (position B in Figure 3.1). Similarly to the adsorber, the sorbent is transported from the top of the column to the bottom, and again returned back to the adsorber. Alongside temperature swing regeneration, purge gas stripping is implemented as well. The desorber is fluidized with a purge gas (steam, N_2 or a mixture thereof) causing a gradient in CO_2 concentration from top to bottom, as the sorbent gets leaner. In addition to the copper heat exchangers, the desorber has a double-wall design that allows for thermal oil heating, in order to supply a sufficiently large heated surface for the high temperature regeneration.

The closed riser-loops of the system each consist of a recirculation gas blower (position 5 & 6 in Figure 3.1), a riser section, a gas-solid separator (PSEP) and a particle filter (position J in Figure 3.1). Since these loops are closed, the equilibrium composition of the recycled gas depends on operating conditions of the BSU, as well as on gaseous slip from the columns into the risers. The voidage of the moving beds, in the stand-pipe between the columns and the BSCs, can contain and therefor transport unwanted gases. To diminish the amount of unwanted gas in the moving bed, there is the possibility of injecting purge gas (position 7 & 8 in Figure 3.1) in form of CO_2, N_2 or steam into the respective stand-pipe.
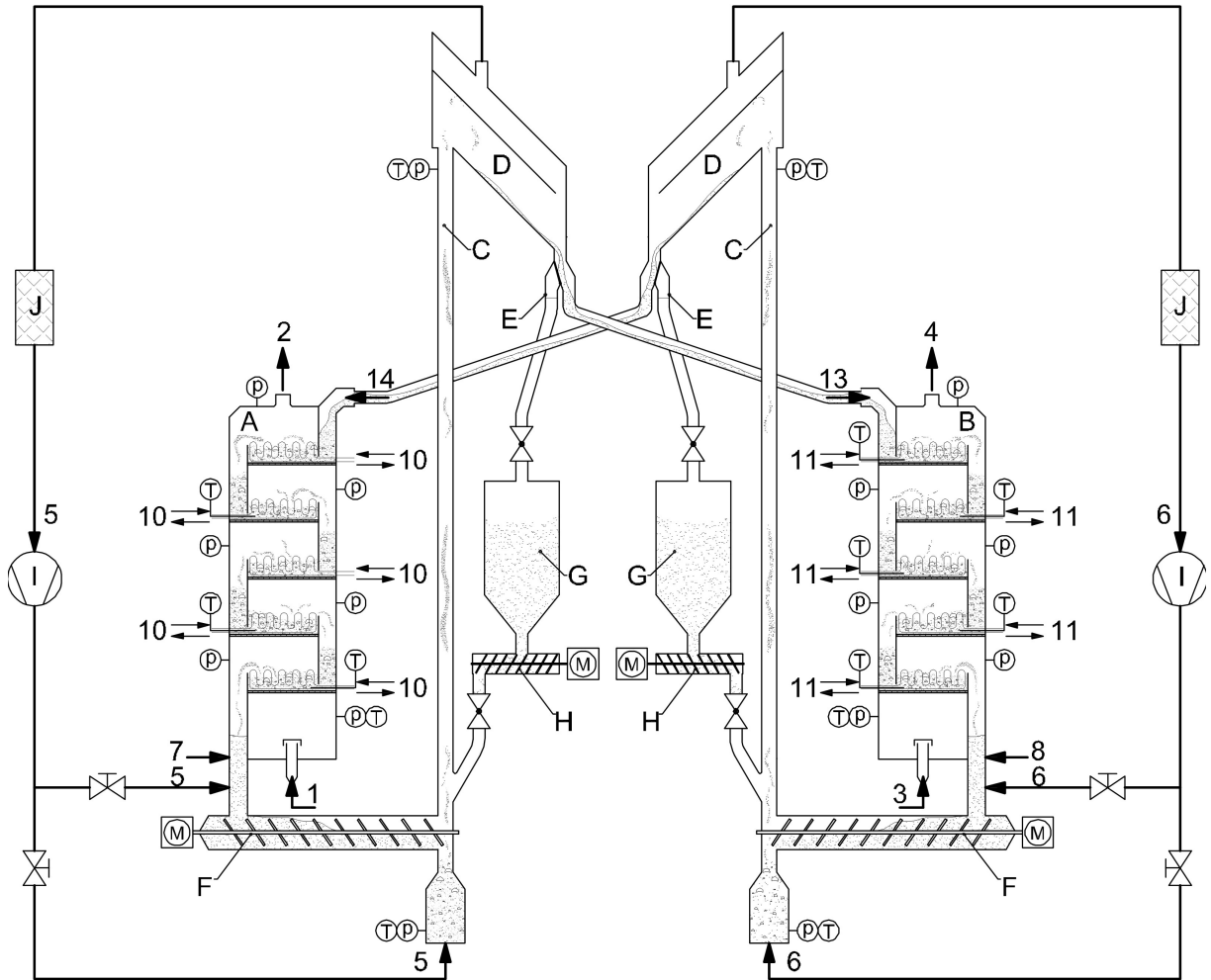
A	adsorber	1	raw flue gas	11	desorber stage heating
B	desorber	2	clean flue gas	12	lean-rich heat exchange
C	riser	3	stripping gas (steam)	13	high loaded solids
D	gas-solid separator	4	CO_2 enriched stripping gas	14	regenerated solids
E	mechanical flap	5	recirculation gas (ads.)		
F	solids transport screw	6	recirculating gas (des.)		
G	particle hopper	7	purge gas		
H	solids feeding screw	8	purge gas	P	pressure sensor
I	gas recycle compressor	9	dilution stream (N_2)	T	temperature sensor
J	particle filter	10	adsorber stage cooling	M	driving motor

Figure 3.1: Basic scheme of a double loop staged fluidized bed system for continuous TSA

All inflowing gas streams are controlled by needle valves and measured by means of flow indicators. As the gas inlets of both columns are equipped with connections to N_2, CO_2 and steam, the production of gas mixtures is done simply by setting the desired volumetric flow on the respective rotameters. A boiler produces steam which, after additional electronic preheating, is superheated to approximately $140°C$ and is introduced to the desorber. Mechanical flaps (position E in Figure 3.1) aid in the removal of sorbent material from the BSU into hoppers. The hoppers are equipped with screw conveyors, which can be used for inventory make-up in cases where entrainment is high. Further, the frequency of the motors driving the BSCs and hopper screw conveyors (HSCs) are manually controlled via a frequency converter.

Three sockets, two of which are located at the gas-outlet of each column, as well as one at the gas-inlet of the adsorber, are connected to a gas analyzer via hoses. Further, one off-gas filter is installed between the adsorber gas-outlet and the off-gas duct. As to avoid condensation of desorbate in the off-gas duct a condenser, in form of a liquid-gas heat exchanger is installed after the desorber gas outlet. The condenser is cooled by external cooling water, which is also used to cool the coolant in a plate heat exchanger.

3.2 Data Acquisition & Evaluation

Throughout the BSU the pressure, or rather differential pressure between relevant positions, is measured by means of 18 "Kalinsky DS2" pressure sensors. The connections between the pressure sensors and the pressure taps on the unit, is established by pressure hoses. In order to protect the pressure sensors from moisture a negligibly small purge gas flow ($<0.1 Sm^3/h$) is utilized. As shown in Figure 3.2 & 3.3, six pressure sensors are connected to each of the columns, two are connected to each of the risers, one is connected to the outlet of the off-gas filter and one is connected to the outlet of the condenser to detect potential blocking of the unit.

Pressure sensor	1	2	3	4	5	6	7	8	9	10
Measured pressure	$\Delta p_{Ads,St1}$	$\Delta p_{Ads,St2}$	$\Delta p_{Ads,St3}$	$\Delta p_{Ads,St4}$	$\Delta p_{Ads,St5}$	$\Delta p_{Ads,BSC}$	$\Delta p_{Ads,Riser}$	$\Delta p_{Ads,PSEP}$	$p_{Ads,Feed}$	$\Delta p_{Ads,Filter}$
Operating range in $mbar$					0 - 10				0 - 250	0 - 25
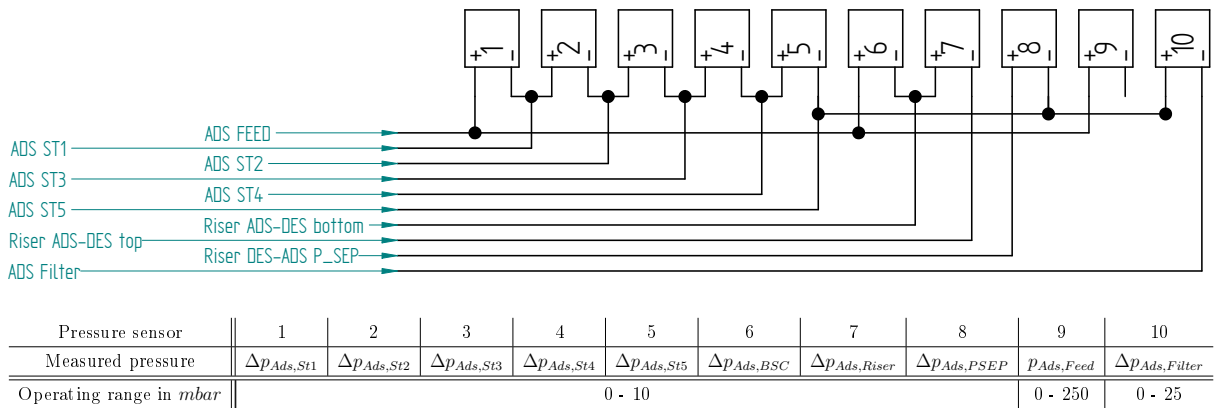
Figure 3.2: Connection scheme of pressure sensors including naming and pressure range of each pressure sensor connected to the adsorber column.

Pressure sensor	11	12	13	14	15	16	17	18	19	20
Measured pressure	$\Delta p_{Des,St1}$	$\Delta p_{Des,St2}$	$\Delta p_{Des,St3}$	$\Delta p_{Des,St4}$	$\Delta p_{Des,St5}$	$\Delta p_{Des,BSC}$	$\Delta p_{Des,Riser}$	$\Delta p_{Des,PSEP}$	$p_{Des,Feed}$	$\Delta p_{Des,Cond.}$
Operating range in $mbar$	0 - 10								0 - 250	0 - 25
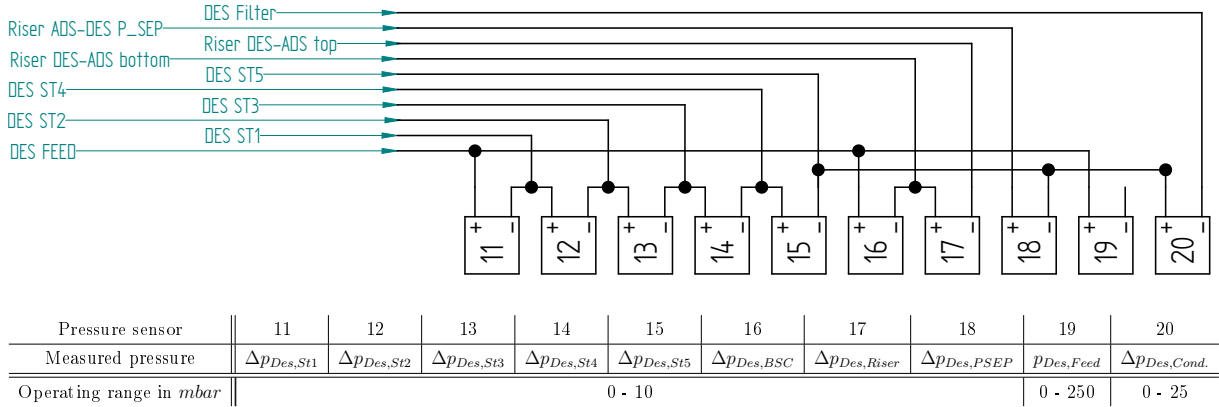
Figure 3.3: Connection scheme of pressure sensors including naming and pressure range of each pressure sensor connected to the desorber column.

As seen in Figure 3.1 the temperature at 16 locations is measured using "Jumo CANtrans T" resistance temperature detectors, with an operating range from $-50°C$ to $150°C$ and an accuracy of $\pm0,1°C$. The temperature probe in each of the ten stages is installed closely above the distributor plate and is immersed in the bed of solids. The remaining temperature probes are located below each of the bottom-most stages of the columns to measure the inlet gas temperatures, as well as two in each of the risers. Further, "$PT-100$" resistance thermometers are used to measure the temperature of thermal oil and coolant leaving the heat-exchangers (return flow temperature), as well as the forward flow temperatures of these media, as they leave their reservoirs.

To be able to calculate values for sorbent loading, at least one of the BSCs (in this case the desorber BSC) must be calibrated with the sorbent material which is used. By doing so, the circulation rate of solids (SCR), in terms of kg sorbent circulating between the adsorber and the desorber column per hour, can be calculated (according to Equation 3.1).

$$SCR = k_{BSC} \cdot f_{BSC} \qquad (3.1)$$

The calibration procedure is carried out by measuring the mass of solids that the screw conveyor can transport in a certain time span; this is done with several different frequencies. For the sake of simplicity, cali-

Figure 3.4: BSC calibration line fit to calibration data

bration data is fit to a line intersecting the origin of the graph (see Figure 3.4), to obtain the constant k_{BSC}.

An "Emerson X-STREAM X2GP" general purpose gas analyzer, with a non-dispersive infrared detector, is used to measure the CO_2 concentration in various gas streams. The analyzer is equipped with a cooler, as to decrease the steam dew point of the analyzed gas to $4°C - 5°C$; thus the measured concentrations must be understood in terms of dry gas. Further, the detector was calibrated with test gas containing 0,49 $vol\%CO_2$, 5,1 $vol\%CO_2$ and 12 $vol\%CO_2$ and the gas analyzer linearity is $\leq 1\%$.

All temperature and pressure measurements as well as data from the gas analyzer are electronically transmitted to the process control system, is then elaborated in a LabView application with a sample rate of half a second, further these values are averaged over a time-span of two seconds. As can be seen in Figures 3.5, an organized interface was designed to display all relevant temperatures, pressures and performance indicators as well as the SCR.

Figure 3.5: User interface of the process control system programmed in LabView.

All flow rates must be entered manually and are saved to a file together with the acquired process data and calculated values. Further, the program is capable of controlling the CANopen-compatible frequency converters of the BSCs. The capture efficiency is one of three performance indicators, which is constantly calculated from the CO_2 concentrations ($c_{CO_2,Ads}$) in the adsorber gas-inlet and gas-outlet; this value is defined by a mass balance in the adsorber and its derivation is shown in Equations 3.2 - 3.7.

$$\eta_{captured} = \frac{\dot{V}_{CO_2,captured}}{\dot{V}_{CO_2,in}} = \frac{\dot{V}_{CO_2,Ads,in} - \dot{V}_{CO_2,Ads,out}}{\dot{V}_{CO_2,Ads,in}} \tag{3.2}$$

$$\dot{V}_{CO_2,Ads,in} = c_{CO_2,Ads,in} \cdot (\dot{V}_{N_2,Ads,in} + \dot{V}_{CO_2,Ads,in}) = \frac{c_{CO_2,Ads,in} \cdot \dot{V}_{N_2,Ads,in}}{1 - c_{CO_2,Ads,in}} \tag{3.3}$$

$$\dot{V}_{CO_2,Ads,out} = c_{CO_2,Ads,out} \cdot (\dot{V}_{N_2,Ads,out} + \dot{V}_{CO_2,Ads,out}) = \frac{c_{CO_2,Ads,out} \cdot \dot{V}_{N_2,Ads,out}}{1 - c_{CO_2,Ads,out}} \tag{3.4}$$

Assuming no gas leakage out or into the adsorber allow for equaling the inlet flow-rate of N_2 with the outgoing flow-rate N_2:

$$\dot{V}_{N_2,Ads,in} = \dot{V}_{N_2,Ads,out} = \dot{V}_{N_2,Ads} \tag{3.5}$$

With Equation 3.2 - 3.5, the capture efficiency amounts to:

$$\eta_{captured} = \frac{\frac{c_{CO_2,Ads,in} \cdot \dot{V}_{N_2,Ads}}{1-c_{CO_2,Ads,in}} - \frac{c_{CO_2,Ads,out} \cdot \dot{V}_{N_2,Ads}}{1-c_{CO_2,Ads,out}}}{\frac{c_{CO_2,Ads,in} \cdot \dot{V}_{N_2,Ads}}{1-c_{CO_2,Ads,in}}} \tag{3.6}$$

Hence, the capture efficiency can be continuously calculated from the measured CO_2 concentrations in the adsorber inlet and outlet:

$$\eta_{captured} = 1 - \frac{c_{CO_2,Ads,out} \cdot (1 - c_{CO_2,Ads,in})}{c_{CO_2,Ads,in} \cdot (1 - c_{CO_2,Ads,out})} \tag{3.7}$$

The dynamic sorbent loading is an indicator for the working capacity of the sorbent material at specific operating conditions in terms of $kg_{CO_2capt.}$ per $kg_{Sorbent}$; it is defined by Equation 3.8:

$$dSl = \frac{\dot{m}_{CO_2captured}}{\dot{m}_{Sorbent}} \cdot 100 = \frac{\dot{V}_{CO_2,Ads,in} \cdot \frac{M_{CO_2}}{V_m} \cdot \eta_{Captured}}{SCR} \cdot 100 \tag{3.8}$$

As the absolute amount of CO_2 which could be captured in a day (24 hours) at specific operating conditions is also of interest. This value is also continuously calculated, according to Equation 3.9:

$$\dot{m}_{CO_2capt.} = \dot{V}_{CO_2,Ads,in} \cdot \eta_{captured} \cdot \frac{M_{CO_2}}{V_m} \cdot 24 \tag{3.9}$$

3.3 Experimental Procedure

3.3.1 Start-up

For start-up of the BSU, a special start-up procedure must be followed. First of all, the off-gas fan is activated, the LabView data acquisition program is started and all acquired pressure values are zeroed. Ideally, both columns are empty and must be filled with a specified amount of material to begin with. In order to be able to do this, mechanical flaps in the downcomer section, at the height of the distributor plates, are installed. Before the start-up procedure begins, these flaps are closed, to simulate a pressure drop across the downcomer, which, when in a steady-state, is created by a moving bed to fluidized bed regime. Filling the columns with sorbent material is done by first activating both recirculation gas blowers and setting a specified flow rate of N_2 to be used as a fluidization gas in each of the columns. In the next step the HSCs are activated and solids are transported from the hoppers into the risers, past the gas-solid separators and into each of the columns. The closed flaps cause the fluidization gas to flow through the distributor plates, rather than the downcomer section. This condition is held until the top

most stages are appropriately filled with material; this is determined either optically, in the adsorber, or by means of the pressure drop across the stage ($2 - 3mbar$, depending on the used sorbent and weir height), in the desorber. Subsequently, the flaps are repeatedly opened and closed, so the downcomer is progressively filled with sorbent. The pressure seal of the moving bed is sufficient, when there is no noticeable change in pressure drop across the stage, between opening and closing the flap. This procedure is done for all ten stages. The HSCs can be turned off when there is a sufficiently high inventory in the bottom-most stages, or buffers, of both columns (approximately $4mbar$ in the adsorber and around $3mbar$ in the desorber, depending on the used sorbent). The buffers in each of the columns result from the fact that the remaining fluidized bed stages can only hold a limited amount of bed material at a given fluidization rate. Any excess bed material is subsequently transported over the weirs and accumulates at the bottom-most stages. Further the BSCs are set to the desired SCR; however it must be taken into account that an inventory shift can take place if the BSCs don't transport the same amount of solids. In the worst case this can lead to the depletion of one of the buffers, and to the loss of the respective pressure seal between riser and column. To avoid an inventory shift, the pressure drops across each of the columns must be monitored at all times, as the pressure drop in a fluidized bed is proportional to the mass of solids therein, according to the following Equation 3.10 [Hofbauer, 2012]:

$$\Delta p = \frac{m_{Solids} \cdot g}{A} \qquad (3.10)$$

If there is a noticeable change in pressure drop across the lower-most stage of the columns, the SCR of one BSC is left unchanged, while the other is adjusted to control the inventory distribution.

In the next step, the thermal oil pump is activated as well as electrical heating of the thermal oil reservoir and gas feed lines. To induce the needed temperature ($70°C$ - $75°C$) in the adsorber, the N_2 stream used to fluidize the adsorber can be partially replaced by a simulated FG (containing CO_2). When a simulated FG is used, the heat of adsorption released within the first 15 minutes, especially in the two top-most stages, is so high, that the coolant pumps must be activated to not exceed the optimal operating temperatures. As soon as the temperature of all desorber stages are heated to approximately $100°C$, N_2 is gradually replaced by steam.

3.3.2 Steady-state Operation

Once the start-up procedure is complete, the desired FG mixture is used to fluidize the adsorber column. In cases where the unit's performance at specific SCRs are tested, the desired SCR is set on the surveyed BSC (desorber BSC) and the other BSC is continuously

adjusted, until the inventory of both columns is constant. In the process of adjusting the unsurveyed BSC, it must be kept in mind, that there must be a sufficient buffer in both columns. Depending on the imposed change on operating conditions e.g. SCR, CO_2 concentration in the FG or coolant flow, it can take up to 30 minutes, until temperatures, differential pressure and, above all, the adsorber off-gas concentration is at a steady state. When steady-state operation is reached, an operating point is set in LabView and is recorded at a specific recording interval, for at least 10 minutes. Reported values in Chapter 4 are averaged values from the recording intervals of the respective operating points.

3.3.3 Base-case operating conditions

In previous work conducted within the Zero Emission Technologies (ZET) group at the University of Technology in Vienna, the potential of the TSA process, using amine functionalized sorbents for commercial scale application, has been assessed by means of mass and energy balance based simulations. This process evaluation was made for specified operating conditions, such as CO_2 concentration, dynamic sorbent loading, operating temperature etc. So called "base-case" operating conditions (shown in Table 3.1) were chosen to align with the operating conditions during evaluation; thus making BSU results comparable to evaluation results.

U/U_{mf}	Flue-gas feed		CO_2 in feed			CO_2 capture rate		Purge-gas feed		Recirculation gas		SCR	dSl
$-$	m^3/h	Sm^3/h	$vol\%$	Sm^3/h	kg/h	$\%$	$kg_{CO_2capt.}/day$	m^3/h	Sm^3/h	m^3/h	Sm^3/h	$kg_{Sorbent}/h$	$wt\%$
10	21,1	16,8	7,7	1,28	2,5	90	54,8	11,5	8	15,2	11,7	≈ 28 / $\approx 32^*$	$\approx 7,1$ / $\approx 6,5^*$

Table 3.1: Base-case operating conditions in the BSU, whereas * indicates BC conditions with corrected bulk density values for the sorbent.

In some experiments incorrect values for the sorbent material's bulk density were used; however, this was corrected after the experiments and lead to an apparent increase of the SCR ($\approx 32kg/h$) together with a decrease of the dynamic sorbent loading ($\approx 6,5wt\%$). The flow regimes of the fluidized beds at BC conditions as well as the Geldart classification of the utilized sorbent material can be seen in Figure 3.6:
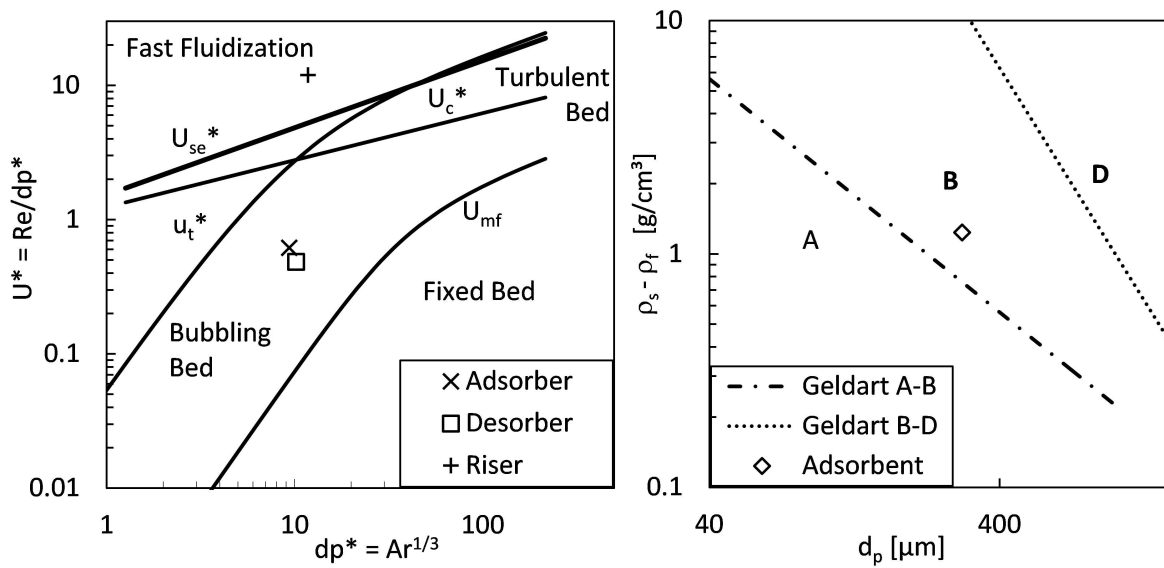
Figure 3.6: Flow regime map of the BSU's fluidized beds (left) & Geldart classification of adsorbent particles used (right)

The experiments included variations of U/U_{mf} of the adsorber feed gas or stripping gas, variation of the compositions of these gases and a variation of the SCR, while all other parameters were left at BC settings. Usually, the stripping agent which is used, is steam; cases where N_2 was used instead, are referred to as "base-case dry" (or BC dry) conditions.

3.3.4 Shutdown

After an experiment was conducted, the sorbent must be dried before heating is turned off. In this way avoiding agglomeration of sorbent material caused by condensation of trapped steam in the pores of the sorbent. For this reason, the steam used to fluidize the desorber is replaced by N_2 and the BSU is operated for another 30 - 45 minutes. After this time, electrical heating of all components is deactivated, together with the flow of CO_2 into the adsorber. Only when all measured temperatures are approximately at room temperature, the coolant flow can be deactivated and the mechanical flaps can be alter, to direct solids into the hoppers.

Chapter 4

Results

In Table 4.1, an overview of the operating conditions as well as variations that were investigated throughout the experimental campaign is given:

Variation	Weir height in mm		Operating Conditions
	Ads.	Des.	
H_2O in stripping gas	60	60	BC dry BC with 25 $vol\%H_2O$ in stripping gas BC with 50 $vol\%H_2O$ in stripping gas BC
Stripping steam flow rate	60	60	BC with variation of stripping gas flow rate
H_2O in adsorber feed gas	60	60	BC with 6,6 $vol\%H_2O$ in feed gas BC with 11,9 $vol\%H_2O$ in feed gas
SCR	60	60	BC dry with variation of SCR
$c_{CO_2,Ads,in}$	60	60	BC with $dSl \approx 6,5wt\%$
U/U_{mf} in the adsorber	60	60	BC with $dsl \approx 7,1wt\%$
Weir height	60	60	BC dry; BC; BC with $\eta_{Captured} = 90\%$; BC with $dSl \approx 7,1wt\%$; BC with $c_{CO_2,Ads,in} = 12vol\%CO_2$ & $dSl \approx 7,1wt\%$
	60	80	
	80	60	
	80	80	

Table 4.1: Summary of variations carried out during the experimental campaign, including weir heights used and a brief description of operating conditions

As can be seen, a vast variation of operating conditions was tested, hence a greater understanding of the coherence between the unit's performance and the tested operating conditions was gained. In the following, each series of variations are summarized by two graphs. The overview displays the averaged temperatures of all fluidized bed stages in $^\circ C$ as well as the SCR in kg/h, whereas the unit performance graph shows averaged

performance data, such as the capture efficiency in %, the capture rate in $kg_{CO_2capt.}/day$ and the dynamic sorbent loading in $wt\%$, at each operating point. Further, all presented results are averaged data acquired over a time-span of at least ten minutes at steady-state conditions.

4.1 Variation of H_2O in stripping gas
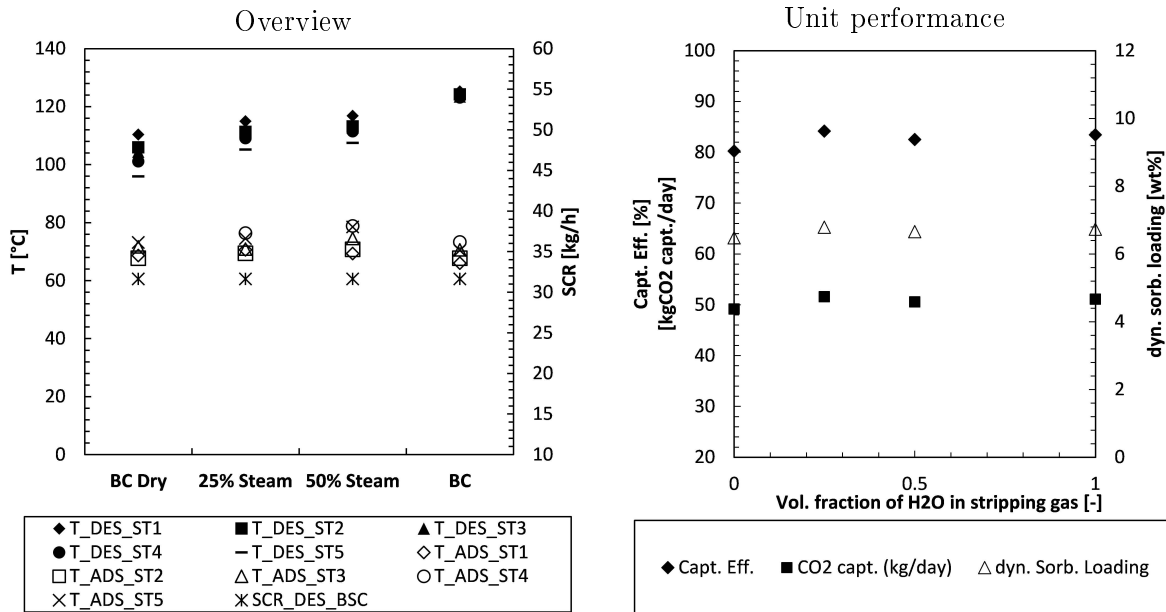
Figure 4.1: Experimental data from the variation of H_2O in stripping gas at BC conditions.

This experiment was conducted in order to determine the impact of steam in the stripping gas, on the BSU's, or rather the utilized PEI impregnated sorbent material's, CO_2 capture performance. This factor had obviously improved the results Zhao et al. [2013] had obtained during their experiments (see Chapter 2.3). BC dry operating conditions, with a SCR of $32kg/h$, were set as an operating point; the steam content in the stripping gas (N_2) was successively increased from $25vol\%H_2O$ to $50vol\%H_2O$ and finally N_2 was entirely replaced by steam at a flow rate of $8Sm^3/h$ resulting in BC conditions. For dry regeneration the forward flow temperature of the cooling medium was chosen quite low to achieve the required process temperatures within the adsorber. The condensation of steam followed by the adhesion of particles, on the cold heat-exchanger surfaces in the adsorber was observed when the desorber was fluidized entirely by steam. This indicates, that there is a slip of steam from the desorber to the adsorber column; this can happen by two means. Firstly, steam may have been co-adsorbed on the sorbent surface in the desorber, followed by its desorption in the adsorber. Secondly, steam which is trapped within the voidage of the moving bed in the stand-pipe leading to the desorber BSC, is transported to the corresponding riser, followed by an enrichment of the respective

recirculation-gas with steam and a subsequent slip thereof into the adsorber column via the solids inlet (at the top-most stage). As the coating of heat-exchanger surfaces by the sorbent material decreases heat-transfer, the forward flow-temperature of the coolant was increased. Differently to the temperatures in the adsorber stages, shown in the overview of Figure 4.1, which only change slightly throughout this variation, an increase of the H_2O concentration in the stripping gas, apparently increases the desorber stage temperatures as well as decreases the axial temperature dispersion in the desorber. The desorber temperatures narrowed from $96°C$ in the top-most stage and $106°C$ in the bottom-most stage at 0% steam in the stripping gas, to $123°C$ in the first and $125°C$ in the fifth desorber stage when only steam was used for regeneration. The adsorber stage temperatures stayed between $68°C$ and $79°C$, whereas a noticeable drop in adsorber stage temperatures as well as decrease in axial temperature dispersion occurs when increasing the H_2O concentration in the stripping gas to 100%. This behavior indicates that steam is continuously adsorbed (exothermically) onto the sorbent material during regeneration and evaporates or is desorbed (endothermically) in the dry environment of the adsorber column. This "internal heat-pump effect" enhances the process of CO_2 adsorption, as the heat of reaction caused by adsorption and desorption of water counterbalances the heating and cooling demand in both columns. This positive effect also leads to a narrower temperature distribution in the columns. As to the performance indicators, the dynamic sorbent loading as well the capture rate are both directly proportional to the capture efficiency in this experiment, as neither the SCR nor the adsorber feed composition and flow rate had been varied. BC dry conditions resulted in the lowest capture efficiency with 80%, and the maximum was measured with $25 vol\% H_2O$ in the stripping gas, where 84% of CO_2 was separated from the flue-gas.

4.2 Variation of stripping steam flow rate
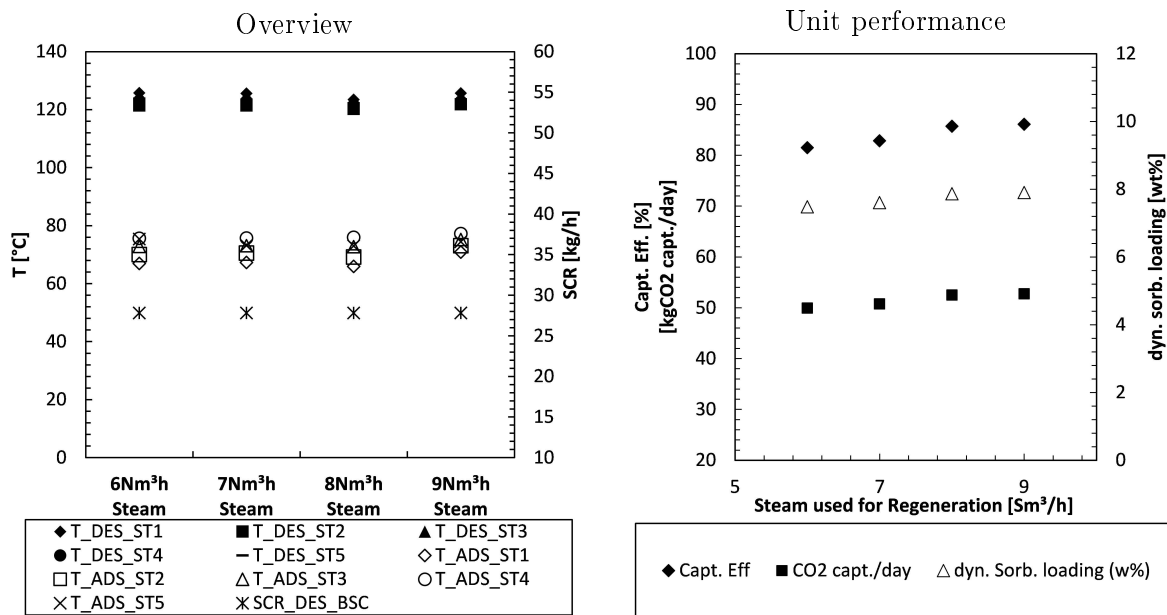
Figure 4.2: Experimental data from the variation of stripping gas flow rate in the desorber at BC conditions.

As mentioned in Chapter 2.1, the energy demand of the desorption step of an adsorption process influences its thermodynamic efficiency. Since the production of less steam would result in a lower energy demand, it was investigated to what extent the BSU's performance depends on the stripping gas (steam) flow rate, and whether a lower steam flow rate, relative to BC conditions, can be considered. For this reason, the BSU was set to BC conditions and the flow rate of steam to the desorber was altered; after steady-state conditions were reached, each operating point was recorded. A decrease in fluidization rate at constant inventory, is accompanied by a decrease in bed voidage and a decrease in bubble size, which are both essential for solids transport over the weirs. To avoid the depletion of the buffer, the flow rate of stripping steam was not adjusted to values below $6 Sm^3/h$. As can be seen in the overview of Figure 4.2 the flow rate of stripping agent has no considerable effect on the temperatures of either columns; the temperatures in the adsorber column varied between $67°C$ and $77°C$, whereas the temperatures of the desorber stages were between $120°C$ and $126°C$. In the graph showing the performance indicators as a function of the total feed rate of stripping steam, the same correlation between the capture efficiency and the capture rate as well as the dynamic sorbent loading, as in the variation of H_2O in stripping gas persists, since the SCR or adsorber feed gas had not been varied. It can also be seen, that by increasing the total feed rate of steam, the capture efficiency increases from $81,5\%$ at $6 Sm^3/h$ to $86,1\%$ at $9 Sm^3/h$. The largest change in capture efficiency can be seen between $7 Sm^3/h$ and $8 Sm^3/h$, where an

improvement in capture efficiency of $2,9\%$ was observed. A further increment of steam fed to the desorber (from $8Sm^3/h$ to $9Sm^3/h$) barely had an effect on the unit's performance (capture efficiency improvement of $0,9\%$). Additionally, the dynamic sorbent loading was between $7,5wt\%$ and $7,9wt\%$, and the capture rate was between $49,9kg$ and $52,7kg$ of CO_2 per day.

4.3 Variation of H_2O in adsorber feed gas
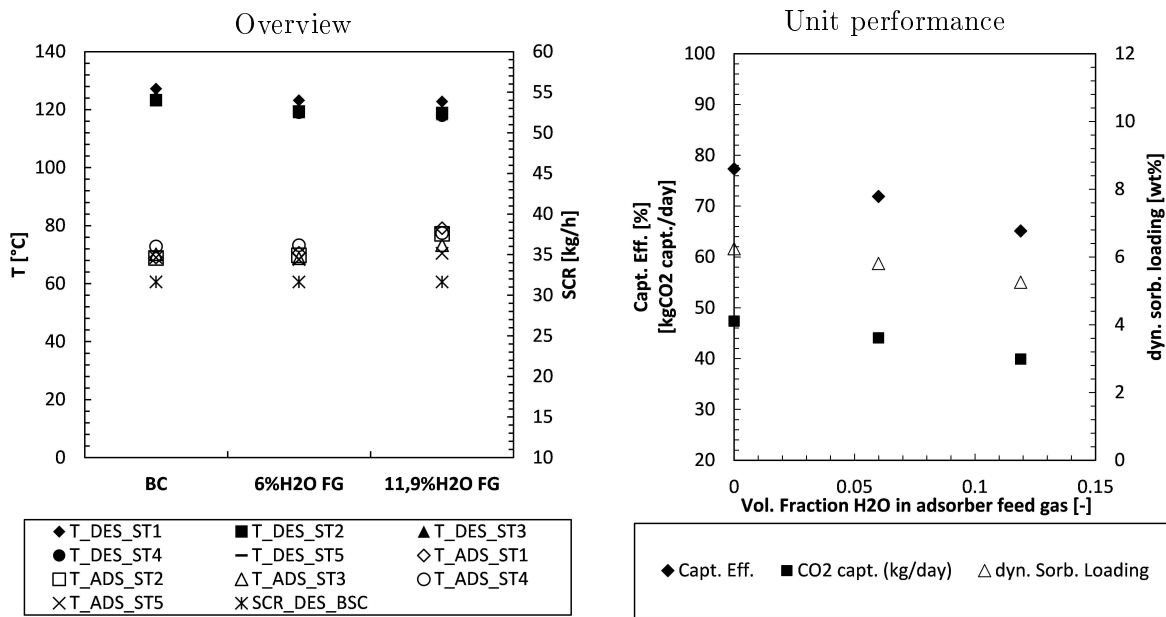
Figure 4.3: Experimental data from the variation of H_2O in adsorber feed gas at BC conditions.

As it is unlikely that a PCC unit at a demonstration scale would treat dry flue-gases, wet flue-gases were tested to spot potential means of improvement. Further, the internal heat-pump effect observed in Chapter 4.1 can easily be confirmed, as this effect should weaken with increasing humidity of the adsorber feed gas. This variation was conducted simply by setting BC conditions, with a SCR of $32kg/h$, and successively increasing the amount of steam entering the adsorber from $0vol\%H_2O$ to $6vol\%H_2O$ (steam dew point at $\approx 37°C$) and finally to $11,9vol\%H_2O$ (steam dew point at $\approx 50°C$), while keeping the total flow rate of adsorber feed gas at $16,8Sm^3/h$ with a CO_2 concentration of $7,7vol\%CO_2$. The behavior of the desorber and adsorber stage temperatures (see overview of Figure 4.3) is in accordance with the predictions concerning the weakening of the internal heat-pump effect. The desorber stage temperatures decreased (from $127°C-123°C$ to $123°C-117°C$) as less steam was adsorbed onto the sorbent material; further, the adsorber stage temperatures increased (from $69°C-73°C$ to $70°C-79°C$), as the desorption of steam got unfavorable in the already humid environment of the adsorber. Further, the axial temperature dispersion in both columns increases with increasing adsorber feed gas humidity;

$4°C$ in both adsorber and desorber at BC versus $9°C$ in the adsorber and $6°C$ in the desorber column at $11,9vol\%H_2O$ in the adsorber feed gas. As to compensate the increasing temperatures in the adsorber, the coolant flow rate was increased, which lead to the condensation of steam; this was accompanied by the adhesion and accumulation of solids, on the heat-exchanger surfaces, especially in the top-most adsorber stages. For this reason, the necessary amount of heat could not be displaced from the adsorber column, resulting in a poor performance (see unit performance in Figure 4.3). Obviously, the low forward-flow temperature of the coolant significantly contributed to the condensation of steam; to avoid potential damage of the particles, the steam content of the adsorber feed gas was not increased above $11,9vol\%H_2O$.

4.4 Variation of SCR
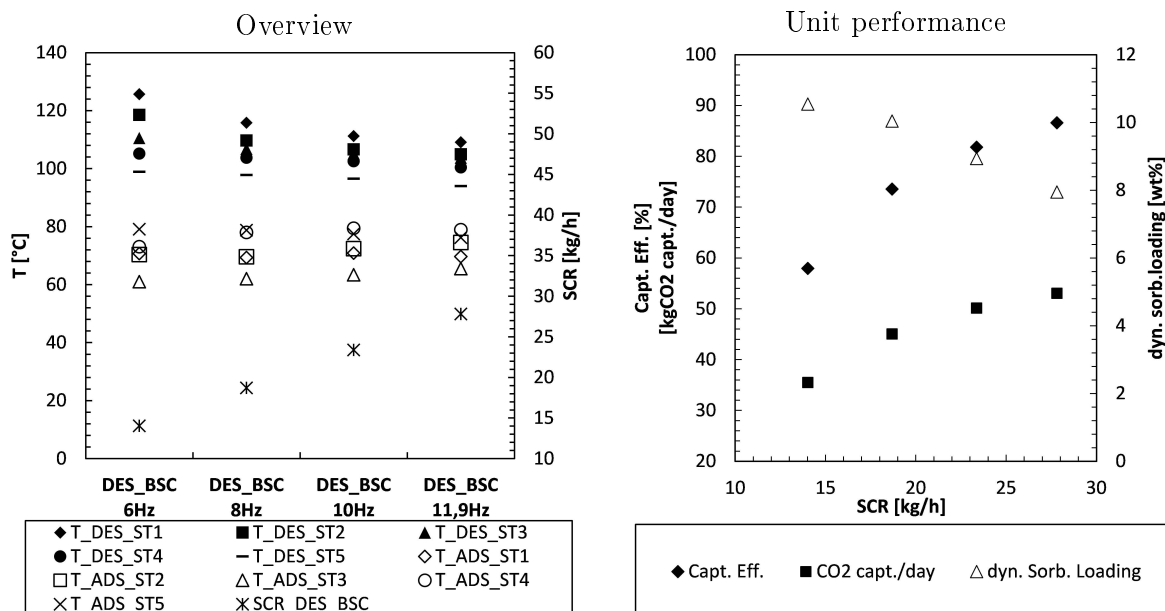
Figure 4.4: Experimental data from the variation of the solids circulation rate at BC dry conditions.

By varying the sorbent circulation rate between both contactors, the residence time of the particles in each of the reactors is altered as well. To investigate the effects of the SCR on the unit's operating stability, performance as well as temperatures, the solid circulation rate was varied in four steps from $14kg/h$ to $28kg/h$ (based on unloaded sorbent mass), whereas all other parameters were kept at BC dry settings. During the SCR variation, a significant drop in stage temperatures as well as in axial temperature dispersion in the desorber column was observed as the SCR was increased. The temperatures in the adsorber column stayed in the range of $61°C$ and $79°C$, with a fairly constant axial temperature dispersion (see overview of Figure 4.4); however coolant flow was increased to accommodate the increasing cooling demand. At a SCR of $14kg/h$ (or desorber BSC

frequency of $6Hz$), the temperatures in the desorber column varied between $99°C$ in stage 5 (uppermost stage) and $126°C$ in stage 1 (lowermost stage). The temperature range gets lower and narrower until the maximum SCR ($28kg/h$ or $11,9Hz$) is reached, with $94°C$ in the top-most and $109°C$ in the lower-most stage. This effect is owed to the limited heat input in the desorber together with the decreasing residence time of solids in each stage. Hence, causing the solids to be further away from thermal equilibrium at higher SCRs. The adsorber stages on the other hand, could be sufficiently cooled even at high SCRs, as the coolant forward-temperature was low enough. Increasing the SCR significantly improves the BSU's capure efficiency and capture rate at the cost of a lower dynamic sorbent loading, as can be seen in the graph showing the unit's performance in Figure 4.4. The dynamic sorbent loading, reached a maximum of $10,5wt\%$ at a circulation rate of $14kg/h$ and decreased with increasing solids circulation rate to $7.9wt\%$ at $28kg/h$. The capture efficiency went from 58% at 14 kg/h to 87% at $28kg/h$ and the amount of CO_2 captured by day increased from $35kg$ to $53kg$. High capture efficiencies correspond to low CO_2 partial pressures (relative to the CO_2 partial pressure in the treated flue gas) in the offgas of the adsorber. These low CO_2 partial pressures in turn correspond to a relatively low loading of sorbent material in the uppermost stage of the adsorber. As increasing sorbent circulation rates allow for achieving lower adsorbent loadings the equilibrium CO_2 partial pressure in the uppermost stage decreases; thus, the capture efficiency increases. Above $\eta_{captured} = 90\%$, a large increase of the SCR is necessary to achieve a significant increase of the capture efficiency. Hence, even though the amount of captured CO_2 increases, the dynamic sorbent loading decreases as the increase of the SCR dominates.

4.5 Variation of $c_{CO_2,Ads,in}$
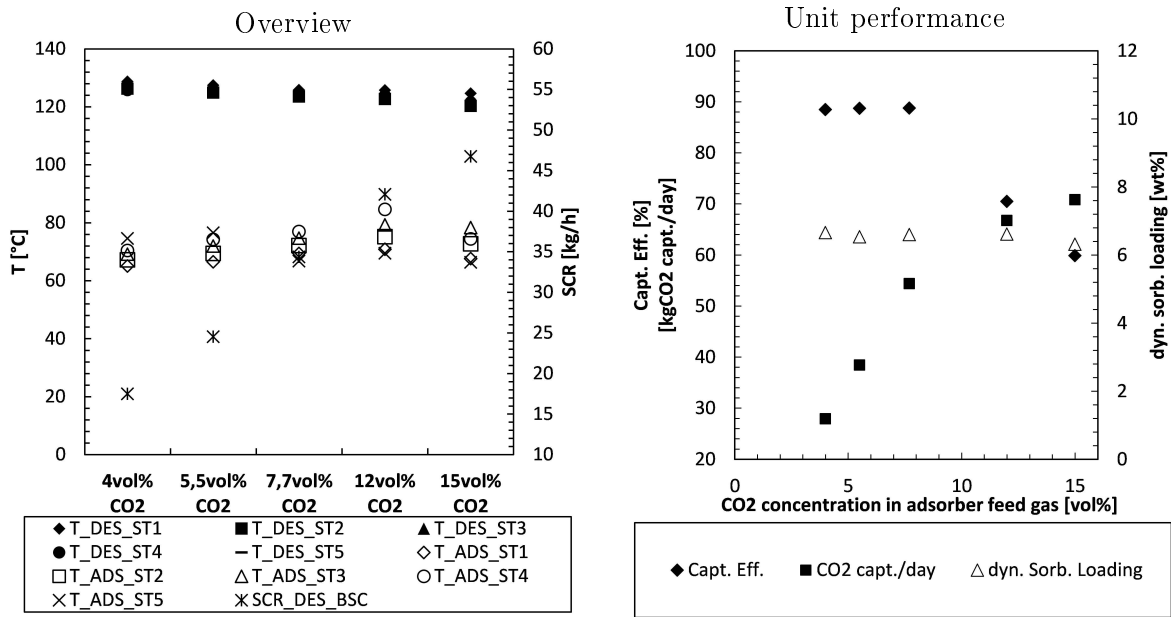
Figure 4.5: Experimental data from the variation of the CO_2 concentration in the adsorber feed at base-case conditions with $U/U_{mf} = 10$ in the adsorber and an SCR adaptation to achieve a dynamic sorbent loading of approximately $6,5wt\%$.

As shown in Table 1.2, the CO_2 concentration of flue-gases from natural gas or coal fired power plants can range from $4vol\%CO_2$ to $15vol\%CO_2$ respectively. In order to test the BSU's flexibility in terms of CO_2 concentration, five operating points each with a different CO_2 concentration in the adsorber feed gas were tested. The CO_2 concentration was successively increased from $4vol\%CO_2$ to $15vol\%CO_2$, while the SCR was altered to obtain a dynamic sorbent loading of approximately $6,5wt\%$; the remaining operating parameters were kept at BC conditions. Initially, the calculated dynamic sorbent loading was $7,1wt\%$. However, as incorrect bulk density data was utilized and corrected after the experiment, the dynamic sorbent loading turned out to be around $6,5wt\%$. The overview of Figure 4.5, shows that the SCR had to be increased with increasing CO_2 concentration in the adsorber feed-gas, to achieve the dynamic sorbent loading which was agreed upon. Since super-heated steam with a temperature of approximately $140°C$ was used as a stripping agent, desorber stage temperatures of $126°C - 129°C$ at a CO_2 concentration of $4vol\%CO_2$ and a SCR of $17,5kg/h$, and $120°C - 125°C$ at $15vol\%CO_2$ and $46,8kg/h$, were reached. Differently to the variation of the SCR, the high SCRs at $12vol\%CO_2$ and $15vol\%CO_2$ lead to a slight increase of axial temperature dispersion in the desorber column. As can be seen in the graph showing the unit performance in Figure 4.5, the capture rate in $kg_{CO_2capt.}/day$ increases considerably and seems to flatten out beyond $12vol\%CO_2$ in the adsorber feed gas. These high capture rates require an appropriately high heat input for

regenerating the loaded sorbent material. The correlation between the flattening of the capture rate and the increase of the axial temperature dispersion of the desorber indicate, that the required heat input had considerably exceeded the actual heat input. Similarly to the SCR variation, a slight increase of adsorber stage temperatures was observed with increasing SCR, between $4vol\%CO_2$ and $12vol\%CO_2$ ($65°C - 75°C$ and $70°C - 85°C$). During the $15vol\%CO_2$ operating point, coolant flow was drastically increased leading to temperatures between $66°C$ in the top-most stage and $78°C$ in the third stage. The capture efficiency was fairly stable (between $88,5\%$ and $88,8\%$) up to $7,7vol\%CO_2$ and underwent a drastic drop with $67,7\%$ at $12vol\%CO_2$ and $59,9\%$ at $15vol\%CO_2$. However, the CO_2 capture rate increase with an increasing CO_2 concentration in the adsorber feed gas. Since the capture efficiency is quite stable, between $4vol\%CO_2$ and $7,7vol\%CO_2$, the capture rate is almost proportional to the SCR, and shows nearly linear behavior in this range; with $27,9kg_{CO_2capt.}/day$ at $4vol\%CO_2$, $38,5kg_{CO_2capt.}/day$ at $5,5vol\%CO_2$ and $54,4kg_{CO_2capt.}/day$ at $7,7vol\%CO_2$. As mentioned, the capture rate slightly flattens, with $66,8kg_{CO_2capt.}/day$ at $12vol\%CO_2$ after reaching a maximum of $70,8kg_{CO_2capt.}/day$ at $15vol\%CO_2$. At high SCRs the slip of steam, from the desorber to the adsorber column, was observed; as to avoid this slip, a relatively low flow rate of N_2 ($0,1Sm^3/h - 0,3Sm^3/h$) was set as a purge gas stream at the standpipe above the desorber BSC. This minor flow of purge gas significantly decreased the amount of solids which coated the surfaces of heat-exchangers in the top-most adsorber stages.

4.6 Variation of U/U_{mf} in the adsorber
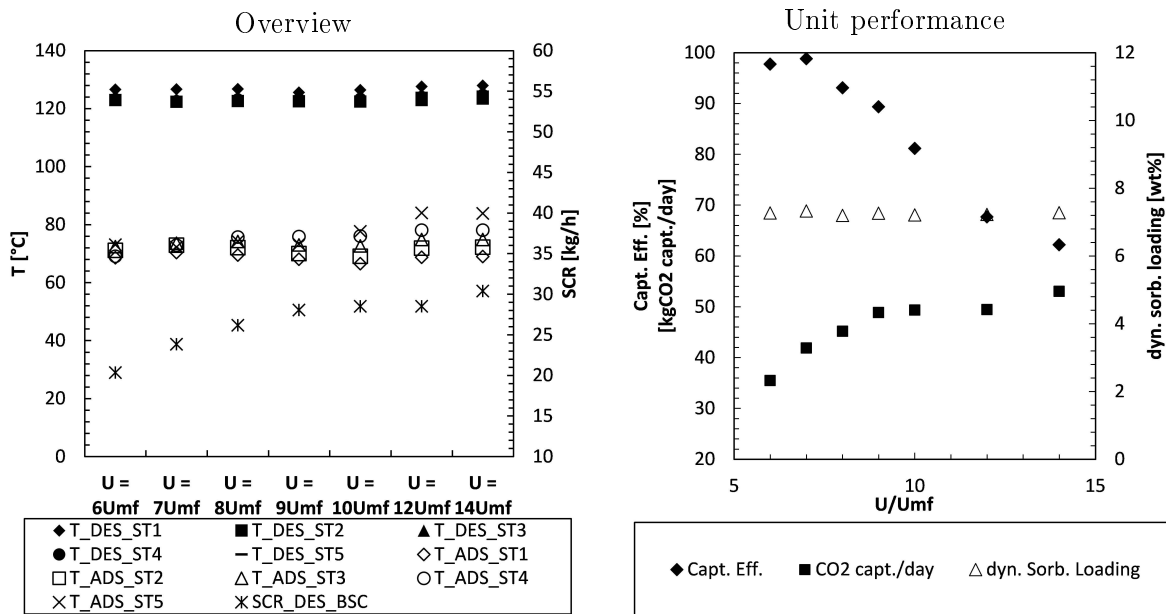
Figure 4.6: Experimental data from the variation of U/U_{mf} in the adsorber at base-case conditions with $7,7vol\%CO_2$ in the adsorber feed gas and a SCR adaptation to achieve a dynamic sorbent loading of approximately $7,1wt\%$.

The flexibility in terms of the volumetric flow rates of flue-gas, is essential, as the flow rate of flue-gas streams can alter with e.g. the electrical power demand of a power plant, or heat demand in industrial processes. To ensure optimal incineration of combustibles, the air-to-fuel-ratio wouldn't be drastically altered when decreasing the fuel feed, this would resulting in a similar CO_2 concentration and a decreasing flow rate of flue-gas. For this reason, the flow rate of simulated flue-gas, with $7,7vol\%CO_2$, was varied from $U/U_{mf} = 6$ to $U/U_{mf} = 14$, resulting in a volumetric flow rate of $10,1Sm^3/h$ to $23,4Sm^3/h$. The SCR at each operating point was adapted to reach a dynamic sorbent loading of $7,1wt\%$. The desorber stage temperatures stayed fairly constant and within a range of $122°C$ and $128°C$ (see overview of Figure 4.6). The adsorber stage temperatures on the other hand, slightly increased with increasing fluidization rates and exhibited an increase in axial temperature dispersion, at values exceeding $U/U_{mf} = 9$. Additionally, the SCR had to be successively increased with increasing fluidization rates; from $20,3kg/h$ at $U/U_{mf} = 6$ to $30,4kg/h$ at $U/U_{mf} = 14$. With a smaller change of SCR ($2,4kg/h$) between $U/U_{mf} = 9$ and $U/U_{mf} = 12$. As can be seen by the unit performance in Figure 4.6, more or less the same amount of CO_2 is captured (per day), beyond $U/U_{mf} = 9$, while the adsorber's axial temperature dispersion increases; this indicates that the necessary amount of heat could not be displaced to continue the steep trend of the capture rate which was observed between $U/U_{mf} = 6$ and $U/U_{mf} = 9$. Further, it is possible that an increase

in bubble size, leads to an increasing surface of the heat-exchangers to be engulfed by bubbles, making heat transfer unfavorable (see Chapter 2.2.1). Decreasing residence times of flue-gas in the adsorber column, as well as decreasing inventory in each of the adsorber stages, caused by an increasing voidage of the fluidized beds, contribute to the unfavorable CO_2 capture performance (see unit performance in Figure 4.6) at increasing ratios of U/U_{mf}. The capture efficiency drastically decreases between $U/U_{mf} = 7$ with $98,8\%$ and $U/U_{mf} = 14$ with $62,2\%$. The initial increase of the capture efficiency, from $97,7\%$ to $98,8\%$ between $U/U_{mf} = 6$ and $U/U_{mf} = 7$, suggests that the operating conditions at $U/U_{mf} = 7$, were optimal for gas-solid mixing and for the displacement of the heat of adsorption, as both inventory and residence time was higher at $U/U_{mf} = 6$. Yet this cannot be said for sure, as a difference in capture efficiency of $1,1\%$, is equal to a change of approximately $0,09 vol\% CO_2$ in the adsorber gas outlet, which in turn is the range of gas-analyzer linearity. The amount of CO_2 captured per day, increases steadily from $35,5 kg_{CO_2capt.}/day$ to $48,8 kg_{CO_2capt.}/day$, between $U/U_{mf} = 6$ and $U/U_{mf} = 9$; the greatest increase being between $U/U_{mf} = 6$ and $U/U_{mf} = 7$ with $6,4 kg_{CO_2capt.}/day$ (to $41,9 kg_{CO_2capt.}/day$). A further increase of the fluidization rate merely affected the capture rate; as an additional increase from $U/U_{mf} = 7$ to $U/U_{mf} = 14$ increased the capture rate by only $4,3 kg CO_2/day$ to $53 kg CO_2/day$.

4.7 Variation of weir height

So far, all experiments were conducted with $60mm$ weirs installed in both columns. Increasing the weir weight, or the distance between gas distributor and weir edge, of a fluidized bed stage can have various positive effects. These advantages include an increased solids residence time, caused by an increased solids inventory in the stages, or improved tube to bed heat transfer, as a larger portion of the heat-exchanger is immersed in the bed. However, these advantages are at the cost of an increased pressure drop. In order to test the influence of an increased weir height on the BSU's performance, $80mm$ weirs were installed in both columns; additionally, the effect of $80mm$ weirs in the adsorber and $60mm$ weirs in the desorber, as well as vice versa, were investigated. These weir height variations were conducted at five different operating points. Comparison of the results should indicate the influence of increased active inventory as well as of the inventory distribution between adsorber and desorber.
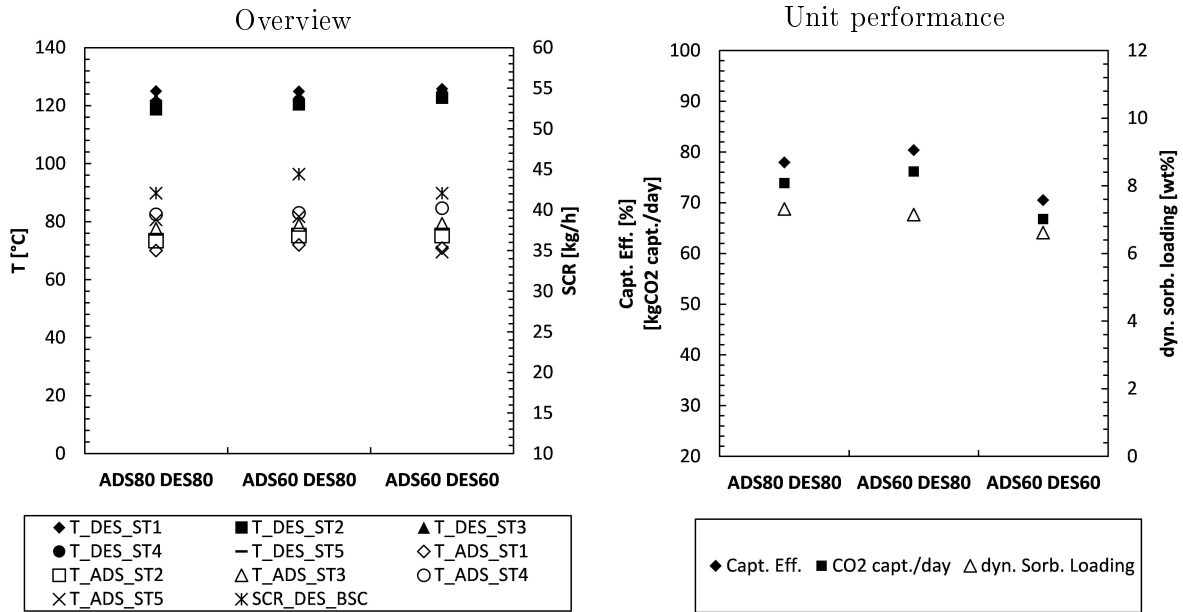
4.7.1 Base-case dry at a constant SCR
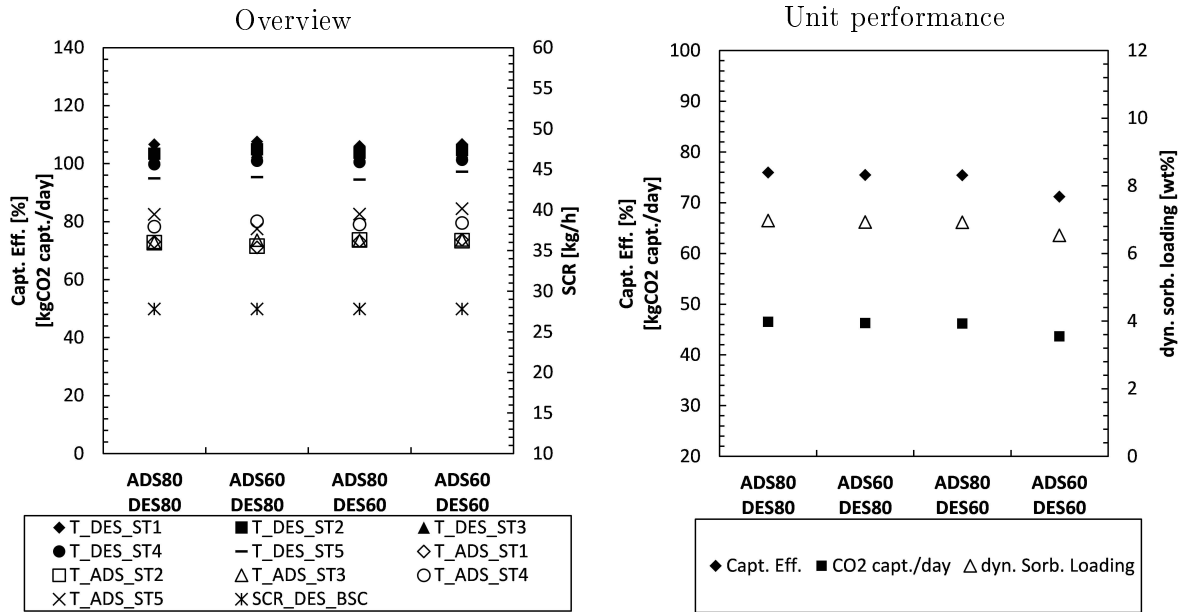
Figure 4.7: Experimental data from the variation of adsorber and desorber weir heights at base-case dry conditions.

As can be seen in Figure 4.7, the adsorber or desorber stage temperatures seem to be independent from the weir height at BC dry operating conditions; the stage temperatures range from $71°C$ to $84°C$ in the adsorber, and from $94°C$ to $108°C$ in the desorber stages. A minor decrease in axial temperature dispersion in the desorber, from $11,7°C$, when both columns were equipped with $80mm$ weirs, to $9,5°C$ in the $ADS60 - DES60$ configuration, was measured. The unit's performance (see Figure 4.7) on the other hand, is significantly better when $80mm$ weirs are used in either, or both of the columns. In these cases, the capture efficiency is between 75% and 76%, the amount of captured CO_2 ranged from $46,2kg_{CO_2capt.}/day$ to $46,5kg_{CO_2capt.}/day$, and the dynamic sorbent loading was between $6,9wt\%$ and $7wt\%$. When $60mm$ weirs were installed in both columns, the capture efficiency only reaches 71%; further, the dynamic sorbent loading was $6,5wt\%$ and the capture rate was $43,6kg_{CO_2capt.}/day$.

4.7.2 Base-case at a constant SCR
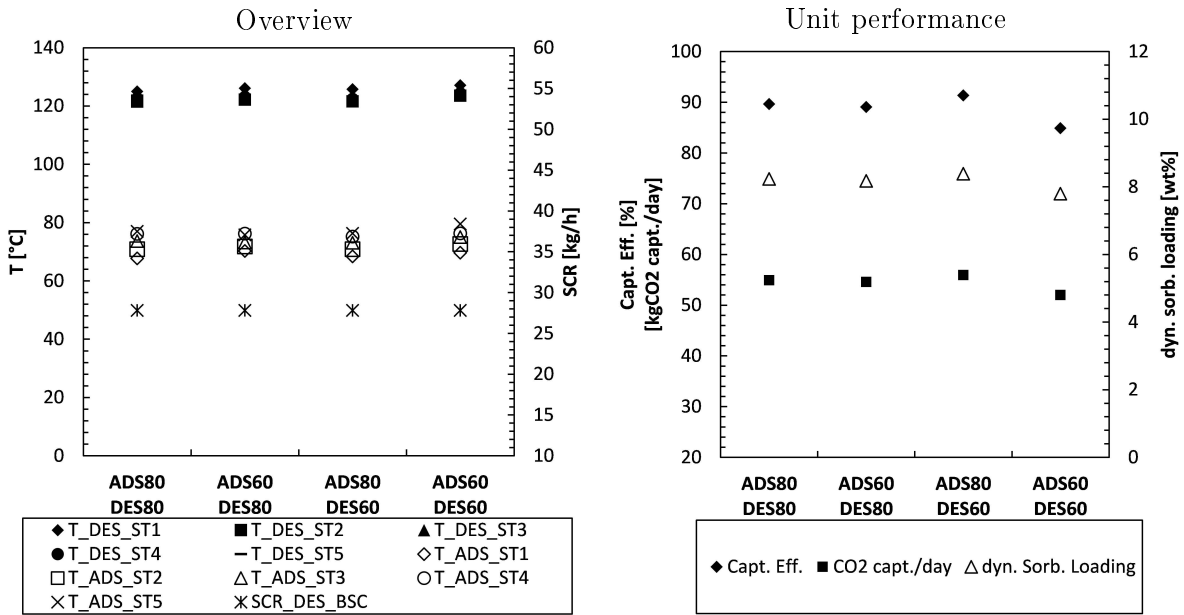
Figure 4.8: Experimental data from the variation of adsorber and desorber weir heights at base-case conditions.

Similarly to the weir height variation during BC dry conditions, the stage temperatures of both column stay rather constant during the weir height variation at BC conditions. However, decreased adsorber temperatures ($68°C - 80°C$) and increased desorber temperatures ($124°C - 129°C$) relative to the weir height variation at BC dry conditions, again indicate the presence of an internal heat-pump effect when regenerating with steam. The unit's performance, shown in Figure 4.8, reveals that the combination of $80mm$ weirs in the adsorber and $60mm$ weirs in the desorber shows a slightly better performance ($\eta_{Captured} = 91\%$, $dSl = 8,4wt\%$ and $55,9kg_{CO_2capt.}/day$) than is the case when $80mm$ weirs are used in both columns ($\eta_{Captured} = 90\%$, $dSl = 8,2wt\%$ and $54,9kg_{CO_2capt.}/day$). When the adsorber is equipped with $60mm$ weirs, the capture efficiency falls below 90%, with 89% when $80mm$ weirs were installed in the desorber and 85% with $60mm$ weirs in the desorber. When both columns were equipped with $60mm$ weirs, a considerably worse dynamic sorbent loading (7,8wt%) and amount of CO_2 captured ($52kg_{CO_2capt.}/day$) than in the $ADS60 - DES80$ configuration ($dSl = 8,2wt\%$ and $54,6kg_{CO_2capt.}/day$) was observed.

4.7.3 BC with $\eta_{Captured} = 90\%$
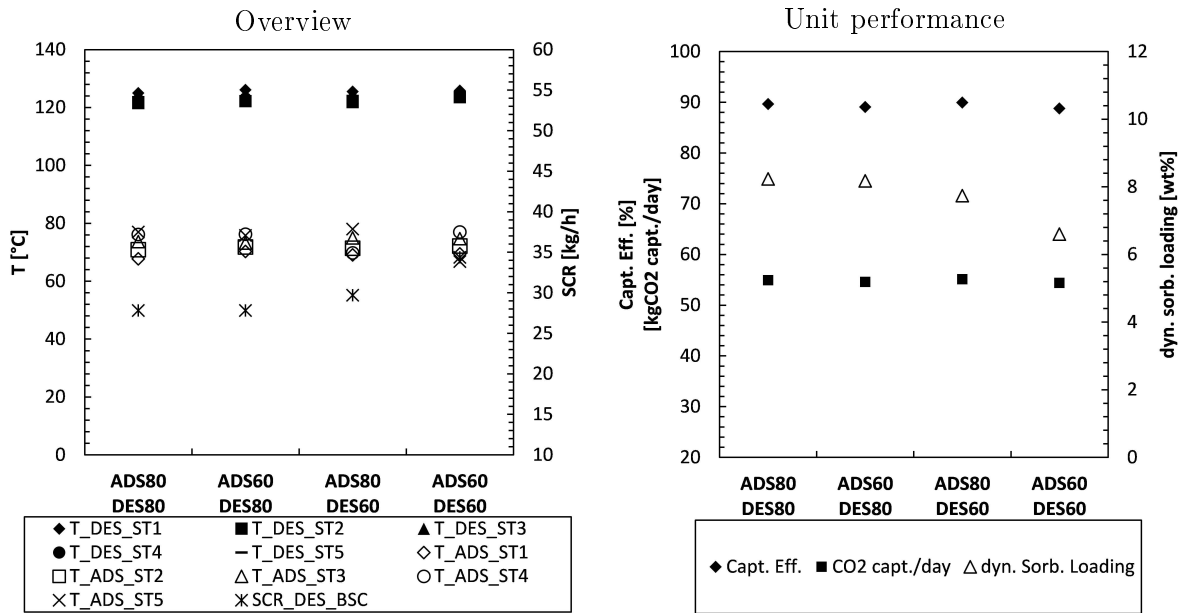
Figure 4.9: Experimental data from the variation of adsorber and desorber weir heights at base-case conditions with a SCR adaptation to achieve a capture efficiency of 90%.

In this experiment, BC conditions were set, and the SCR was adapted to reach a capture efficiency of 90%. As shown in the overview of Figure 4.9, the SCR had to be increased beyond $28kg/h$, for configurations where $60mm$ weirs were installed in the desorber; e.i $32kg/h$ when the adsorber was equipped with $80mm$ weirs and $35kg/h$ when $60mm$ weirs were used in both columns. The lowest SCR ($27kg/h$) had to be set in the configuration $ADS60 - DES80$. Similarly to the SCR variation, the axial temperature dispersion in the desorber decreases slightly with increasing SCR, nevertheless the desorber stage temperatures stayed between $122°C$ and $126°C$ during all experiments. The adsorber stage temperatures could be kept within a range of $67°C$ and $78°C$ by adjusting the cooland flow. As can be seen in the graph showing the unit's performance indicators at different unit configurations in Figure 4.9, the capture efficiency could be kept between 89% and 90%. As the adsorber feed gas was left unchanged, the amount of CO_2 captured is directly proportional to the capture efficiency and was within $54,4kg_{CO_2capt.}/day$ and $55,1kg_{CO_2capt.}/day$. For the same reason, the dynamic sorbent loading is approximately inversely proportional to the SCR, and decreases from $8,2wt\%$, when $80mm$ weir were installed in the desorber, to $7,7wt\%$ at the $ADS80 - DES60$ configuration. Yet, the greatest decrease ($1,1wt\%$) was observed when both columns were equipped with $60mm$ weirs, where a dynamic sorbent loading of only $6,6wt\%$ was achieved.

4.7.4 BC with $dSl \approx 7,1wt\%$
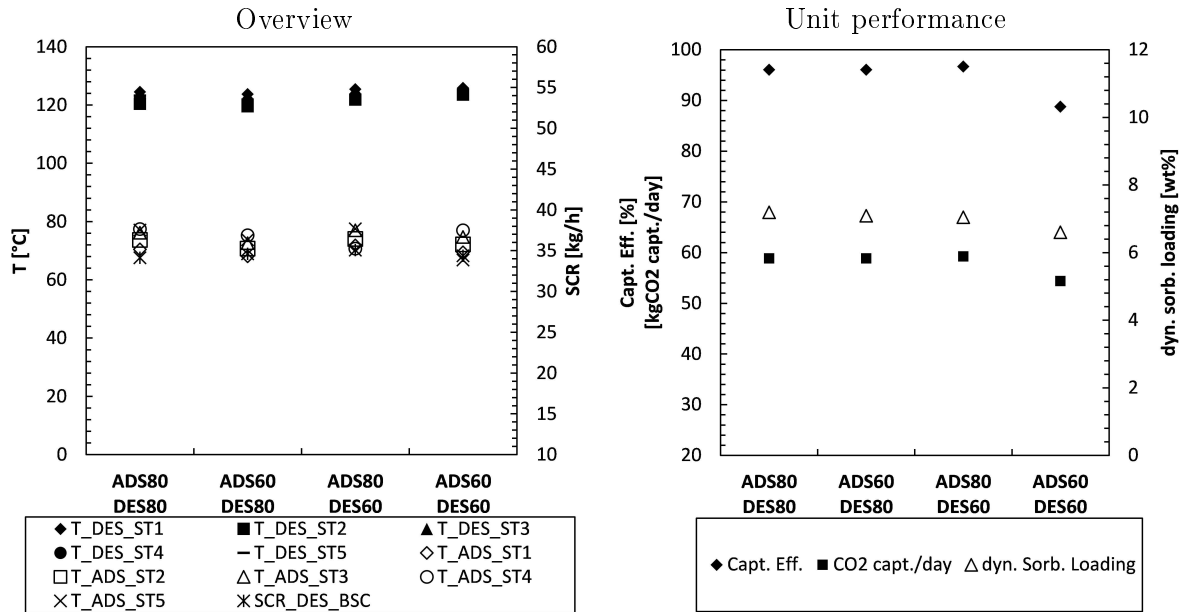
Figure 4.10: Experimental data from the variation of adsorber and desorber weir heights at base-case conditions with a SCR adaptation to achieve a dynamic sorbent loading of approximately $7,1wt\%$.

In this series of experiments, the weir heights of both columns was varied; base-case conditions were set and the SCR adapted to reach a value of approximately $7,1wt\%$ dynamic sorbent loading. The adsorber as well as desorber stage temperatures, as seen in the overview of Figure 4.10, stay within a temperature range of $67°C$ to $78°C$ in the adsorber and $120°C$ to $126°C$ in the desorber. Similarly to the weir height variation at BC dry conditions, a mere decrease in the axial temperature dispersion (from $\approx 4,1°C$ to $2,3°C$) in the desorber is observed, when $60mm$ weirs were used in both columns, relative to the remaining unit configurations. The SCR stayed within a narrow range for this weir height variation, ranging from $27kg/h$ to $35kg/h$. However, it must be stated that for the $ADS60 - DES60$ unit configuration, an incorrect value for the bulk density of the sorbent material was used; the dynamic sorbent loading was around $6,6wt\%$ rather than $7,1wt\%$, and the SCR had increased (inversely proportional to the change in dynamic sorbent loading) upon correction. The unit's performance in Figure 4.10 shows, that the BSU's performance was quite similar when $80mm$ weirs were used in either or both columns; the capture efficiency was within a range of $96\% - 97\%$ and the capture rate between $58,8kg_{CO_2capt.}/day$ and $58kg_{CO_2capt.}/day$. The configuration where $60mm$ weirs were used in both, adsorber and desorber, columns showed the worst performance and would have probably performed even worse, were the SCR reduced to meet a dynamic sorbent loading of $7,1wt\%$ (see Figure 4.4).

4.7.5 BC with $c_{Ads,in} = 12vol\%CO_2$ & $dSl \approx 7,1wt\%$

Figure 4.11: Experimental data from the variation of adsorber and desorber weir heights at base-case conditions with $12vol\%CO_2$ in the adsorber feed gas and an SCR adaptation to achieve a dynamic sorbent loading of approximately $7,1wt\%$.

In this weir height variation, a simulated flue-gas with $12vol\%CO_2$ was fed to the adsorber, to investigate whether the weir height also influences the BSU's capture performance at particular high CO_2 concentrations. Due to a lack of time, the unit configuration $ADS80 - DES60$ was not tested under these conditions. Similarly to the weir height variations at BC dry and BC with $dSl \approx 7,1wt\%$, the overview in Figure 4.11 shows, that the axial temperature dispersion in the desorber again decreases (from $6,3°C$ to $3,1°C$) when both columns had $60mm$ weirs installed. It can also be seen that the necessary amount of heat could not be discharged from the adsorber column by means of increasing the coolant flow, as the temperatures in the column were within a rather broad range (from $69°C$ to $85°C$). When $60mm$ weirs were installed in both columns, the axial temperature dispersion of the adsorber rose to an unprecedented level ($15,1°C$); this indicates, that the bed height in the adsorber stages were too low to engulf the necessary heat-exchanger surface area. This lead to insufficient heat displacement, which was also reflected by a poor capture efficiency (see Figure 4.11) of only 70%; nevertheless, compared to the previous variations a large amount of CO_2 was captured ($70,5kg_{CO_2capt.}/day$). During this variation, the SCR had to be increased considerably, relative to the previous experiments, in order to achieve the low dynamic sorbent loading of approximately $7,1wt\%$; $42kg/h$ was set in the configurations ADS60-DES60 as well as ADS80-DES80, and $44kg/h$ in the $ADS60 - DES80$ configuration. However, these high SCRs showed, similarly to the variation of CO_2 in the adsorber feed gas, high amounts of steam slip from the

desorber to the adsorber. A significant improvement of the unit's performance is seen, when $80mm$ weirs were installed in the desorber column. An adsorber stage weir height of $80mm$ resulted in a capture efficiency of 78% and $76, 1kg_{CO_2capt.}/day$. $60mm$ weirs in the adsorber and $80mm$ weirs in the desorber further improved the capture efficiency and amount of CO_2 captured, with 80% and $76, 2kg_{CO_2capt.}/day$ respectively. As in the weir height variation at BC with $dSl = 7, 1wt\%$, the $ADS60 - DES60$ configuration was also carried out with an incorrect bulk density of the sorbent material; upon correction, the dynamic sorbent loading was calculated to $6, 5wt\%$.

Chapter 5

Discussion

The decrease of the axial temperature dispersion in the desorber column, when steam is used as a fluidization gas, indicates that a higher contribution to the heat demand is made by steam than by N_2. This can be explained by the internal heat-pump effect, where, in the desorber column, steam is adsorbed on the sorbent material's surface and the corresponding heat of adsorption is released; this heat partially compensates the energy required for the regeneration of loaded sorbent material. At this stage however, it is not clear, whether the observed internal heat-pump effect is caused by chemisorption or physisorption of steam, nor is it known whether steam is involved in the reaction with adsorbed CO_2 and the formation of bicarbonates. In order to fully understand the effect steam had on the conducted experiments, the behavior of the utilized sorbent material in the presence of different gas mixtures consisting of N_2, CO_2 and steam at the BSU's operating temperatures should be investigated using TGA or a fixed bed configuration. A configuration of the TGA with differential scanning calorimetry (DSC), for measuring the corresponding heats of adsorption and regeneration, is recommended.

A problem which was encountered quite often during the experimental campaign, particularly at high SCRs, was the condensation of steam on the surface of the heat-exchangers in the top-most adsorber stages; this was accompanied by the adhesion of particles thereon and reduced tube-to-bed heat transfer. A particularly low purge gas stream in the stand-pipe leading to the desorber BSC, diminishes the slip of steam; the increase of the coolant temperature considerably reduced the subsequent condensation of steam on the adsorber heat-exchangers. Yet, since a certain transport of steam from the desorber to the adsorber, by whichever means (slip or co-adsorption), is favorable for the process, either the coolant flow, the coolant temperature, or the heat-exchanger surface altogether, must be altered in such a way, that the heat-exchanger surface temperature does not fall below the dew point of the flue-gas, while the necessary amount of heat is discharged, to attain an acceptable unit performance, even when humid flue-gases are fed to the adsorber.

As it was shown, the capture efficiency undergoes a mere decreases when the flow rate of steam to the regenerator was decreased. In particular, decreasing the amount of stripping

steam by 30% reduced the process performance by only 4,7%. This minor loss can be explained by two means; lower tube-to-bed heat transfer, as a consequence of lower particle convection at decreased fluidization velocities, and by a decreased dilution of CO_2 with steam.

The desorber configurations with an increased weir height, which entailed an increased solids inventory as well as enhanced tube-to-bed heat transfer, were at an advantage over lower weir heights, regarding CO_2 capture performance. This indicates that there is a trade-off between the amount of steam used to fluidize the desorber column, the inventory of solids needed therein and the unit's performance. As to reduce the steam demand of the desorber without a performance penalty, yet at the cost of a higher pressure drop across the column, reducing the desorber cross-section, while simultaneously increasing the desorber stage inventories and the fraction of heat-exchanger surface immersed in the fluidized bed, can be considered. Alternatively, an additional desorber stage could have a similar effect.

The dominance of the SCR over the dynamic sorbent loading of particles regarding the capture efficiency suggests, that if high capture efficiency should be achieved, high SCRs should be pursued at the cost of lower dynamic sorbent loadings. However, since a slip of steam from the adsorber to the desorber was observed at high SCRs, a slip of gases in the opposite direction can also be expected. The latter is more problematic, as this would threaten the purity of the desorbate. For this reason, it is recommended to investigate the slip from the adsorber to the desorber at different SCRs, as well as the possibility of its reduction by means of a suitable purge gas flow into the standpipe above the adsorber BSC.

Should the capture efficiency be increased without alteration of the SCR, an increase of heat transfer between heat exchanger tubes and the fluidized bed as well as an increase of the solids residence time in either, or both columns, can be considered. This can be done, by means of higher weirs; this possibility is again connected to an increase of the pressure drop across the columns and a potential increase of the mechanical power demand of the flue-gas blower.

Additionally, increasing the contact time between flue-gas and sorbent in the adsorber by means of an additional adsorber stage or an increased adsorber cross-section, allowing for lower U/U_{mf} at the same volumetric flow of flue-gas, could allow for higher capture efficiencies. However, it must be stated that changes regarding the adsorber column, can only improve the unit performance if the desorption step does not limit process performance.

In Figure 5.1 the amount of CO_2 captured (in $kg_{CO_2capt.}/day$) from the CO_2 concentration variation in the adsorber feed gas, at a constant ratio U/U_{mf}, as well as from the variation of U/U_{mf} in the adsorber, at a constant CO_2 concentration, can be seen as a function of the

amount of CO_2 fed to the adsorber (in $kg_{CO_2capt.}/day$). The two sets of experiments were not carried out at the same dynamic sorbent loading (detailed explanation in Chapters 3 & 4), therefore the results do not match at BC conditions. The different trends for the two variations can be explained by the following: higher CO_2 partial pressures in the adsorber feed gas allow for higher sorbents loadings in the adsorber. Due to the already mentioned dominance of the SCR over the dynamic sorbent loading regarding the capture efficiency, a higher amount of CO_2 can be captured when higher concentrated flue-gases are treated.

In most weir-height variation experiments where the SCR was not altered between the different unit configurations, the $ADS60 - DES60$ configuration exhibited an inferior performance, relative to the unit configurations where $80mm$ weirs were installed in either or both columns. This indicates, that either an increase in tube-to-bed heat transfer, an increased solids residence time in the contactors or a combination thereof induced an improved unit performance. Whether one of these effects dominates the observed performance enhancement cannot be said for sure at this stage.

The impact of sorbent degradation on the BSU's performance could not be clarified within this experimental campaign. A slight increase of the capture efficiency at BC conditions was

Figure 5.1: Graph showing the results of the CO_2 concentration variation in the adsorber feed gas as well as the results of the U/U_{mf} variation in the adsorber at constant CO_2 concentration in the adsorber feed gas.

noticed, when a fresh batch of sorbents was used, however this effect lasted for less than an hour. Furthermore, the entrained solids were replaced by fresh sorbent material (make-up) between the experimental variations; this inevitably lead to a wide age distribution of solids and above all a higher share of "fresh" solids in experiments which were conducted after high amounts of solids were entrained. This could explain the contradictory improvement of the the BSU's performance, when using the $ADS60 - DES80$ configuration during the weir height variation at $12vol\%CO_2$ and a dynamic sorbent loading of $7,1wt\%$, relative to the case where $80mm$ weirs were installed in both reactors.

Chapter 6

Conclusion & Outlook

Using adsorption for post-combustion CO_2 capture has the potential of overcoming several shortcoming compared to absortion, which is currently considered as the state-of-the-art technology. In the bench scale unit that has been used for experimental investigations in this work, temperature swing adsorption is realized by circulating an amine functionalized solid sorbent between two multistage fluidized bed columns. Thus, continuous CO_2 capture from a simulated flue-gas was put into practice, while counter-current flow of solids relative to the gas phase, maximizes the working capacity of the adsorbents. In the course of an experimental campaign, the performance of the bench scale unit was extensively investigated under a wide variety of operating conditions and unit configurations. To summarize the results shown in Chapter 4, the following statements can be made:

- The axial temperature dispersion of the desorber column decreases when steam is used as a stripping gas.

- Within the parameters tested, the flow rate of steam in the desorber, has a rather small influence on the capture efficiency.

- An internal heat displacement from the desorber to the adsorber occurs when steam is used as stripping gas (most likely through co-adsorption of H_2O in the desorber and subsequent desorption in the adsorber). It was shown that this enhances the performance of the CO_2 adsorption process.

- Higher SCRs improve the BSU's performance at the cost of lower dynamic sorbent loading.

- Proper gas sealing by means of introduction of low flow rates of purge gas is possible.

- By increasing the CO_2 concentration of the adsorber feed gas at a constant dynamic sorbent loading, the amount of CO_2 which could be captured per day increases at the cost of a significantly lower capture efficiency.

- Increasing the flow rate of flue-gas leads to an increase of the amount of CO_2 captured per day and a steep decrease of the capture efficiency.

- Higher weirs installed in either contactors, allow for higher dynamic sorbent loadings and lower SCRs, at constant capture efficiencies.

Due to recent constructive measures like higher freeboards in both columns, particle entrainment has been minimized, allowing for long term operation without adding significant amounts of material make-up. In the near future, a long term operating test, with more than 100 regeneration cycles, is planned to determine the degradation of the adsorbent material. Further experiments with a variation of the inventory by variation of the numbers of stages in the adsorber and desorber are planned. As mentioned in Chapter 5 it will be necessary to investigate the observed co-adsorption of steam by means of a thermogravimetric analysis of the utilized sorbent material. As tube-to-bed heat exchange obviously plays a major role in this process, an increase of the heat-exchanger surface by altering its design will be considered; this measure is expected to improve the BSU's performance and is also key for the reactor design of such a system.

Bibliography

[ACS, 2014] ACS (2014). "American Chemical Society - National Historic Chemical Landmarks: The Fluid Bed Reactor http://www.acs.org /content/acs/en/education/whatischemistry/landmarks/fluidbedreactor.html".

[Berger and Bhown, 2011] Berger, A. and Bhown, A. (2011). "Comparing Physisorption and Chemisorption Solid Sorbents for use Separating CO2 from Flue Gas using Temperature Swing Adsorption". *Energy Procedia*, 4, pp. 562–567.

[Canadella, 2007] Canadella, J. (2007). "Contributions to accelerating atmospheric CO2 growth from economic activity, carbon intensity, and efficiency of natural sinks; Proceedings of the National Academy of Sciences".

[Dabrowski, 2001] Dabrowski, A. (2001). "Adsorption from theory to practice". *Advances in Colloid and Interface Science*, 93, pp. 135–224.

[de Rosset et al., 1981] de Rosset, A.; Neuzil, R. W.; and Broughton, D. B. (1981). "Percolation Processes: Theory and Applications". page 249.

[Dinca and Badea, 2012] Dinca, C. and Badea, A. (2012). "The parameters optimization for a CFBC pilot plant experimental study of post-combustion CO2 capture by reactive absorption with MEA".

[Drage et al., 2008] Drage, T.; Arenillas, A.; Smith, K.; and Snape, C. (2008). "Thermal stability of polyethylenimine based carbon dioxide adsorbents and its influence on selection of regeneration strategies". *Microporous and Mesoporous Materials*, 116(1-3), pp. 504–512.

[Drage et al., 2009] Drage, T.; Smith, K.; Arenillas, A.; and Snape, C. (2009). "Developing strategies for the regeneration of polyethylenimine based CO2 adsorbents". *Energy Procedia*, 1, pp. 875–880.

[ESRL, 2014] ESRL (2014). "Earth System Research Laboratory - Global Monitoring Devision: Atmospheric CO2 at Mauno Loa Observatory".

[Fauth et al., 2012] Fauth, D.; Gray, M. L.; and Pennline, H. (2012). "Investigation of Porous Silica Supported Mixed-Amine Sorbents for Post-Combustion CO2 Capture". *Energy Fuels*, 26, pp. 2483–2496.

[GCCSI, 2012a] GCCSI (2012a). "Global Carbon Capture and Storage Institute: CO2 Capture Technologies - Post Combustion Capture (PCC)".

[GCCSI, 2012b] GCCSI (2012b). "Global Carbon Capture and Storage Institute: CO2 Capture Technologies - Pre Combustion Capture".

[Geldart, 1973] Geldart, D. (1973). "Types of gas fluidization". *Powder Technology*, 7, pp. 285.

[Grace, 1986] Grace, J. R. (1986). "Contacting modes and behaviour classification of gas-solid and other two-phase suspensions". *Canadian Journal of Chemical Engineering*, 64, pp. 353.

[Grace, 2006] Grace, J. R. (2006). "Multiphase Flow Handbook - 5.1 Hydrodynamics of Fluidization".

[Gray et al., 2005] Gray, M.; Soong, Y.; Champagne, K.; Pennline, H.; Baltrus, J.; Stevens Jr., R.; Khatri, R.; Chuang, S.; and Filburn, T. (2005). "Improved immobilized carbon dioxide capture sorbents". *Fuel Processing Technology*, 86, pp. 1449–1455.

[Gray et al., 2008] Gray, M. L.; Champagne, K. J.; Fauth, D.; Baltrus, J. P.; and Pennline, H. (2008). "Performance of immobilized tertiary amine solid sorbents for the capture of carbon dioxide". *International Journal of Greenhouse Gas Control*, 2(1), pp. 3–8.

[Grewal and Cheung, 1985] Grewal, N. S. and Cheung, T. K. (1985). "Heat Transfer between Horizontal Finned Tubes and a Gas-Solid Fluidized Bed". *Industrial & Engineering Chemistry Process Design and Development*, 24, pp. 458–471.

[Haita, 2012] Haita, C. (2012). "The State of Compliance in the Kyoto Protocol". *International Centre for Climate Governance Reflection*, 12.

[Hammache et al., 2013] Hammache, S.; Hoffman, J. S.; McMahan, G. L.; Fauth, D. J.; Howard, B. H.; and Pennline, H. W. (2013). "Comprehensive Study of the Impact of Steam on Polyethyleneimine on Silica for CO2 Capture". *Energy Fuels*, 27, pp. 6899–6905.

[Heyardi-Gorji and Sayari, 2012] Heyardi-Gorji, A. and Sayari, A. (2012). "Thermal, Oxidative, and CO2-Induced Degradation of Supported Polyethylenimine Adsorbents". *Industrial & Engineering Chemistry Research*, 51, pp. 6887–6894.

[Hofbauer, 2012] Hofbauer, H. (2012). "Unterlagen zur Vorlesung: Wirbelschichttechnik".

[Houshmand et al., 2012] Houshmand, A.; Daud, W.; Lee, M.; and Shafeeyan, M. (2012). "Carbon Dioxide Capture with Amine-Grafted Activated Carbon". *Water, Air, & Soil Pollution*, 223(2), pp. 827–835.

[IEA, 2013] IEA (2013). "International Energy Agency Technology Roadmap: Carbon Capture and Storage".

[IPCC, 2005] IPCC (2005). "IPCC Special Report on Carbon Dioxide Capture and Storage".

[IPCC, 2007] IPCC (2007). "IPCC Fourth Assessment Report - Climate Change 2007: Synthesis Report".

[IPCC, 2012] IPCC (2012). "Intergovernmental Panel on Climate Change - Glossary of terms. In: Managing the Risks of Extreme Events and Disasters to Advance Climate Change Adaptation". pages 555–564.

[IPCC, 2013] IPCC (2013). "Anthropogenic and Natural Radiative Forcing; Climate Change 2013: The Physical Science Basis. Contribution of Working Group I to the Fifth Assessment Report of the Intergovernmental Panel on Climate Change".

[Kayser, 1881] Kayser, H. (1881). *Wiedemann's Annalen der Physik und Chemie*, 12.

[Keller and Saudt, 2005] Keller, J. and Saudt, R. (2005). "Gas Adsorption Equilibria - Experimental Methods and Adsorption Isotherms". pages 2–6.

[Kim et al., 2003] Kim, S. W.; Ahn, J. Y.; Kim, S. D.; and Hyun Lee, D. (2003). "Heat transfer and bubble characteristics in a fluidized bed with immersed horizontal tube bundle". *International Journal of Heat and Mass Transfer*, 46(3), pp. 399–409.

[Knudsen et al., 2009] Knudsen, J.; Jensen, J.; Vilhelmsen, P.; and Biede, O. (2009). "Experience with CO2 capture from coal flue gas in pilot-scale: Testing of different amine solvents".

[Kolbitsch et al., 2009] Kolbitsch, P.; Pröll, T.; Bolhar-Nordenkampf, J.; and Hofbauer, H. (2009). "Operating experience with chemical looping combustion in a 120kW dual circulating fluidized bed (DCFB) unit".

[Kunii and Levenspiel, 1991] Kunii, D. and Levenspiel, O. (1991). "Fluidization Engineering".

[Langmuir, 1918] Langmuir, I. (1918). "The adsorption of gases on plane surfaces of glass, mica and platinum". *Journal of the American Chemical Society*, 40.

[LeVan et al., 1997] LeVan, M. D.; Carta, G.; and Yon, C. M. (1997). "Adsorption and Ion Exchange". *Perry's Chemical Engineers' Handbook*, 7.

[Masel, 1996] Masel, R. I. (1996). "Principles of Adsorption and Reaction on Solid Surfaces". pages 108–197.

[NETL, 2007] NETL (2007). "U.S. Department of Energy: The National Energy Technology Laboratory - Carbon Dioxide Capture from Existing Coal-Fired Power Plants".

[Palchonok et al., 1998] Palchonok, G. I.; Breitholtz, C.; Borodulya, V. A.; and Leckner, B. (1998). "Effect of turbulence on heat transfer in the freeboard of stationary and circulating fluidized beds". *Proceedings of the ninth Engineering Foundation Conference on Fluidization*, pages 413–420.

[Petit et al., 1999] Petit, J.; Jouzel, J.; Raynaud, D.; Barkov, N. I.; Barnola, J.-M.; Basile, I.; Benders, M.; Chappellaz, J.; Davis, M.; Delayque, G.; Delmotte, M.; Kotlyakov, V. M.; Legrand, M.; Lipenkov, V.; Lorius, C.; Pepin, L.; Ritz, C.; Saltzman, E.; and Stievenard, M. (1999). "Climate and atmospheric history of the past 420,000 years from the Vostok ice core, Antarctica". *Nature*, 399.

[Pirngruber et al., 2013] Pirngruber, G. D.; Guillou, F.; Gomez, A.; and Clausse, M. (2013). "A theoretical analysis of the energy consumption of post-combustion CO2 capture processes by temperature swing adsorption using solid sorbents". *International Journal of Greenhouse Gas Control*, 14(0), pp. 74–83.

[Ratnasamy and Wagner, 2009] Ratnasamy, C. and Wagner, J. P. (2009). "Water Gas Shift Catalysis". *Catalysis Reviews*, 51(3), pp. 325–440.

[Rouquerol et al., 1999] Rouquerol, F.; J., R.; and Sing, K. (1999). "Adsorption by Powders and Porous Solids". pages 1–21.

[Ruthven, 1984] Ruthven, D. M. (1984). "Principles of Adsorption & Adsorption Processes". pages 1–43; 336–408.

[Saxena, 1989] Saxena, S. C. (1989). "Heat Transfer between Immersed Surfaces and Gas-Fluidized Beds". *Advances in Heat Transfer*, 19.

[Sjostrom and Krutka, 2010] Sjostrom, S. and Krutka, H. (2010). "Evaluation of solid sorbents as a retrofit technology for CO2 capture". *Fuel*, 89(6), pp. 1298–1306.

[Su et al., 2010] Su, F.; Lu, C.; Kuo, S.; and Zeng, W. (2010). "Adsorption of CO2 on Amine-Functionalized Y-Type Zeolites". *Energy Fuels*, 24, pp. 1441–1448.

[Suzuki, 1990] Suzuki, M. (1990). "Adsorption Engineering". pages 35–37.

[Vattenfall, 2014] Vattenfall (2014). "http://www.vattenfall.com/en/ccs/illustrations.htm".

[Veneman et al., 2012] Veneman, R.; Li, Z.; Hogendoorn, J.; Kersten, S.; and Brilman, D. (2012). "Continuous CO2 capture in a circulating fluidized bed using supported amine sorbents". *Chemical Engineering Journal*, 207-208, pp. 18–26.

[Wang et al., 2011] Wang, M.; Stephenson, L. P.; Sidders, J.; Ramshaw, C.; and Yeung, H. (2011). "Post-combustion CO2 Capture with Chemical Absorption: A State-of-the-art Review". *Chemical Engineering Research and Design*, 8(9), pp. 1609–1624.

[Xu et al., 2009] Xu, G.; Murakami, T.; Suda, T.; Matsuzaw, Y.; and Tani, H. (2009). "Two-stage dual fluidized bed gasification: Its conception and application to biomass". *Fuel Processing Technology*, 90(1), pp. 137–144.

[Xu et al., 2002] Xu, X.; Song, C.; Andresen, J.; Bruce, G.; and Scaront, A. (2002). "Novel Polyethylenimine-Modified Mesoporous Molecular Sieve of MCM-41 Type as High-Capacity Adsorbent for CO2 Capture". *Energy & Fuels*, 16, pp. 1463–1469.

[Yang and Hoffman, 2009] Yang, W. and Hoffman, J. (2009). "Exploratory Design Study on Reactor Configurations for Carbon Dioxide Capture from Conventional Power Plants Employing Regenerable Solid Sorbents". *Industrial & Engineering Chemistry Research*, 48, pp. 341–351.

[Yu et al., 2012] Yu, C.; Huang, C.; and Tan, C. (2012). "A Review of CO2 Capture by Absorption and Adsorption". *Aerosol and Air Quality Research*, 12, pp. 745–769.

[Zhao et al., 2013] Zhao, W.; Zhang, Z.; Li, Z.; and Cai, N. (2013). "Continuous CO2 Capture in Dual Fluidized Beds Using Silica Supported Amine". *Energy Procedia*, 37, pp. 89–98.

List of Figures

List of Tables